Viroid evolution and viroid-induced pathogenesis networks in host plants

Inaugural-Dissertation

zur Erlangung des Doktorgrades
der Mathematisch-Naturwissenschaftlichen Fakultät
der Heinrich-Heine-Universität Düsseldorf

vorgelegt von

Rajen Julian Joseph Piernikarczyk
aus Hamburg

Düsseldorf, Mai 2016

aus dem Institut für Physikalische Biologie
der Heinrich-Heine-Universität Düsseldorf

Gedruckt mit der Genehmigung der
Mathematisch-Naturwissenschaftlichen Fakultät der
Heinrich-Heine-Universität Düsseldorf

Referent: apl.Prof. Dr. Ing. Gerhard Steger
Korreferent: Prof. Dr. Martin J. Lercher

Tag der mündlichen Prüfung: 17. Juni 2016

Erklärung

Ich versichere an Eides Statt, dass die Dissertation von mir selbstständig und ohne unzulässige fremde Hilfe unter Beachtung der „Grundsätze zur Sicherung guter wissenschaftlicher Praxis an der Heinrich-Heine-Universität Düsseldorf“ erstellt worden ist. Die Dissertation habe ich in dieser oder in ähnlicher Form noch bei keiner anderen Institution eingereicht. Ich habe bisher keine erfolglosen oder erfolgreichen Promotionsversuche unternommen.

Düsseldorf, den 11. Mai 2016

_____

Rajen Julian Joseph Piernikarczyk

The New Colossus

Not like the brazen giant of Greek fame,
With conquering limbs astride from land to land;
Here at our sea-washed, sunset gates shall stand
A mighty woman with a torch, whose flame
Is the imprisoned lightning, and her name
Mother of Exiles. From her beacon-hand
Glows world-wide welcome; her mild eyes command
The air-bridged harbor that twin cities frame.

"Keep, ancient lands, your storied pomp!" cries she
With silent lips. "Give me your tired, your poor,
Your huddled masses yearning to breathe free,
The wretched refuse of your teeming shore.
Send these, the homeless, tempest-tost to me,
I lift my lamp beside the golden door!"

Emma Lazarus

Abstract

Pathogens exploit host resources for replication and spread to adapt and survive in dynamic environments. Small pathogenic elements like viruses and transposons composed of 10^4–10^6 nucleotides (nt) infect hosts from all domains of life and introduce deleterious as well as beneficial effects. These pathogens employ a broad range of genome-encoded exploits like proteins and RNA secondary structures and diversify their genome to evade host defense systems. Host-pathogen interactions drive selection, which is acting on the host-genotype as well as on the pathogen-genotype. Pathogenic elements shape the evolutionary history and adaptions of the host among others by lateral gene transfer, gene duplication, genomic reorganization, reprogramming and rewiring pathways. The class of subviral particles includes the smallest known pathogens like prions and hepatitis δ, a satellite RNA. The plant-pathogenic viroids are subviral particles that compress all essential information into single-stranded, circular and non-coding RNA genomes of about 250–400 nt length depending on the viroid species. Viroids are obligate parasites of the host's transcriptional machinery. Hosts of viroids are species from *Solanaceae* like *Solanum lycopersicum* (tomato) and *Solanum tuberosum* (potato), but also *Prunus persica* (peach), *Cocos nucifera* (coconut) and others. The pathogenesis of viroids depends on the genotype of the pathogen and its host, different host cultivars might be (in-)tolerant to viroid-induced symptoms like dwarfism, epinasty and necrosis that cause significant yield losses of diverse crops worldwide. Although the genome of the Potato spindle tuber viroid (PSTVd)—the type strain of the *Pospiviroidae* family—was the second genome to be sequenced, a comprehensive pathogenesis theorem that explains viroid genotype-dependent symptoms of host plants is lacking. *Pospiviroidae* exploit the DNA-dependent RNA polymerase II (Pol II) for replication in an asymmetric rolling-circle mechanism. Based on the RNA substrate, the replication process constantly introduces an increased number of mutations compared to Pol II-error rates on DNA substrates. This error-prone replication rapidly leads to the accumulation of error copies of the original infecting master copy that gives rise to a so-called "mutant swarm" or quasispecies. The thermodynamically stable as well as metastable RNA secondary structures and structural motifs of PSTVd recruit host factors at least for replication and systemic trafficking, but do not explain the far reaching host reprogramming and evasion of the host defense system. Viroid infections induce viroid-specific small RNAs (vsRNA) that are hypothesized within one pathogenicity theorem to direct the host post-transcriptional gene silencing (PTGS) pathway to host transcripts resulting in a viroid-instructed and favored environment.

The first part of this thesis focuses on the evolution of PSTVd during infections of the tomato hosts. Based on deep-sequenced vsRNAs we developed a method to reconstruct quasispecies and extract viable PSTVd variants that evolved from the master copy. These newly emerged variants competed with the original master sequence and in some instances have overgrown them. We estimated the replication efficiency of Pol II with an RNA substrate as a template and determined an error rate of $\sim 5 \times 10^{-3}$ for PSTVd. We identified ornamental plants as viroid reservoirs.

The second part of this thesis focuses on viroid-induced pathogenesis networks. We performed degradome sequencing of PSTVd-infected tomato plants to determine degradation regimes of the mild symptoms inducing PSTVd variant QFA and severe symptoms inducing variant AS1. We computationally identified viroid-induced differentially degraded host transcripts that belong to diverse pathways. The most significant differentially cleaved host transcripts were pathogenesis-related transcripts that are assumed to suppress the host defense systems. We assume that tomato plants activate a PAMP/pattern-triggered immunity (PTI) response to viroid infections, which is countered by the viroid-induced pathogenesis networks that lead to the cleavage of transcripts related to pathogenesis-critical host pathways. We investigated the differential expression and degradation of a tomato morphogenesis-regulating SANT/HTH Myb transcript in healthy and PSTVd infected plants. We determined that the expression dynamics correlated to the viroid-induced pathogenesis and to the PSTVd (in-)tolerant tomato cultivar.

Zusammenfassung

Pathogene befallen Wirte, um sich zu replizieren und an dynamische Lebensräume anzupassen und darin zu bestehen. Kleine pathogene Elemente, wie Viren und Transposons, die aus 10^4–10^6 Nukleotiden (nt) bestehen, befallen Wirte aus allen Domänen des Lebens und lösen in ihnen sowohl schädliche als auch nützliche Effekte aus. Diese Pathogene kodieren eine große Bandbreite von gegen den Wirt gerichteten Proteinen und RNA-Sekundärstrukturen. Ausserdem diversifizieren sie ihr Genom, um sich den Abwehrmechanismen des Wirts zu entziehen. Die Interaktionen zwischen Pathogen und Wirt beeinflussen die Selektion, die sich auf das Genom beider auswirkt. Pathogene Elemente formen die Evolutionsgeschichte und Anpassung des Wirts unter anderem durch lateralen Gentransfer, Genduplikation, genetische Reorganisation, Neuprogrammierung und Neuverschaltung von Synthesewegen. Die Klasse der subviralen Partikel beinhaltet die kleinsten bekannten Pathogene, wie zum Beispiel Prione und die Satelliten-RNA Hepatitis δ. Ebenfalls zu den subviralen Partikeln zählen die pflanzeninfizierenden Viroide, die ihre gesamte essentielle Information auf ein einzelsträngiges, zirkuläres und nicht-kodierendes RNA-Genom mit einer Länge von 250–400 nt komprimieren. Viroide sind obligate Parasiten der Transkriptionsmaschinerie des Pflanzenwirtes. Bekannte Viroidwirte sind unter anderem Spezies der *Solanaceae*, wie zum Beispiel *Solanum lycopersicum* (Tomate) und *Solanum tuberosum* (Kartoffel), aber auch *Prunus persica* (Pfirsisch) und *Cocos nucifera* (Kokosnuss). Die Pathogenese der Viroide hängt vom Genotypen des Pathogens und des Wirts ab. Verschiedene Kulturvarietäten der Wirtspflanzen können (in-)tolerant gegenüber den vom Viroid hervorgerufenen Symptomen sein, wie Zwergwuchs, Epinastie und Nekrosen. Diese Symptome sind weltweit verantwortlich für signifikante Ernteausfälle der betroffenen Nutzpflanzen. Obwohl das Genom des Kartoffel-Spindelknollen-Sucht-Viroids („Potato spindle tuber viroid"; PSTVd), dem namensgebenden Viroid der Familie *Pospiviroidae*, das zweite sequenzierte Genom überhaupt ist, fehlt es bislang an einem Pathogenitätstheorem, das die vom Viroidgenotypen abhängigen Symptome in der Wirtspflanze erklärt. Mitglieder der *Pospiviroidae* nutzen die DNA-abhängige RNA Polymerase II (Pol II) für die Replikation in einem asymmetrischen rollenden Ring-ähnlichen Mechanismus. Bei der Replikation dient die Viroid-RNA somit als falsches Substrat, weswegen im Replikationsprozess im Vergleich zur Pol II-Fehlerrate mit DNA Substrat kontinuierlich eine erhöhte Anzahl von Mutationen eingeführt werden. Die erzeugten fehlerhaften Genomkopien, welche von der ursprünglich infizierenden – der Mastersequenz – stammen, formen eine sogenannte Quasispezies. Die thermodynamischen stabilen und metastabilen Sekundärstrukturen und andere Motive rekrutieren Wirtsfaktoren unter anderem für die Replikation und Ausweitung von einer lokalen zu einer systemischen Infektion. Diese erklären jedoch nicht die weitreichende Umprogrammierung des Wirts und das Ausweichen der Abwehrantwort. Viroid-Infektionen induzieren Viroid-spezifische kleine RNAs (vsRNA), die innerhalb eines Pathogenitätstheorems die Fähigkeiten des Wirts zum posttranskriptionelles Gen-Silencing (PTGS) übernehmen und dieses wiederum gegen Wirtstrankripte einsetzen. Diese Viroid-instruierte Wirtsregulation führt zu einer Viroid-bevorzugten Zellumgebung.

Im ersten Teil dieser Arbeit wird die Evolution von PSTVd-Genomen in infizierten Tomatenpflanzen untersucht. Basierend auf sequenzierte vsRNAs haben wir eine Methode zur Rekonstruktion von Quasispezies entwickelt und lebensfähige PSTVd-Varianten extrahiert, die von der Mastersequenz evolviert sind. Die durch Mutationen neu enstandenen PSTVd-Varianten konkurrierten mit der ursprünglich infizierenden Mastersequenz und überwuchsen diese in einzelnen Fällen. Wir haben die Replikationseffizienz der Pol II mit dem fehlerhaften PSTVd-RNA-Substrat abgeschätzt und eine Fehlerrate von $\sim 5 \times 10^{-3}$ festgestellt. Wir konnten Zierpflanzen als Viroid-Reservoirs identifizieren.

Im zweiten dieser Arbeit werden Viroid-induzierte Pathogenitätsnetzwerke untersucht. Wir haben das s Degradom von PSTVd-infizierten Tomatenpflanzen sequenziert, um Viroid-induzierte differentielle Degradierungsregime der mit milden Symptomen verbundenen QFA-Variante

und mit schwersten Symptomen verbundenen AS1-Variante zu beschreiben. Wir konnten computergestützt Viroid-induzierte differentielle Degradierung verschiedener Wirtssynthesewege feststellen. Interessanterweise gehörten die meisten geschnittenen Wirtstranskripte zu den sogenannten pathogenitätsbezogenen Proteinen, was vermutlich dem Unterdrücken von Abwehrwegen des Wirts dient. Wir vermuten, dass infizierte Tomatenpflanzen eine PAMP/pattern-triggered immunity (PTI) Antwort generieren und diese vom Viroid-induzierten Pathogenitätsnetzwerk gekontert wird. Dies wird sichtbar durch Schnitte von pathogenesekritischen Wirtstranskripten. Wir untersuchten die differenzielle Expression und Degradierung von morphogeneseregulierenden Tomaten SANT/HTH Myb Transcripten in gesunden und PSTVd infizierten Pflanzen. Wir haben festgestellt, dass die Expressionsdynamik mit der viroid-induzierten Pathogenese und den PSTVd (in-)toleranten Tomaten Kulturvarietäten korreliert.

Preface

This work was conceptualized as a cumulative thesis in accordance with "Promotionsordnung der Mathematisch-Naturwissenschaftlichen Fakultät der Heinrich-Heine-Universität Düsseldorf" from January 09, 2014 § 6 (4) with the amendments from December 10, 2014, March 20, 2015, and March 03, 2016. Contributions for each manuscript are listed in accordance with § 6 (3). Four manuscripts are presented along with an introduction to the field of study and a conclusion.

- Viroid evolution

    1. **Viroid quasispecies revealed by deep sequencing.**
    Rajen J.J. Piernikarczyk, Robert A. Owens, Jaroslav Matoušek and Gerhard Steger
    (Submitted)
    Contribution: Theoretical framework, method, bioinformatics, manuscript concept and writing.
    2. **Characterization of Potato spindle tuber viroid (PSTVd) incidence and new variants from ornamentals.**
    Jaroslav Matoušek, Rajen J.J. Piernikarczyk, Anna Týcová, Ganesh S. Duraisamy, Tomáš Kocábek and Gerhard Steger
    European Journal of Plant Pathology (2014)
    Contribution: Bioinformatics.
    Reprint license: Springer: 3861341402687; issued on May 03, 2016.

- Viroid-induced pathogenesis networks

    3. **Expression of SANT/HTH Myb mRNA, a plant morphogenesis-regulating transcription factor, changes due to viroid infection.**
    Jaroslav Matoušek, Rajen J.J. Piernikarczyk, Petr Dědič, Josef Mertelík, Kateřina Uhlířová, Ganesh S. Duraisamy, Lidmila Orctová, Kateřina Kloudová, Jiří Ptáček and Gerhard Steger
    Journal of Plant Physiology (2015)
    Contribution: Bioinformatics.
    Reprint license: ELSEVIER: 3861351332734; issued on May 03, 2016.
    4. **Characterization of the PSTVd-induced tomato degradome.**
    Rajen J.J. Piernikarczyk, Jaroslav Matoušek, Sophie de Vries and Gerhard Steger
    Manuscript
    Contribution: Theoretical framework, bioinformatics, manuscript concept and writing.

Acknowledgements

I thank the following people:

Gerhard Steger	for awakening my interest for viroids and plant pathology; extensive discussions, supervision and trust.
Jaroslav Matoušek	for collaboration and experimentally exploration of bioinformatics-derived theory.
Detlev Riesner	for mentoring and support.
Dieter Wilbold	for hosting me.
Martin J. Lercher	for paving the way for this work and the support in the years before.
Sophie de Vries	for collaboration and supporting this work with plant pathology expertise.
David Heckmann	for support and discussion.
C. Jonathan Fritzemeier	for support and discussion.
Konny Aigner	for support and discussion.
My family.	

I am grateful to the following institutions for funding this work:
The interdisciplinary Graduate School: Evolutionary Networks: Organisms, Reactions, Molecules (E-Norm)
Alexander von Humboldt Foundation

Contents

Chapter 1

Introduction

Subviral particles represent the smallest known pathogens with genomes of 10^2–10^4 nucleotides (nt) that infect all kingdoms of life. Satellite RNAs like hepatitis δ are dependent on helper virus infections (Makino et al., 1987). Prions are structured protein aggregates that adopt special disease-causing conformations leading f. e. to Creutzfeldt–Jakob disease (for review see Prusiner, 1998). The genomes of viroids are non-coding RNAs that infect plants and cause devastating and economically important diseases in crop plants (Diener, 2003; Palukaitis, 2014). Despite their small genomic size the exact mechanism of pathogenesis of most subviral particles remains unknown. In this thesis viroids are investigated. First, viroids and their molecular hallmarks are introduced. Second, the evolution of viroids is presented as an interesting field to study Eigen's quasispecies concept (Eigen, 1971). Third, the current viroid pathogenicity theorem and resulting viroid-induced pathogenesis networks are introduced. The small genome of viroids carry all required information to infect, replicate and spread in host plants.

Viroids

Viroids are minimal biotrophic plant pathogens belonging to the class of subviral particles. In contrast to satellite RNAs like the Hepatitis δ satellite, viroids are autonomously infecting entities. Viroids are composed of a single-stranded, unencapsulated, circular and non-coding RNA (ncRNA) genome with a length of 250–400 nt. The broad host range of viroids comprises *Solanacea* hosts like *S. lycopersicum* (tomato), *S. tuberosum* (potato), and *Nicotiana benthamiana* as well as *Humulus lupulus* (hop) and others (Hadidi et al., 2003). Viroids are subdivided into two families:

Members of the *Avsunviroidae*, like the Peach latent mosaic viroid (PLMVd), replicate in a symmetrical rolling-circle mechanism located in host chloroplasts and exploiting a host nuclear-encoded DNA-dependent RNA-polymerase (NEP). These viroids feature a hammerhead ribozyme activity for self-cleavage and ligation (Flores et al., 2011).

Members of the *Pospiviroidae*, like the *Potato spindle tuber viroid* (PSTVd), adopt a rod-like secondary structure (see Fig. 1.1) and replicate in the host cell nucleus (Harders et al., 1989; Zhao et al., 2001) via the DNA-dependent RNA polymerase II (Pol II; Schindler and Mühlbach, 1992) in an asymmetric rolling-circle mechanism (see Fig. 1.3 Branch et al., 1988; Feldstein et al., 1998). Common to all members of *Pospiviroidae* is a central conserved region (Keese and Symons, 1985). In experiments, PSTVd was transmissible by diverse mechanisms; mechanically (Verhoeven et al., 2010), hitchhiking within an encapsulated virus (Francki et al., 1986), aphidborne (Syller and Marczewski, 2001), and in pollen and seeds (Matsushita and Tsuda, 2014). The pathogenesis of PSTVd-induced symptoms

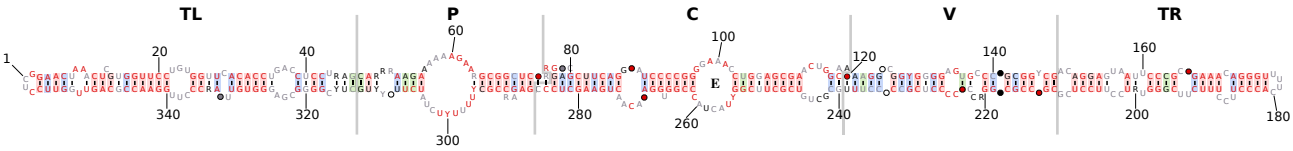

Figure 1.1: Structure of (+)-stranded PSTVd variants. The consensus sequence and structure were predicted for an alignment of 234 variants with MAFFT/G-INS-I (Katoh et al., 2005) optimized in CONSTRUCT (Wilm et al., 2008) at 37 ℃, excluding lonely base pairs, and drawn with R2R (Weinberg and Breaker, 2011). Borders of the five domains are marked by gray lines (TL, terminal left; P, pathogenicity-related; C, central; V, variable; TR, terminal right; Keese and Symons, 1985). Basepairs on green and blue background are supported by covarying mutations and compatible mutations, respectively; no mutations are observed for basepairs in red.

in *S. lycopersicum* and other host plants exhibits a host cultivar-specific and viroid variant-specific genotype dependency. In *S. lycopersicum*, the PSTVd pathogenesis induces symptoms like dwarfism, epinasty, stunting, and necrosis. The severity of symptoms is dependent on the viroid as well as on the host genotype. For example, the PSTVd variants QFA and KF5M5 induce mild, RG1 intermediate (Gruner et al., 1995), and AS1 "lethal" symptoms in tomato cultivar Heinz1706 (see Fig. 1.2).

Although viroids infect a broad range of hosts the tolerance to symptoms is dependent on the host cultivar rather then host species (Matousek et al., 2007) f. e. in *S. lycopersicum* and *Humulus lupulus* (hop). Hence, sensitivity to PSTVd pathogenesis is an intraspecies rather than an interspecies trait. In the PSTVd-intolerant *S. lycopersicum* cultivars Heinz1706 and Rutgers PSTVd pathogenesis-induced symptoms emerge over time. In contrast, *S. lycopersicum* cv. Moneymaker and UC82B are susceptible for PSTVd infections but no significant symptoms accompany the pathogenesis. Mutations like single-nucleotide polymorphisms (SNPs) convert PSTVd variants between different symptom severity classes (Gruner et al., 1995) and mediate host shifts (Wassenegger et al., 1996). Viroids, as autonomously infecting pathogens, encode all required information in their small genomes to invade, overcome, control the host defensive systems, replicate, establish a systemic infection, and spread. The stable and metastable secondary structures of PSTVd integrate motifs that recruit and hence exploit host proteins (for review see Steger and Perreault, 2016).

The high self-complementarity leads secondary structure with a high fraction of base pairings that protects PSTVd from host-driven degradation (Wang et al., 2004; Itaya et al., 2007). Viroid secondary structures are important for trafficking (for review see Takeda and Ding, 2009). Other known secondary structure motifs for recruitment of host factors are: A tetraloop-hairpin loop E motif that implements the switch from cleavage to ligation within the replication cycle (Baumstark et al., 1997; Gas et al., 2007), the ligation of monomeric linear (+)-strands is mediated by DNA ligase 1 (Nohales et al., 2012), and the viroid RNA-binding protein 1 (VIRP1) is a host protein, which binds to a secondary structure motif in the TR region and was identified as critical for PSTVd pathogenesis (Martínez de Alba et al., 2003; Gozmanova et al., 2003; Kalantidis et al., 2007).

Viroid evolution

Every replication of information faces constraints by the amount of information that can be reliably and error-free duplicated irrespectively of their original physical system. Based on information theory (Shannon, 1948), every information bit sends through communication channels is exposed to channel noise leading to errors between source and sink. In biological systems the replication machinery represents such a communication channel. Errors during replication result in inexact genome

Figure 1.2: PSTVd-induced symptoms in tomato cultivar 'Heinz1709'. MOCK, control plant; QFA, a mild, nearly no visible symptoms inducing PSTVd variant; Intermediate, dwarfism, and epinasty inducing PSTVd variant; AS1, "lethal" PSTVd variant with enhanced symptoms in comparison to Intermediate: progressed dwarfism, epinasty, stunting, and necrosis (not shown). Modified from Diermann et al. (2010).

copies (Steinhauer et al., 1992). Based on redundancy, error correction ensures information integrity *in silico* and *in vivo*. In biological systems error correction evolved in form of proof reading of polymerases that enables genomes with billions of nucleotides.

In biological entities, replication-introduced mutations–nucleotide exchange, deletion, insertion, crossing-over or recombination–give rise to error copies of a template genome–the master copy. The emerging aggregate of master and error copies is described by Eigen (1971) with the quasispecies concept. Erroneous information transmission is a source of innovation and enables biological entities to adapt to dynamic environments (Elena and Sanjuán, 2005). Whether a newly acquired mutation is deleterious, neutral or beneficial for a biological entity is decided by selection, i. e. the replication success of the information (Darwin, 1859).

The error rate of polymerases is the primary limitation of the information content and genome size, respectively (Eigen, 1971). If the error rate of a polymerase exceeds the inverse of the genome length the replication copies accumulate errors up to a so-called "error catastrophe". Within this catastropic event the introduced mutations in each replication round result in loss of essential information rendering replicated genomes nonviable. PSTVd replication in plants is thermosensitive, elevated temperatures induce the formation of broad distribution of quasispecies resulting from increased polymerase error-rates (Matoušek et al., 2004).

The error threshold represents the minimal error rate that still supports a replication with a given genome length. Hence, from Eigen's paradox (Eigen, 1971) follows that genomes encode, on the one hand, means for replication that ensures replication fidelity above the error threshold. On the other

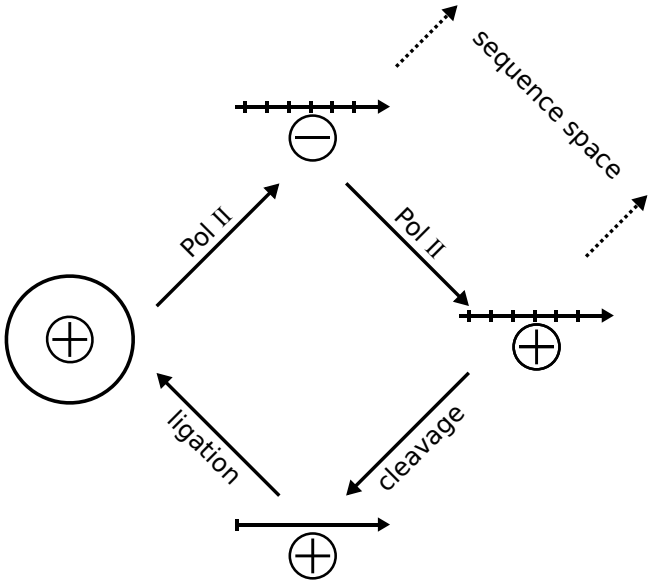

Figure 1.3: PSTVd asymmetrical rolling-circle replication. The replication starts (left) with the circular $(+)$–stranded molecule recruiting Pol II resulting in linear oligomeric $(-)$–stranded replication intermediates (top). This replication intermediate again recruits Pol II for a second passage to produce a linear oligomeric $(+)$–standed replication intermediate (right). Linear monomeric $(+)$-standed molecule are excised from the oligomeric $(+)$-stands (bottom). Ligation converts the linear into a circular molecule. Based on the RNA substrate for the DNA-dependent Pol II PSTVd replication is error-prone. The increased error rate constantly introduces and rapidly accumulates mutations, giving rise to quasispecies that explore the PSTVd sequence space.

hand, genomes ensure that the replication fidelity does not exceed a certain cutoff to allow genome evolution. For example, the replication fidelity of RNA viruses is optimized to operate near the error catastrophe; this ensures adaptability in an arms race with the host defense systems and simultaneously retaining the genome integrity (Crotty et al., 2001). The evolutionary origin of viroids remains controversial; viroids where proposed as descendants of the hypothesized RNA world (Diener, 1989) or as *de novo* emerged plant pathogens (Diener, 2016).

In the paper "Viroid quasispecies revealed by deep sequencing" (submitted) we investigated the error rate, error threshold, and formation of quasispecies guided by Eigen's thereom.

In the paper "Characterization of Potato spindle tuber viroid (PSTVd) incidence and new variants from ornamentals" (Matoušek et al., 2014) we describe ornamental plant as PSTVd hosts. Previously, plants like *Matricaria chamomilla* (chamomile) were identified to constitute symptomless viroid reservoirs (Matoušek et al., 2012) in close proximity to crop fields. Hence, viroid reservoirs in *M. chamomilla* or ornamental plants conserve viroid populations and might feed infection cycles that potentially enable viroids to evolve and adapt to new host.

Viroid-induced pathogenesis networks

Viroids exploit hosts by adopting secondary structure motifs, but the viroid genotype-dependent pathogenesis in plants remains largely unknown. Viroid infections are accompanied by viroid-specific small RNAs (vsRNAs) ranging in size between 19–26 nt (Papaefthimiou et al., 2001) that derive at least from DICER-like proteins (DCL) activity directed against the viroid genome (Itaya et al., 2007).

Plant small RNAs derive from diverse endogenous and exogenous origins. These small effector molecules trigger and maintain epigenetic and transcript regulation (for review see Voinnet, 2009; Borges and Martienssen, 2015). In cooperation with pathogen-derived small RNAs, endogenous small RNAs defend against viruses (Voinnet, 2001). Through cell-to-cell movement small RNAs establish communication between cells to propagate f. e. information on pathogen infections (Yoo et al., 2004).

The small RNA-mediated regulation and host reprogramming is based on two distinct pathways. First, small RNAs guide methylation of genomic sequences (Wassenegger et al., 1994) in the transcriptional gene silencing (TGS) pathway; f. e., transposon-derived small RNAs lead to methylation and heterochromatin formation (Lippman et al., 2004). Silencing of transposal elements (TE) by transposon-derived small RNAs establish an arms race between these and other integrated genomic selfish elements that shaped plant genome evolution (for review see Lisch, 2013). Second, small RNAs guide ARGONAUTE proteins (AGO) for post-transcriptional gene silencing (PTGS) to host RNA transcripts (for review see Vaucheret, 2008) within the RNA interfernce (RNAi) pathway (Hannon, 2002). The focus of this thesis is PTGS.

Genome-encoded microRNAs (miRNA) originate from DCL-processed non-coding pre-miRNA transcripts or introns that adopt stem-loop secondary structures that are subsequently cleaved by DCL (for review see Voinnet, 2009). Host exogenous and endogenous small-interfering RNAs (siRNA) derive from diverse sources (for review see Axtell, 2013). These diverse small RNAs are recruited as guide strands by different AGO proteins (for review see Hutvagner and Simard, 2008; Zhang et al., 2015) forming a binary complex. Different AGOs implement specific regulatory functions f. e. endonucleolytic cleavage-competent AGOs (for review see Czech and Hannon, 2011). The binary complex scans RNAs—f. e. messenger RNAs (mRNA), ncRNA or foreign RNAs—for accessible regions (Tafer et al., 2008) of extensive complementarity to the incorporated guide strand. A ternary complex is formed upon binding to the designated transcript target site. The ternary complex mediates regulation of translation; either the ternary complex stably binds leading to repression of translation or to cleavage of the target site (for review see Rogers and Chen, 2013). The mode of action is dependent on the specific AGO protein, extent of sequence complementarity and (un-)cooperative interactions between multiple ternary complexes on the same transcript (two-hit trigger; Axtell et al., 2006) and other factors. Following cleavage of the targeted transcript between position ten and eleven relative to the guide strand, the 3'-end fragment exhibits a 5'-monophosphorylated end. This feature is exploited to determine small RNA-induced cleaved transcripts including the cleavage site within the so-called degradome sequencing (Degradome-Seq) or parallel analysis of RNA ends (PARE) (German et al., 2008, 2009).

Double-stranded RNAs (dsRNA), which are constantly encountered by plants as virus genomes (Mérai et al., 2006), are targeted by DCL that slice and phase these molecules into 21–24 nt long small RNAs (Allen et al., 2005). Similarly, single-stranded RNA (ssRNA) transcripts are converted into dsRNA by RNA-dependent RNA polymerase 6 (RDR6), which constitute once more a substrate for DCL resulting in 21–24 nt small RNAs. This latter fragment class is called phased secondary small interfering RNAs (phasiRNAs) that can be recruited by AGO and subsequently target additional transcripts (for review see Fei et al., 2013). Based on the sequence homology to their originating transcript, these small RNAs are able to regulate and propagate through multiple layers of related and distant pathway networks (MacLean et al., 2010).

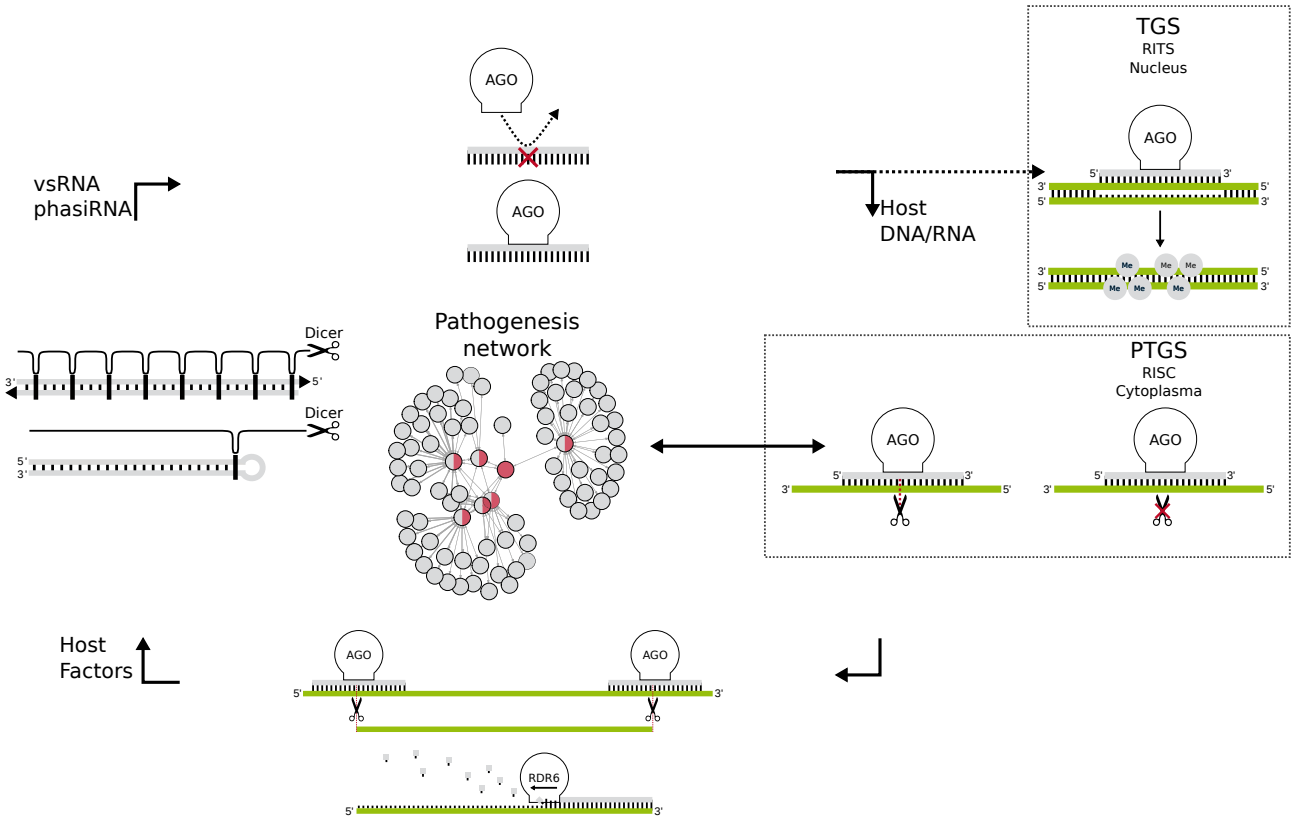

Figure 1.4: Viroid pathogenesis theorem. (left) $(+)$ and $(-)$-stranded PSTVd genomes are templates for presumingly DCL-mediated cleavage to generate vsRNAs (Itaya et al., 2007). (top) functional vsRNAs recruit AGO and form a binary complex. Non-functional vsRNAs fail to recruit AGO and may engage in other mechanisms. (right) Binary complexes scan for extensive sequence complementarity between the guiding vsRNA and host transcripts; upon binding to a target sites a ternary complex is formed. In PTGS, transcripts are either cleaved or translation is repressed by stably bound complexes depending on the sequence complementarity and AGO type. In TGS, vsRNA-guided AGO activity may result in genomic methylation rendering whole genomic regions inaccessible. (bottom) Upon cleavage host transcripts that are cleaved multiple times by either cooperative vsRNAs or combined with host endogenous small RNAs may be converted into dsRNA by RDR6. The dsRNA is a substrate for DCL, which mediates phased cleavage of the molecule leading to the formation of secondary phasiRNA. This process gives rise to far-reaching viroid-induced regulatory networks by converting transcripts into small RNAs that regulate homologues and distant sequences effectively shutting down whole pathways. (central) Illustration of a regulatory network, the initial cleavage event (red) initiates a regulatory cascade by inducing the production of secondary small RNAs from cleaved transcripts. The emerging secondary small RNAs establish a regulatory network that propagates and effectively reprograms the host cell into a viroid-favored environment.

From one established pathogenesis hypothesis of viroids follows that vsRNAs mimic host endogenous small RNAs, based on the molecular similarity. That is, host transcripts are targeted by vsRNAs and are subsequently degraded by the host RNA-induced silencing complex (RISC) as part of the plant post-transcriptional gene silencing (PTGS) pathway; i. e. vsRNAs hijack and redirect a host defensive system against itself (Hammann and Steger, 2012; see Fig. 1.4). Aspects of the pathogenesis theorem were shown for three viroids. For a PLMVd variant, two vsRNAs target the chloroplastic heat shock protein 90 (HSP90) and induce a severe albinism 'peach calico' in affected peach leaves (Navarro et al., 2012). For the *Pospiviroid* Tomato planta macho viroid (TPMVd), a vsRNA was identified that targets a conserved tomato WD40-repeat protein (Avina-Padilla et al., 2015). For

PSTVd, two tomato transcripts CalS11-like and CalS12-like are targeted by vsRNAs inducing characteristic symptoms (Adkar-Purushothama et al., 2015). However, this small number of established vsRNA-transcript relations after a decade of active research illustrates the experimental elusiveness of the current pathogenesis theorem. Currently, a vsRNA-instructed large scale host reprogramming, which is usually required by pathogens to neutralize host defense and exploit host resources, is not attributable to viroids.

In the paper "Expression of SANT/HTH Myb mRNA, a plant morphogenesis-regulating transcription factor, changes due to viroid infection" (Matoušek et al., 2015) we follow a transcript that is cleaved upon viroid infection.

In the manuscript "Characterization of viroid-induced tomato degradome" we sequenced the degradome of PSTVd-infected *S. lycopersicum* to elucidate degradation-mediated host reprogramming as a result of viroid infection and vsRNA-mediated cleavage of host transcripts.

Chapter 2

Conclusion

We elucidated the viroid evolution in the course of infection by the reconstruction of viroid-induced quasispecies. The minimalistic RNA genomes of *Pospiviroidae* are replicated as incorrect substrates by the DNA-dependent RNA polymerase II (Pol II) in an asymmetric rolling circle. Each replication includes two passages of this error-prone process that results in rapid accumulation of mutations and gives rise to a genotypically heterogeneous quasispecies. The mutated master copies—or error copies—with replication competence aggregate and compete with the original master copy rendering them viable. Replication incompetent error copies are considered nonviable. The small genome of PSTVd includes many invariable nucleotide positions (see Fig. 1.1) because of critical structural elements necessary to recruit host proteins like Pol II, DCL, and DNA ligase 1 for replication and processing. Selection acts against mutants lacking these motifs. Hence, error copies are constantly cleared from the emerging quasispecies populations by selection, which was deduced from the background expression of mutated vsRNAs.

With NETMAP we developed a graph-theory-based method for SNPs discovery in deep-sequenced small RNAs derived from circular RNA molecules. By considering the polarity and removal of non-integrable mutations into a circular graph, we were able to extract viroid variants considered to be viable and determined their relative fitness. We hypothesized that the viroid-induced quasispecies are in themselves coding for important pathogenesis-related signals like vsRNAs, that are incompatible with the original infecting master copy—we call this the quasispecies-derived pathogenesis theorem (see Fig. 2.1). In this framework the original infecting master copy variants shape the course of quasispecies formation; i. e., the probability of emergence of specific mutations might diverge significantly in time between viroid variants. This framework would also account for the plasticity and rapid host adaptions of viroids. As a consequence of this hypothesis, future endeavors to relate vsRNAs to host transcript target sites should consider vsRNA that derive from quasispecies.

Based on the deep-sequencing-derived quasispecies we determined an error rate of $\sim 5 \times 10^{-3}$ for PSTVd, a member of *Pospiviroidae*. The accumulation of SNPs led to the formation of viable and previously known PSTVd variants, f. e. QFA→KF5M5. We confirmed that a *Pospiviroid* operates near the error threshold in a narrow fitness landscape—illustrated by the small number of emerged viable error copies—shaped by the high error rates and small genome sizes, which was previously shown for an *Avsunviroidae* (Gago et al., 2009). Similar to viroids, viruses operate close to the error threshold (Crotty et al., 2001). The viroid genome simultaneously represents a legislative, as an information storage and retrieval system, and an executive entity, which mimicks host binding motifs to reshape

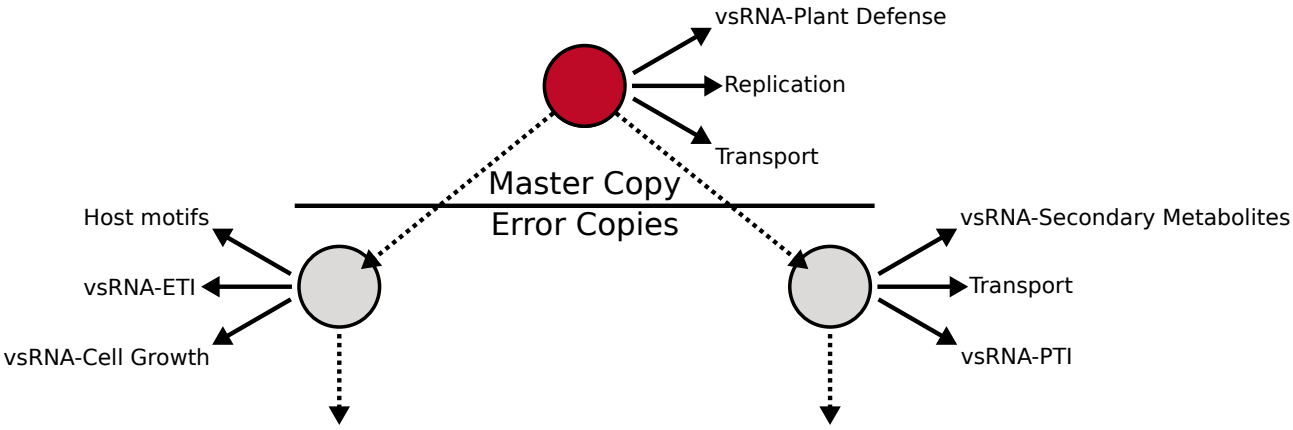

Figure 2.1: Quasispecies pathogenesis theorem. The infecting viroid master sequence encodes signals, f. e. vsRNAs targeting defense-related host transcripts or secondary structure motifs, to reprogram the host. Based on the error-prone Pol II replication, error copies forming a quasispecies that encode new signals, effectively increasing the plasticity of the entire pathogenic sequence assemble or master and error copies.

the host environment. The concept of this duality of legislative and executive was previously described by Eigen (1971). We identified ornamental plants to harbor viroids as symptomless hosts. Hence, ornamentals may constitute hard-to-identify viroid reservoirs from which viroid constantly spread to crop fields. The ability of viroids to afflict ornamentals and induce latent infections underscores the plasticity of these tiny molecules. The broad host range of viroids indicates that they target and exploit fundamental plant pathways.

We investigated viroid-induced pathogenesis networks that enable the minimalistic viroid genomes to modulate signals like vsRNAs. These exogenous small RNAs are hypothesized to cleave host transcripts leading to the formation of host endogenous secondary small RNAs like phasiRNA. Based on these vsRNA-instructed pathogenesis networks, phasiRNA-mediated regulation cascades in host plants potentially establish viroid-favored environments including suppression of host defense pathways. We determined that a viroid-favorable degradation regime is induced upon infection by differentially degraded PR-1 proteins, Phytophthora-induced protein 1 (PIP1) and other proteins belonging to the phenylpropanoid pathway. These findings show that *S. lycopersicum* modulates an appropriate response to PSTVd infections, thus arguing for an evolved and established plant-pathogen interaction.

We are not able to confirm or reject the vsRNA-pathogenesis hypothesis. On the background of the small amount of conclusive degradome reads, plausible and experimentally verified relation between vsRNAs and host transcripts remain elusive. We investigated a viroid-specific degradome of SANT/HTH Myb, but were unable to establish a relation to a host exogenous vsRNA or endogenous primary or secondary small RNA. Based on the following reasoning, we assume that viroid infection-related host reprogramming—including degradation of targeted host transcripts—is orchestrated in an early and narrow time frame. First, in the analyzed degradome data we observed a host pattern-triggered immunity (PTI) response to viroid-infection that must be overcome in a very early infection stage. Second, we previously predicted vsRNA host targets that would lead to plausible symptom-like phenotypes in null-mutants (Piernikarczyk, 2013) that exhibited conclusive expression dynamics in response to viroid-infections but the target sites could not be verified by specific degradomes (not

shown). We therefore recommend to study transcript expression levels at smaller time windows to determine an optimal timeframe for transcript-specific degradomes.

We further advocate to study viroid-infection in time-dependent datasets to establish links between vsRNAs and host transcripts in the frame of the pathogenesis theorem. The time-dependent deep sequencing of the small RNA population will be able to elucidate the viroid quasispecies formation, dynamics and selection process. Additionally, time-dependent investigations would allow to identify transient vsRNA and other signals like secondary structure motifs that are critical in small time frames. The minimalistic viroid genomes offer a unique opportunity to reveal plant-pathogen interactions in the absence of pathogen-encoded proteins. The viroid-induced pathogenesis remains largely unknown despite extensive research effort. Viroids as subviral particles employ diverse exploits, which maximize their informational output. Hence, pathogenesis-related signals may derive from multiple sources including quasispecies which might form in a PSTVd variant-specific manner explaining the diverse variant-specific symptoms. The time-dependent dynamics of viroid-induced pathogenesis and associated host reprogramming appears as a promising field for the future.

Bibliography

Adkar-Purushothama, C. R., Brosseau, C., Giguère, T., Sano, T., Moffett, P., and Perreault, J.-P. (2015). Small rna derived from the virulence modulating region of the potato spindle tuber viroid silences callose synthase genes of tomato plants. *Plant Cell*, 27:2178–94.

Allen, E., Xie, Z., Gustafson, A. M., and Carrington, J. C. (2005). microRNA-directed phasing during trans-acting siRNA biogenesis in plants. *Cell*, 121:207–21.

Avina-Padilla, K., Martinez de la Vega, O., Rivera-Bustamante, R., Martinez-Soriano, J. P., Owens, R. A., Hammond, R. W., and Vielle-Calzada, J.-P. (2015). In silico prediction and validation of potential gene targets for pospiviroid-derived small RNAs during tomato infection. *Gene*, 564:197–205.

Axtell, M. J. (2013). Classification and comparison of small RNAs from plants. *Annu. Rev. Plant Biol.*, 64:137–59.

Axtell, M. J., Jan, C., Rajagopalan, R., and Bartel, D. P. (2006). A two-hit trigger for siRNA biogenesis in plants. *Cell*, 127:565–77.

Baumstark, T., Schröder, A. R., and Riesner, D. (1997). Viroid processing: switch from cleavage to ligation is driven by a change from a tetraloop to a loop E conformation. *EMBO J.*, 16:599–610.

Borges, F. and Martienssen, R. A. (2015). The expanding world of small RNAs in plants. *Nat. Rev. Cell Biol.*, 16:727–41.

Branch, A. D., Benenfeld, B. J., and Robertson, H. D. (1988). Evidence for a single rolling circle in the replication of potato spindle tuber viroid. *Proc. Natl. Acad. Sci. U.S.A.*, 85:9128–32.

Crotty, S., Cameron, C. E., and Andino, R. (2001). RNA virus error catastrophe: direct molecular test by using ribavirin. *Proc. Natl. Acad. Sci. U.S.A.*, 98:6895–900.

Czech, B. and Hannon, G. J. (2011). Small RNA sorting: matchmaking for Argonautes. *Nat. Rev. Genet.*, 12:19–31.

Darwin, C. (1859). On the origin of species.

Diener, T. O. (1989). Circular RNAs: relics of precellular evolution? *Proc. Natl. Acad. Sci. U.S.A.*, 86:9370–4.

Diener, T. O. (2003). Discovering viroids–a personal perspective. *Nat. Rev. Microbiol.*, 1:75–80.

Diener, T. O. (2016). Viroids: "living fossils" of primordial RNAs? *Biol. Direct*, 11:15.

Diermann, N., Matoušek, J., Junge, M., Riesner, D., and Steger, G. (2010). Characterization of plant miRNAs and small RNAs derived from potato spindle tuber viroid (PSTVd) in infected tomato. *Biol. Chem.*, 391:1379–90.

Eigen, M. (1971). Selforganization of matter and the evolution of biological macromolecules. *Naturwissenschaften*, 58:465–523.

Elena, S. F. and Sanjuán, R. (2005). Adaptive value of high mutation rates of RNA viruses: separating causes from consequences. *J. Gen. Virol.*, 79:11555–8.

Fei, Q., Xia, R., and Meyers, B. C. (2013). Phased, secondary, small interfering RNAs in posttranscriptional regulatory networks. *Plant Cell*, 25:2400–15.

Feldstein, P. A., Hu, Y., and Owens, R. A. (1998). Precisely full length, circularizable, complementary RNA: an infectious form of potato spindle tuber viroid. *Proc. Natl. Acad. Sci. U.S.A.*, 95:6560–5.

Flores, R., Grubb, D., Elleuch, A., Nohales, M.-Á., Delgado, S., and Gago, S. (2011). Rolling-circle replication of viroids, viroid-like satellite RNAs and hepatitis delta virus: variations on a theme. *RNA Biol.*, 8:200–6.

Francki, R. I., Zaitlin, M., and Palukaitis, P. (1986). In vivo encapsidation of potato spindle tuber viroid by velvet tobacco mottle virus particles. *Virology*, 155:469–73.

Gago, S., Elena, S. F., Flores, R., and Sanjuán, R. (2009). Extremely high mutation rate of a hammerhead viroid. *Science*, 323:1308.

Gas, M., Hernández, C., Flores, R., and Daròs, J. (2007). Processing of nuclear viroids in vivo: an interplay between RNA conformations. *PLoS Pathog.*, 3:e182.

German, M. A., Luo, S., Schroth, G., Meyers, B. C., and Green, P. J. (2009). Construction of Parallel Analysis of RNA Ends (PARE) libraries for the study of cleaved miRNA targets and the RNA degradome. *Nat. Protoc.*, 4:356–62.

German, M. A., Pillay, M., Jeong, D.-H., Hetawal, A., Luo, S., Janardhanan, P., Kannan, V., Rymarquis, L. A., Nobuta, K., German, R., De Paoli, E., Lu, C., Schroth, G., Meyers, B. C., and Green, P. J. (2008). Global identification of microRNA-target RNA pairs by parallel analysis of RNA ends. *Nat. Biotechnol.*, 26:941–6.

Gozmanova, M., Denti, M. A., Minkov, I. N., Tsagris, M., and Tabler, M. (2003). Characterization of the RNA motif responsible for the specific interaction of potato spindle tuber viroid RNA (PSTVd) and the tomato protein Virp1. *Nucleic Acids Res.*, 31:5534–43.

Gruner, R., Fels, A., Qu, F., Zimmat, R., Steger, G., and Riesner, D. (1995). Interdependence of pathogenicity and replicability with potato spindle tuber viroid (PSTVd). *Virology*, 209:60–69.

Hadidi, A., Flores, R., Randles, J., and Semancik, J. (2003). *Viroids: properties, detection, diseases and their control*. Csiro Publishing.

Hammann, C. and Steger, G. (2012). Viroid-specific small RNA in plant disease. *RNA Biol.*, 9:809–19.

Hannon, G. J. (2002). RNA interference. *Nature*, 418:244–51.

Harders, J., Lukács, N., Robert-Nicoud, M., Jovin, T. M., and Riesner, D. (1989). Imaging of viroids in nuclei from tomato leaf tissue by in situ hybridization and confocal laser scanning microscopy. *EMBO J.*, 8:3941–9.

Hutvagner, G. and Simard, M. J. (2008). Argonaute proteins: key players in RNA silencing. *Nat. Rev. Mol. Cell Biol.*, 9:22–32.

Itaya, A., Zhong, X., Bundschuh, R., Qi, Y., Wang, Y., Takeda, R., Harris, A. R., Molina, C., Nelson, R. S., and Ding, B. (2007). A structured viroid RNA serves as a substrate for dicer-like cleavage to produce biologically active small RNAs but is resistant to RNA-induced silencing complex-mediated degradation. *J. Gen. Virol.*, 81:2980–94.

Kalantidis, K., Denti, M. A., Tzortzakaki, S., Marinou, E., Tabler, M., and Tsagris, M. (2007). Virp1 is a host protein with a major role in Potato spindle tuber viroid infection in Nicotiana plants. *J. Gen. Virol.*, 81:12872–80.

Katoh, K., Kuma, K., Miyata, T., and Toh, H. (2005). Improvement in the accuracy of multiple sequence alignment program MAFFT. *Genome Inform.*, 16:22–33.

Keese, P. and Symons, R. H. (1985). Domains in viroids: evidence of intermolecular RNA rearrangements and their contribution to viroid evolution. *Proc. Natl. Acad. Sci. U.S.A.*, 82:4582–6.

Lippman, Z., Gendrel, A.-V., Black, M., Vaughn, M. W., Dedhia, N., McCombie, W. R., Lavine, K., Mittal, V., May, B., Kasschau, K. D., Carrington, J. C., Doerge, R. W., Colot, V., and Martienssen, R. (2004). Role of transposable elements in heterochromatin and epigenetic control. *Nature*, 430:471–6.

Lisch, D. (2013). How important are transposons for plant evolution? *Nat. Rev. Genet.*, 14:49–61.

MacLean, D., Elina, N., Havecker, E. R., Heimstaedt, S. B., Studholme, D. J., and Baulcombe, D. C. (2010). Evidence for large complex networks of plant short silencing RNAs. *PloS one*, 5:e9901.

Makino, S., Chang, M. F., Shieh, C. K., Kamahora, T., Vannier, D. M., Govindarajan, S., and Lai, M. M. (1987). Molecular cloning and sequencing of a human hepatitis delta (delta) virus RNA. *Nature*, 329:343–6.

Martínez de Alba, A. E., Sägesser, R., Tabler, M., and Tsagris, M. (2003). A bromodomain-containing protein from tomato specifically binds potato spindle tuber viroid RNA in vitro and in vivo. *J. Gen. Virol.*, 77:9685–94.

Matousek, J., Kozlová, P., Orctová, L., Schmitz, A., Pesina, K., Bannach, O., Diermann, N., Steger, G., and Riesner, D. (2007). Accumulation of viroid-specific small RNAs and increase in nucleolytic activities linked to viroid-caused pathogenesis. *Biol. Chem.*, 388:1–13.

Matoušek, J., Orctová, L., Steger, G., Škopek, J., Moors, M., Dědič, P., and Riesner, D. (2004). Analysis of thermal stress-mediated PSTVd variation and biolistic inoculation of progeny of viroid "thermomutants" to tomato and *Brassica* species. *Virology*, 323:67–78.

Matoušek, J., Piernikarczyk, R. J. J., Dědič, P., Mertelík, J., Uhlířová, K., Duraisamy, G. S., Orctová, L., Kloudová, K., Ptáček, J., and Steger, G. (2014). Characterization of Potato spindle tuber viroid (PSTVd) incidence and new variants from ornamentals. *Eur. J. Plant Pathol.*, 138:93–101.

Matoušek, J., Piernikarczyk, R. J. J., Týcová, A., Duraisamy, G. S., Kocábek, T., and Steger, G. (2015). Expression of SANT/HTH Myb mRNA, a plant morphogenesis-regulating transcription factor, changes due to viroid infection. *J. Plant Physiol.*, 183:85–94.

Matoušek, J., Stehlík, J., Procházková, J., Orctová, L., Wullenweber, J., Füssy, Z., Kováčik, J., Duraisamy, G. S., Ziegler, A., Schubert, J., and Steger, G. (2012). Biological and molecular analysis of the pathogenic variant C3 of potato spindle tuber viroid (PSTVd) evolved during adaptation to chamomile (*Matricaria chamomilla*). *Biol. Chem.*, 393:605–15.

Matsushita, Y. and Tsuda, S. (2014). Distribution of potato spindle tuber viroid in reproductive organs of petunia during its developmental stages. *Phytopathology*, 104:964–9.

Mérai, Z., Kerényi, Z., Kertész, S., Magna, M., Lakatos, L., and Silhavy, D. (2006). Double-stranded RNA binding may be a general plant RNA viral strategy to suppress RNA silencing. *J. Gen. Virol.*, 80:5747–56.

Navarro, B., Gisel, A., Rodio, M. E., Delgado, S., Flores, R., and Di Serio, F. (2012). Small RNAs containing the pathogenic determinant of a chloroplast-replicating viroid guide the degradation of a host mRNA as predicted by RNA silencing. *Plant J.*, 70:991–1003.

Nohales, M.-Á., Flores, R., and Daròs, J.-A. (2012). Viroid RNA redirects host DNA ligase 1 to act as an RNA ligase. *Proc. Natl. Acad. Sci. U.S.A.*, 109:13805–10.

Palukaitis, P. (2014). What has been happening with viroids? *Virus Genes*, 49:175–84.

Papaefthimiou, I., Hamilton, A., Denti, M., Baulcombe, D., Tsagris, M., and Tabler, M. (2001). Replicating potato spindle tuber viroid RNA is accompanied by short RNA fragments that are characteristic of post-transcriptional gene silencing. *Nucleic Acids Res.*, 29:2395–400.

Piernikarczyk, R. (2013). Exploration of a relation between viroid-specific small RNAs and symptoms in viroid-infected tomato (*Solanum lycopersicum* L.). Master's thesis, Heinrich-Heine-Universität Düsseldorf.

Prusiner, S. B. (1998). Prions. *Proc. Natl. Acad. Sci. U.S.A.*, 95:13363–83.

Rogers, K. and Chen, X. (2013). Biogenesis, turnover, and mode of action of plant microRNAs. *Plant Cell*, 25:2383–99.

Schindler, I.-M. and Mühlbach, H.-P. (1992). Involvement of nuclear DNA-dependent RNA polymerases in potato spindle tuber viroid replication: a reevaluation. *Plant Sci.*, 84:221–229.

Shannon, C. E. (1948). A mathematical theory of communication. *Bell System Technical Journal*, 27:379–423.

Steger, G. and Perreault, J.-P. (2016). Structure and associated biological functions of viroids. *Adv. Virus Res.*, pages 141–72.

Steinhauer, D. A., Domingo, E., and Holland, J. J. (1992). Lack of evidence for proofreading mechanisms associated with an RNA virus polymerase. *Gene*, 122:281–8.

Syller and Marczewski (2001). Potato leafroll virus-assisted aphid transmission of potato spindle tuber viroid to potato leafroll virus-resistant potato. *J. Phytopathol.*, 149:195–201.

Tafer, H., Ameres, S. L., Obernosterer, G., Gebeshuber, C. a., Schroeder, R., Martinez, J., and Hofacker, I. L. (2008). The impact of target site accessibility on the design of effective siRNAs. *Nat. Biotechnol.*, 26:578–83.

Takeda, R. and Ding, B. (2009). Viroid intercellular trafficking: RNA motifs, cellular factors and broad impacts. *Viruses*, 1:210–21.

Vaucheret, H. (2008). Plant ARGONAUTES. *Trends Plant Sci.*, 13:350–8.

Verhoeven, J. T. J., Hüner, L., Marn, M. V., Plesko, I. M., and Roenhorst, J. W. (2010). Mechanical transmission of potato spindle tuber viroid between plants of *Brugmansia suaveoles*, *Solanum jasminoides* and potatoes and tomatoes. *Eur. J. Plant Pathol.*, 128:417–421.

Voinnet, O. (2001). RNA silencing as a plant immune system against viruses. *Trends Genet.*, 17:449–59.

Voinnet, O. (2009). Origin, biogenesis, and activity of plant microRNAs. *Cell*, 136:669–87.

Wang, M.-B., Bian, X.-Y., Wu, L.-M., Liu, L.-X., Smith, N. A., Isenegger, D., Wu, R.-M., Masuta, C., Vance, V. B., Watson, J. M., Rezaian, A., Dennis, E. S., and Waterhouse, P. M. (2004). On the role of RNA silencing in the pathogenicity and evolution of viroids and viral satellites. *Proc. Natl. Acad. Sci. U.S.A.*, 101:3275–80.

Wassenegger, M., Heimes, S., Riedel, L., and Sänger, H. L. (1994). RNA-directed de novo methylation of genomic sequences in plants. *Cell*, 76:567–76.

Wassenegger, M., Spieker, R. L., Thalmeir, S., Gast, F. U., Riedel, L., and Sänger, H. L. (1996). A single nucleotide substitution converts potato spindle tuber viroid (PSTVd) from a noninfectious to an infectious RNA for *Nicotiana tabacum*. *Virology*, 226:191–7.

Weinberg, Z. and Breaker, R. R. (2011). R2R–software to speed the depiction of aesthetic consensus RNA secondary structures. *BMC Bioinformatics*, 12:3.

Wilm, A., Linnenbrink, K., and Steger, G. (2008). ConStruct: Improved construction of RNA consensus structures. *BMC Bioinformatics*, 9:219.

Yoo, B.-C., Kragler, F., Varkonyi-Gasic, E., Haywood, V., Archer-Evans, S., Lee, Y. M., Lough, T. J., and Lucas, W. J. (2004). A systemic small RNA signaling system in plants. *Plant Cell*, 16:1979–2000.

Zhang, H., Xia, R., Meyers, B. C., and Walbot, V. (2015). Evolution, functions, and mysteries of plant ARGONAUTE proteins. *Curr. Opin. Plant Biol.*, 27:84–90.

Zhao, Y., Owens, R. A., and Hammond, R. W. (2001). Use of a vector based on Potato virus X in a whole plant assay to demonstrate nuclear targeting of Potato spindle tuber viroid. *J. Gen. Virol.*, 82:1491–7.

Chapter 3

Manuscripts

Viroid quasispecies revealed by deep sequencing

Rajen J. J. Piernikarczyk [1], Robert A. Owens [2], Jaroslav Matoušek [3], and Gerhard Steger [1*]

[1]Institut für Physikalische Biologie, Heinrich-Heine-Universität Düsseldorf, 40204 Düsseldorf, Germany
[2]United States Department of Agriculture, Agricultural Research Service, Molecular Plant Pathology Laboratory, Beltsville, MD 20705, USA
[3]Biology Centre, CAS, v. v. i., Institute of Plant Molecular Biology, Branišovská 31, 37005 České Budějovice, Czech Republic

ABSTRACT

Viroids are non-coding single-stranded circular RNA molecules that replicate autonomously in infected host plants causing mild to lethal symptoms. Their genomes contain about 250–400 nucleotides, depending on viroid species. Members of the family *Pospiviriodeae*, like the *Potato spindle tuber viroid* (PSTVd), replicate via an asymmetric rolling-circle mechanism using the host DNA-dependent RNA-Polymerase II in the nucleus, while members of *Avsunviroidae* are replicated in a symmetric rolling-circle mechanism probably by the nuclear-encoded polymerase in chloroplasts. Viroids induce the production of viroid-specific small RNAs (vsRNA) that can direct (post-)transcriptional gene silencing against host transcripts or genomic sequences. Here, we used deep-sequencing to analyze vsRNAs from plants infected with different PSTVd variants to elucidate the PSTVd quasipecies evolved during infection. We recovered several novel as well as previously known PSTVd variants that were obviously competent in replication, and identified common strand-specific mutations. The frequencies of these mutations are consistent with a mean error rate per nucleotide position of less than 5×10^{-3}, quite comparable to the known value of 2.5×10^{-3} for a member of *Avsunviroidae*. The resulting error threshold allows the synthesis of longer-than-unit-length replication intermediates as required by the asymmetric rolling-circle mechanism of members of *Pospiviroidae*.

INTRODUCTION

Viroids are single-stranded circular RNA molecules that replicate autonomously in infected host plants. As non-coding RNAs, viroids do not code for any protein but possess the biological activity and function of a minimal parasite inducing specific diseases in their hosts (1–3). The severity of viroid-induced symptoms depends on the viroid variant as well as on the host and cultivar susceptibility. Members of the family *Pospiviroidae*, including the type strain *Potato spindle tuber viroid* (PSTVd), are transcribed in host cell nuclei in an asymmetric rolling-circle mechanism (see Figure 1) by the host DNA-dependent RNA polymerase II (Pol II); members of the family *Avsunviroidae* are replicated by a nuclear-encoded polymerase (NEP) in chloroplasts (4). Viroids induce these polymerases to accept RNA instead of DNA as template with a resulting increase in error rates. Indeed, for Chrysanthemum chlorotic mottle viroid (CChMVd), a member of *Avsunviroidae*, an error rate of 2.5×10^{-3} has been demonstrated (5). Consequently, an infecting viroid molecule—the master sequence—gives rise to a sequence ensemble of master and error copies termed a 'mutant swarm' or quasispecies (6).

Viroids rely on thermodynamically stable and metastable secondary structures to recruit host factors for replication, processing, ligation, and systemic trafficking (7). These structures mimic host endogenous binding motifs and drive selection during replication and quasispecies formation (see Figure 1). Indeed, viroid infections may spontaneously, or in new hosts adaptively, generate new viable and competitive sequences (8–11). Thus, viroids as minimal biological entities with high replication and error rates provide a unique opportunity to study such quasispecies.

Viroid infections also induce the production of viroid-specific small RNAs (vsRNA) that appear to be involved in pathogenesis (12, 13): sequence complementarity with host transcripts results in (post-)transcriptional gene silencing, and creation of a host environment favoring viroid replication. Thus far, three vsRNA-based pathogenic determinants have been described; the first involves a variant of Peach latent mosaic viroid (PLMVd) (14), the second Tomato planta macho viroid (TPMVd) (15), and a third PSTVd (16).

In this context, three deep-sequencing small RNA datasets isolated from tomato (*Solanum lycopersicum*) infected with PSTVd variants are currently available. The first is from tomato 'Heinz 1706' infected by PSTVd variants QFA, C3, and AS1, that induce mild, severe, and "lethal" symptoms, respectively (11). The second is from tomato 'Rutgers' infected by PSTVd variants M and I that induce mild and intermediate symptoms, respectively (17). The third is from four tomato cultivars infected with variant RG1. RG1 induces intermediate to severe symptoms in 'Heinz 1706' and

*To whom correspondence should be addressed. Tel: +49 211 8114597; Fax: +49 211 8115167; Email: steger@biophys.uni-duesseldorf.de

2

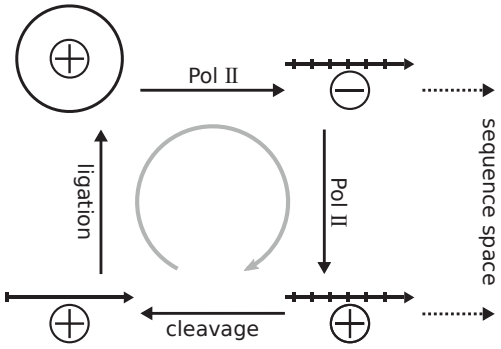

Figure 1. The asymmetric rolling-circle replication of members of the *Pospiviroidae* exploits the host's Pol II. The circular monomeric PSTVd genome, arbitrarily assigned as (+)-strand, is transcribed into an oligomeric linear (−)-strand; the latter is template for synthesis of an oligomeric linear (+)-strand. The oligomeric (+)-strand is cleaved into monomers that are ligated to form the mature circular form. Pol II transcription introduces mutations and generates the quasispecies to explore the sequence space; the grey arrow indicate selection acting against non-viable mutations.

'Rutgers' but only mild symptoms in 'Moneymaker' and 'UC82B'; this dataset was produced following the protocol described in (18).

It is well known that the full sequence of the infecting viroid variant (or larger viruses) can be assembled from such small RNA datasets either using the viroid sequence as reference (19) or even without a reference (20, 21). In this study, we wanted to go a step further; that is, we compared the mutational landscape of different infecting viroid variants; these landscapes reflect replication efficiency, selection, and sequencing error. We estimated the viroids' sequence space from the deep-sequencing data following methods established for RNA viruses (22–26) and applied the quasispecies theorem (6, 27) and associated concepts to viroids.

MATERIALS AND METHODS

Deep-sequencing datasets of small RNAs

We analyzed three published sets of small RNA sequence data, which are abbreviated as D_s (11), D_p (17) and D_o, respectively. D_s is from *S. lycopersicum* 'Heinz 1706' plants infected with the PSTVd variants QFA (mild, GenBank AC U23059.1), C3 (severe, HE575349.1), or AS1 ("lethal", AY518939.1). D_p is from *S. lycopersicum* 'Rutgers' infected with the PSTVd variants Intermediate (I, AY937179.1) and PSTVd Dahlia (M(ild), AB623143.1), respectively. D_o is from four different tomato cultivars infected with the PSTVd variant RG1 (intermediate–severe, U23058.1); these cultivars are the PSTVd-sensitive 'Heinz 1706' and 'Rutgers', and the PSTVd-insensitive, nearly asymptomatic 'Moneymaker' and 'UC82B'.

For D_s, we used PRINSEQ (28) for entropy based removal of uninformative poly-A tails derived from the sequencing procedure. Illumina adapters were removed using TRIMMOMATIC (29). We used SEGEMEHL v. 0.2.0 (30, 31) to map deep-sequenced vsRNAs to their infecting PSTVd variant reference. Parameters for use of these programs are listed in supplemental Table S1.

Sequence evolution

We followed Eigen's formalism for the evolution of sequences (6). In brief, read mappings with 90% accuracy resulted in positions i deviating from the reference sequence S; consecutive insertions were handled as a single mutation at the corresponding first position. The read count with the reference nucleotide at position i is v_i^{ref}, the sum of all reads with nucleotide changes (substitutions, insertions, or deletions) at position i is denoted as v_i^{var}. Then the probability q for exact reproduction of a nucleotide was estimated by the mean error rate P_{error} over all sites:

$$q(S) = 1 - \left(\sum_{i=1}^{|S|} \frac{v_i^{\text{var}}}{v_i^{\text{ref}}} \right) / |S| = 1 - P_{\text{error}} \qquad \textbf{(1)}$$

Under the assumption that master and error copies exhibit the same decay rate, we estimated the average selective advantage σ of the master copy over the error copies under 90 % accuracy mapping (32)

$$\sigma(S) = \sum_{i=1}^{|S|} \frac{v_i^{\text{ref}}}{v_i^{\text{var}}} \qquad \textbf{(2)}$$

and the error threshold

$$t_{\max} < \ln(\sigma)/(1-q). \qquad \textbf{(3)}$$

Sequence network mapping with NETMAP

We developed a graph-orientated method named NETMAP, a PERL script based on SAMTOOLS (33) and Bio::DB::Sam, to assemble the PSTVd sequence space from mapped deep-sequenced small RNA reads. A PSTVd sequence of length l is represented by $|v|^l$ vertices with $v \in \{\text{A,C,G,U,D(eletion),I(nsertion)}\}$ connected by weighted directed edges e. A weight w is the count of two adjacent vertices located in any single read; the edge direction represents (+) and (−) strandedness of reads. The graph $G = (V,E)$ is constructed from short reads mapped by SEGEMEHL with 90% accuracy to a reference sequence, which is the PSTVd variant used for infection.

We applied the following filter steps to vsRNA reads to reduce noise based mainly on sequencing errors:

(1) Two neighboring sequence positions (u,v) are only connected by an edge $e(u,v)$ if they are in the same read with read counts $w(e(u,v)) \geq 20$ and relative counts $w(e(u,v))/w(e(u^{\text{ref}},v^{\text{ref}})) \geq 0.01$.

(2) Mismatching bases at the 5' or 3' end of a read are considered as adapter contamination or sequencing error if no other reads embed these variations.

(3) Only variants present in both polarities are considered competent for replication.

(4) Two (or more) sequence variations are only considered as connected (i. e., derived from one genome) if a read includes both; that is, variations further apart than the length of a read might originate from different PSTVd genomes. If two variants are present on both polarities but are only connected in one polarity, we still considered them as connected.

RESULTS

vsRNA Expression

We identified vsRNAs by mapping small RNA reads from deep-sequencing datasets D_s, D_o and D_p to the respective infecting PSTVd variant with different accuracies (see Figure 2(a)). In the range from 100 to 90% accuracy, only a very small number of small RNAs from mock-inoculated deep-sequenced samples mapped to the PSTVd variants (see Figure S2). Thus, we continued with vsRNAs mapped with 90% accuracy for the remaining results. That is, we tolerated up to 2 mismatches between a standard read, with length below 25 nt, and a viroid sequence to ensure sufficient specificity and to allow some variability.

The numbers of vsRNAs from intermediate and severe PSTVd variants were similar and higher than those from mild variants (see Table S2). In D_p and D_o, $(-)$-stranded vsRNAs were less abundant than $(+)$-stranded vsRNAs. In D_s, vsRNA levels gradually increased from QFA to C3 to AS1. Notably, the lower pathogenicity-related domain (P^+_{lower}; see Fig. S1(a)) of PSTVd variants AS1 and C3 exhibits vsRNA expression peaks in contrast to QFA (see Figure 2(a)).

In all but one case, the numbers of mapped vsRNAs increased by about 10% (Table S2) as the mapping accuracy was decreased from 100 to 90% (Figure 2(a)). The clear exception was the vsRNA profile of variant QFA: here the additional mappings at 90% accuracy revealed sequence variations in the upper central to variable domain ($(\text{C–V})_{\text{upper}}$) and—to a minor extent—in the lower P to terminal-left domain ($(\text{P–TL})_{\text{lower}}$). These mutations show up more clearly in a plot of differences between nucleotides in vsRNAs and the infecting PSTVd sequence (Fig. 2(b)). In QFA, mutations at positions 120–125 and 303–316 are up to 10 times more abundant than the original QFA nucleotides.

With this surprising result in mind, we mapped each deep-sequencing dataset to all PSTVd variants available in the subviral database (34). Indeed, the reads from the QFA-infected sample were more consistent with the sequence of variant KF5M5 (AC M93685) than with QFA (see rows marked by QFA→KF5M5 in Fig. 2). This discrepancy between the infecting sequence and the resulting sequence assembled by small reads prompted us to analyze these deviations in detail.

vsRNA-derived sequence space

To elucidate the distribution of mismatched nucleotides in vsRNAs, we plotted these mismatches along the respective PSTVd sequence in Figure 2(b) and the ratio of these mismatches to the corresponding reference nucleotide in Figure S3. In the latter figure, the few positive values—especially in the QFA mapping—clearly show that the originally infecting PSTVd variant was overgrown by other variant(s). The same mismatch positions dominate in Fig. 2(b); a clear example is again seen in QFA at positions 61, 121, and 315, or, less pronounced, in C3 at positions 308–314.

These mutations with their relative high frequencies emerge from a background of sequence errors, similarly visible in both polarities in all datasets independent of the infecting PSTVd variant or the different tomato cultivars. This background makes it difficult to distinguish replication-competent variants containing changes in both strands from the infecting reference sequence. Furthermore, because our detection of mutations is based on short reads and not on full-length viroid sequences, we can only identify co-appearing mutations that are located on the same read(s). To accomplish both objectives, extraction of relevant mutations and detection of co-appearing mutations, we developed the method NETMAP.

Replication-competent PSTVd variants revealed by graph theory

NETMAP extracts from vsRNAs viable and connected sequence positions. We define mutations as viable if they are present in reads of both polarities and thus are likely to originate from replicating viroids. Mutations are connected and originate from the same genome if they are present on a single read. For further program details see Material & Methods. This network analysis revealed viable sequence variants that co-replicated with the inoculated PSTVd variant or even outgrew it.

From the reads mapping to PSTVd variant QFA in D_s, NETMAP identified three significantly expressed mutations. Fig. 3(a) illustrates the deletion of an A in the A stretch upstream of G_{62}; this deletion was present in about 29% of $(+)$-stranded reads covering this position and in about 76% of $(-)$-stranded reads. Fig. 3(b) illustrates two connected mutations, an $A_{121}\rightarrow U$ transversion and an A deletion upstream of G_{125}; both mutations dominated the reference sequence in both polarities. Fig. 3(c) illustrates five connected mutations including two insertions; these mutations also dominated the reference sequence. Assuming that these mutations (Figures 3(a)–(c)) from regions P_{upper}, V_{upper}, and P_{lower} were present in the same molecule, the inoculated PSTVd variant QFA evolved to variant KF5M5 (AC M93685.1).

For variant C3, NETMAP identified two variable sites: $A_{47}\rightarrow U$ and $A_{59}\rightarrow AA$ in region P_{upper} (Figure 3(g)), and $A_{308}\rightarrow U$, $C_{310}\rightarrow A$, $U_{312}\rightarrow A$, and $U_{314}\rightarrow C$ in P_{lower} (Figure 3(h)). The mutation $C_{310}\rightarrow A$ was only weakly supported (below 0.1% reads in both polarities) and was not connected with the neighboring mutations. The other mutations were supported by 6–15% of reads; that is, these mutations were less expressed than the corresponding reference nucleotides. If these mutations in P_{upper} and P_{lower}, except $C_{310}\rightarrow A$, were present in the same molecule, they point to the possible evolution of the infecting variant C3 to variant AS1; C3 was still the dominant sequence at the time of sampling, however. For variant AS1, NETMAP detected no sequence variations.

For D_o, NETMAP detected only a single mutation (i. e., $U_{309}\rightarrow A$) in about 2 and 4% of $(+)$- and $(-)$-stranded reads

4

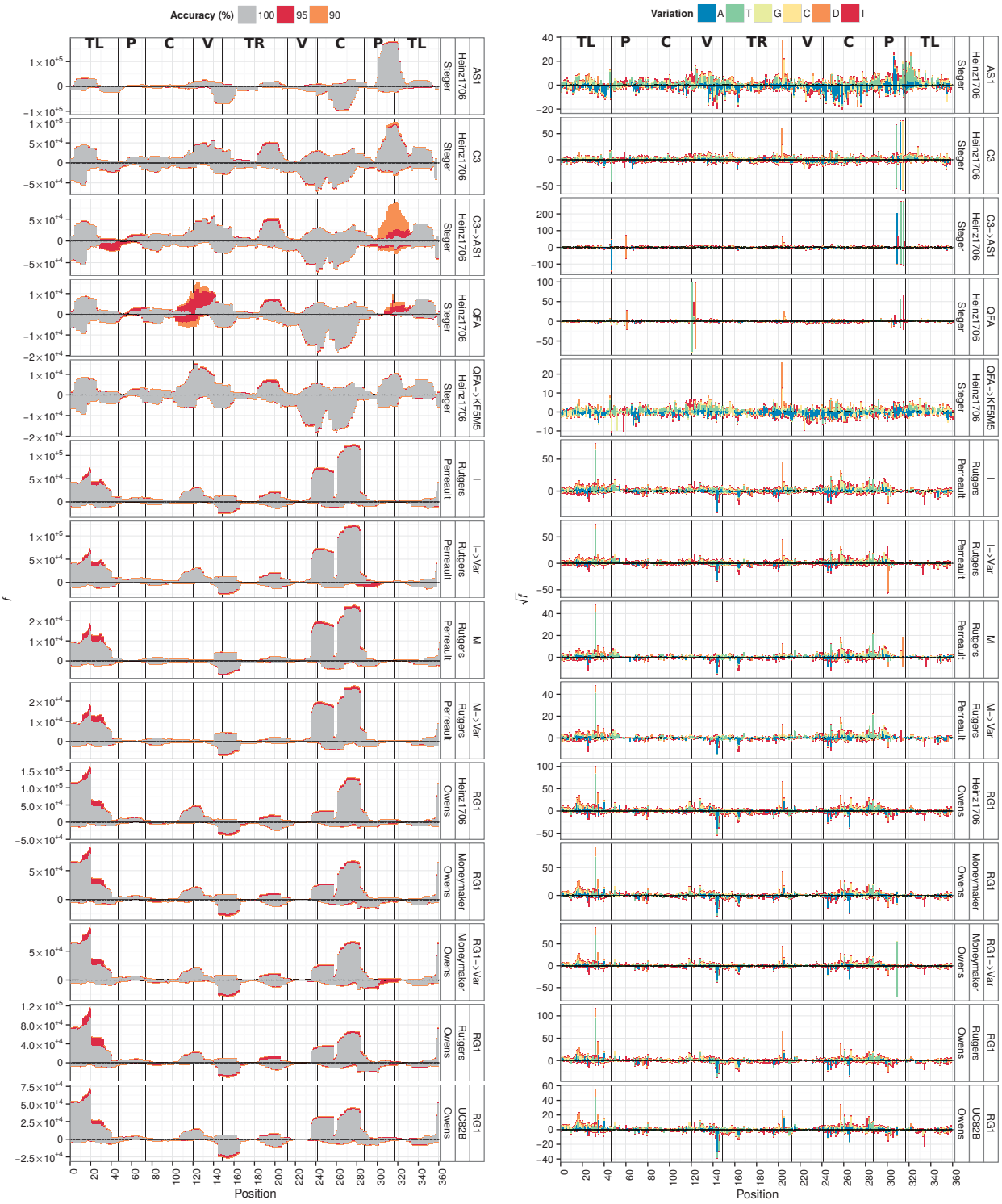

(a) vsRNA expression (b) vsRNA sequence variation

Figure 2. Mapping of small reads to PSTVd variants. (a) Frequency of reads mapping to PSTVd positions with different accuracies (see color code at top). Note the differently scaled y-axes. (b) Sequence variation (see color code at top) at 90% mapping accuracy; stacked bars represent the square root of ratio of a specific variation in relation to all variations (including the reference nucleotide) at one site. All insertions are collapsed into one count regardless of base and length. Viroid domains (see Fig. S1(a)) are marked close to the top. Deletions (D), insertions (I), and mutations to A, U, G, or C are marked by different colors (see legend at top).

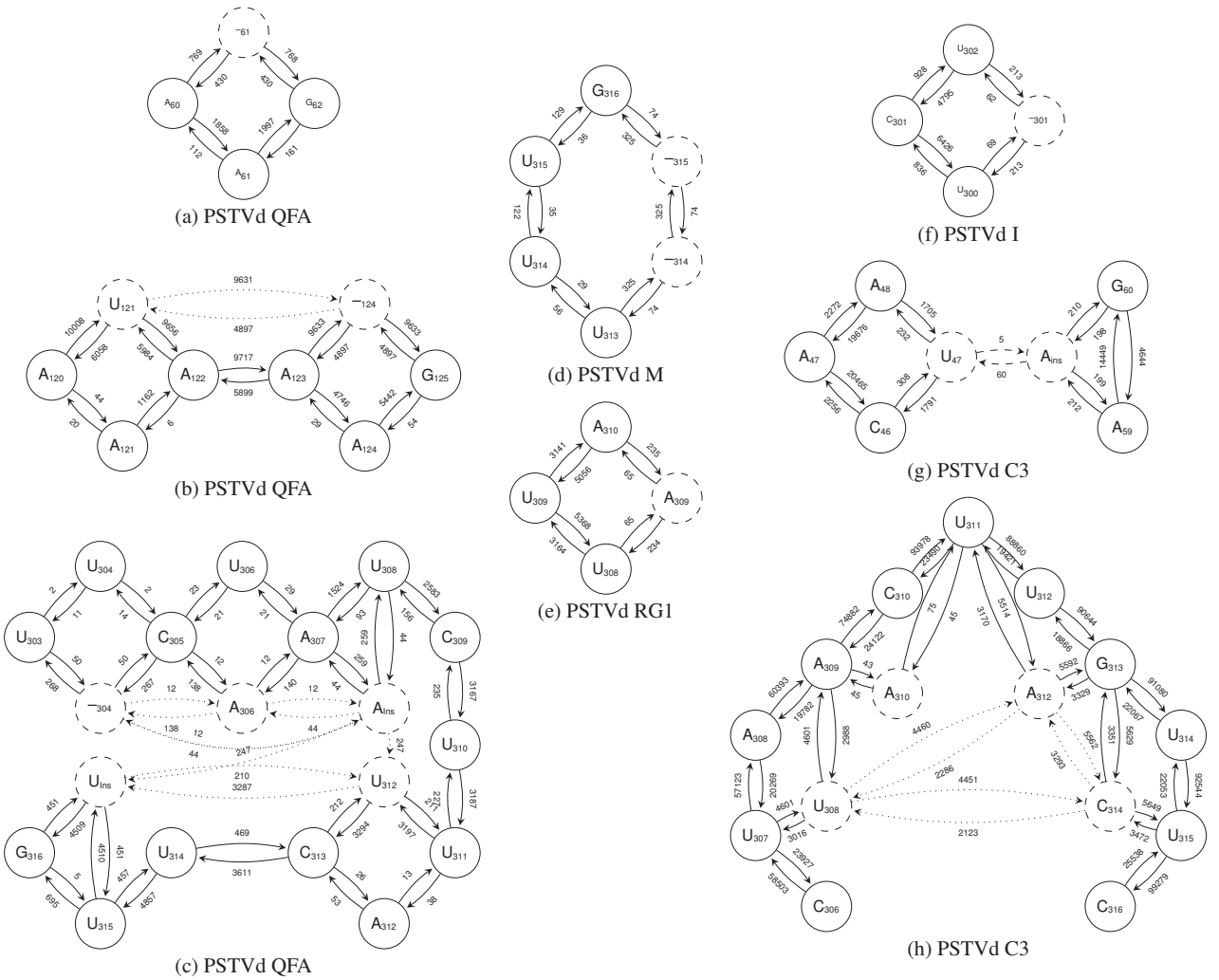

Figure 3. Sequence networks extracted by NETMAP from reads mapping with 90% accuracy to the respective infecting PSTVd variant. Nucleotides in solid circles show sequence positions that are identical to the reference sequence; those in dashed circles show mutations. Insertions and deletions are indicated by (N_{Ins}) and ($-_{position}$), respectively. Solid arrows connect nucleotides; dotted arrows link mutations that are located on the same read. An arrow pointing from position x to position y indicates $(+)$- and $(-)$-polarity if $x > y$ and $x < y$, respectively. Read numbers (edge weights) label the arrows. Positions of mutations in the secondary structure of PSTVd are shown in Fig. S1(d).

from 'Moneymaker' (see Fig. 3(e)). This change is present in several other PSTVd variants (e. g., KF440-2 (X58388.1), X52039.1, X52040.1), but only with additional mutations. No sequence variation of the infecting PSTVd variant RG1 was detected in the other tomato cultivars.

In D_p, network analysis revealed sequence variation in the PSTVd variants M and I. For variant M we identified two linked and dominant mutations (deletions of U_{314} and U_{315} in about 70% of reads; see Figure 3(d)). For variant I we identified a minor mutation (deletion of C_{301} in <7% of the reads; see Figure 3(f)). Sequence comparisons revealed no known variants associated with these changes.

Polarity-specific mutations

Besides the mutations detected by NETMAP, which are potentially replication competent, several other potential mutations were identified in reads of only one polarity. Note that these changes have a higher chance to originate from sequencing or mapping errors because they are not supported by corresponding mutations in the opposite strand.

All datasets contained a deletion at consensus position 202 in the $(+)$-strand with mean expression ratios $v_i^{\text{Deletion}}/v_i^{\text{ref}}$ ($i = 204$ for variants AS1, I, M, and RG1, $i = 203$ for C3, and $i = 205$ for QFA) of 0.09, 0.10, and 0.27 in D_s, D_p, and D_o, respectively. This deletion could disrupt a binding motif for the viroid binding protein 1 (VirP1; see Figure S1(a) and (c)) and result in loss of infectivity (35, 36). The D_o and D_p datasets also contained a significant level of variation at position 32 in TL^+_{upper}. However, because this reflects mainly a $A_{32} \rightarrow U$ change at the end of reads, this variation could be a result of imperfect trimming.

6

Table 1. Parameters of vsRNAs mapping to their respective PSTVd genomes in both polarities.

Data-set	Cultivar	PSTVd	$P_{\text{error}}/10^{-3}$ (+)	$P_{\text{error}}/10^{-3}$ (−)	$P_{\text{error-free}}$ (+)	$P_{\text{error-free}}$ (−)
D_s	Heinz1706	AS1	5.6	4.0	0.13	0.24
		C3	4.4	4.4	0.21	0.21
		C3→AS1	99	71	0.00	0.00
		QFA	196	1170	0.00	0.00
		QFA →KF5M5	4.3	3.5	0.21	0.28
D_p	Rutgers	I	7.7	5.8	0.06	0.12
		I→Var	9.9	9.1	0.06	0.12
		M	24	17	0.00	0.00
		M→Var	10.1	6.5	0.03	0.10
D_o	Heinz1706	RG1	8.6	10.5	0.05	0.02
	Rutgers		9.9	10.9	0.03	0.02
	UC82B		6.3	6.6	0.10	0.09
	Moneymaker		8.0	8.6	0.06	0.05
	Moneymaker	RG1→Var	133	65	0.00	0.00

Cultivar: tomato cultivar used for infection
PSTVd: vsRNAs were determined by mapping the small reads to the sequence S of the respective inoculated PSTVd variant using SEGEMEHL with 90% accuracy; if mutations point to presence of an additional PSTVd variant, the mapping was repeated with this other variant.
$P_{\text{error}} = \left(\sum_{i=1}^{|S|} v_i^{\text{var}}/v_i^{\text{ref}}\right)/|S|$; mean error rate per nucleotide position
$P_{\text{error-free}} = (1-P_{\text{error}})^{|S|} = q^{|S|}$; probability for exact reproduction of the respective viroid sequence

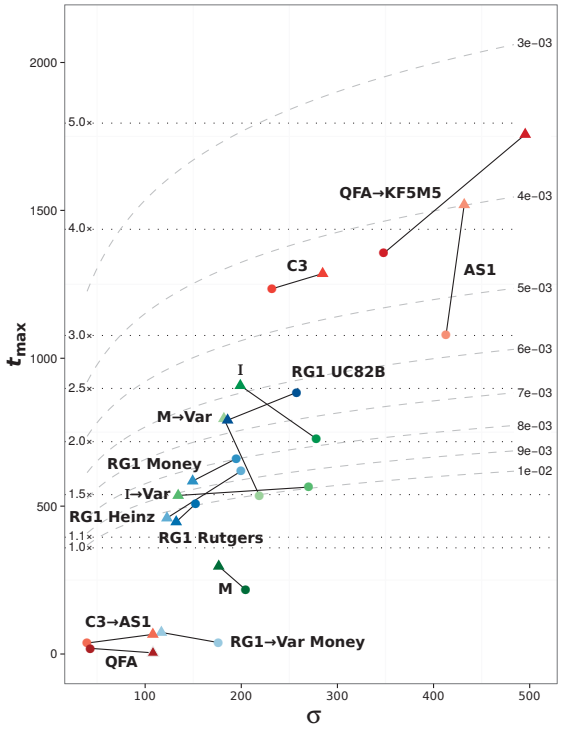

Figure 4. Dependence of the calculated error thresholds ($t_{\max}$; see equation (**3**)) on selective advantage (σ; see equation (**2**)) of the master copy for individual PSTVd variants based on the P_{error} values calculated from analysis of the respective vsRNA populations (see Table 1). Solid lines connect thresholds for (+)- (circles) and (−)-strands (triangles) of the same sample. Dotted horizontal lines indicate the mean PSTVd genome length (359 nt) times the number given on the left end of lines. Dashed curved lines indicate mean error rate per nucleotide P_{error} given on the right end of lines.

We also identified a deletion at consensus position 256 that is located in the loop E motif (see Fig. S1(a)) in all data sets except D_o. Loop E is involved, amongst other processes, in processing of (+) replication intermediates to circles [for review see (7)]. Such a deletion would destroy the tertiary structure of this loop (37), which is consistent with its presence only in (+) strands.

Error rate, error copies, and error threshold

Using the ratio of sites with a variant nucleotide to that with the reference nucleotide, we estimated the probability q for exact reproduction of a single nucleotide in the master copy of a viroid genome during replication (see equation (**1**)). This approach includes at least two inherent limitations: Firstly, we assume that the decay rates of master and error copies, leading to the production of vsRNAs, are equal. Secondly, selection, replication errors, and sequencing errors in the deep sequenced small RNA population are indistinguishable. With these limitations in mind, we calculated the probability q for the originally infecting PSTVd variants as well as any suspected new variants that evolved during infection (see Table 1).

The value of the mean error rate per nucleotide $P_{\text{error}} = 1-q$ was $(7.0\pm2.4)\times10^{-3}$ averaged over variants AS1, C3, QFA→KF5M5, I, M→Var, and RG1. In contrast, for the variant QFA we calculated a much higher error rate, indicating that QFA accumulated mutations leading to the variant KF5M5, which replaced the inoculated QFA as master copy. Similarly, the calculated error rate for variant M would not allow the error-free replication of the originally infecting variant, and this sequence was also overgrown by a variant.

How are these error rates of viroid replication and selection influenced by sequencing errors? To estimate the effect of sequencing errors, we determined the apparent error rates for two tomato microRNAs (see Table S3). These error rates were close to 6×10^{-4} and quite identical for the different datasets. MicroRNAs are replicated by Pol II, but, in contrast to viroids, from a DNA template. Error rates for Pol II transcription of mRNAs are known to be in the range of 1×10^{-5}–1×10^{-6} (38, 39). Consequently, our higher-than-expected error rate for microRNAs is due to the sequencing error. That is, the sequencing error is lower than the error rate of viroid replication and selection by about a factor of 10.

From the estimated error rates of viroid replication we calculated the probability of error-free unit-length copies $P_{\text{error-free}} = (1-P_{\text{error}})^{|S|} = q^{|S|}$ (6). As shown in Table 1, 20% or less of the PSTVd population per replication cycle corresponds to the original variant genome. We also calculated the error threshold based on the determined error rates to estimate the longest possible error-free viroid genome (see Figure 4). Error rates for the original variants M and QFA were clearly too high to support their genome size leading to an error catastrophe (6). In contrast, the error thresholds for the evolved variants M→Var and QFA→KF5M5 were much higher, thereby allowing these sequences to replace the respective original variants. Remarkably, the newly evolved

variant KF5M5 exhibited the highest error threshold, possibly allowing the longest replication intermediate of all PSTVd variants analyzed here.

DISCUSSION

We analyzed three deep-sequencing datasets of small RNAs isolated from PSTVd-infected tomato plants. As expected, we were able to reconstruct the respective genomic sequences after mapping the reads with SEGEMEHL at 100% accuracy to the inoculated PSTVd variants. With a mapping accuracy of 90%, we found additional reads that allowed us to detect sequence variants of the inoculated PSTVd. In the dataset from plants inoculated with QFA, we detected all mutations by which QFA differs from the known mild variant KF5F5. From the small read data alone, however, we cannot be sure that all mutations were present in the same PSTVd genome. In the second dataset the inoculated variant M was present in a comparable amount to a new variant, which differs from variant M by two connected U deletions in the lower P region. In datasets from 'Moneymaker' plants inoculated with RG1, or 'Heinz 1706' inoculated with AS1, C3, and I, respectively, only minor amounts of mutations were present; that is, the inoculated variant remained the master sequence in these four datasets at the sampling time point.

These results appear to fit quite well with quasispecies theory; i. e., that the viroid quasispecies serves as a source of adaptation to new hosts and that changes in selective pressures are able to induce the rapid emergence of new variants within days or weeks (9, 40–45). The fitness landscape of PSTVd seems to contain a quite restricted number of peaks, many of which coincide with known variants.

In addition to replication competent mutants, mutations that are present in only one polarity might also advantageous for viroid evolution. Such mutations may allow fast adaptation to new environments, as shown for example for ribozyme selection (46), and may also increase the spectrum of host targets susceptible to post-transcriptional gene silencing. Thus, a PLMVd variant that contains a specific hairpin insertion sequence and induces a loss of pigmentation known as 'peach calico', expresses a vsRNA that targets the mRNA of chloroplastic heat-shock protein 90 leading to chloroplast malformation (14). Twenty of the 21 nt in this vsRNA basepair with its target. Also, PSTVd variants M and I express a scarce vsRNA from P^{+}_{upper} that pairs with only 14 or 15 nt, respectively, to a tomato CalS11-like mRNA (16). vsRNAs encoded by the mutant swarm rather than the master sequence could allow the viroid to attack additional targets, thereby creating a cellular environment more favorable for viroid replication.

The concept of an error threshold (6) limits the length of a self-replicating molecule to the inverse of the error rate of its replicase. This concept also holds for viroids that utilize a host polymerase for replication. Because the host polymerase, either Pol II for members of *Pospiviroidae* or NEP for members of *Avsunviroidae*, has to act on a foreign RNA rather than its normal DNA template, the error rates could well be higher than those observed with DNA templates. Indeed, the error rate of a member of *Avsunviroidae* was shown to be 2.5×10^{-3} (5), resulting in ~1 mutation per genome replication.

Considering the higher structural constraints on the rod-shaped structure of members of *Pospiviroidae* in comparison to the branched structure of most members of *Avsunviroidae*, Duràn-Vila et al. have proposed that the error rate of *Pospiviroidae* should be ten-fold lower than that of *Avsunviroidae* (47). Our data for PSTVd indicates, however, an upper limit of 5×10^{-3} for the error rate, a value which is not much lower than that for a member of *Avsunviroidae*.

ACKNOWLEDGMENTS

This work was supported by the interdisciplinary graduate school 'Evolutionary Networks: Organisms, Reactions, Molecules' (E-Norm), Prof. em. Dr. Dr. h. c. Detlev Riesner, and a grant from the Alexander von Humboldt Foundation to GS and JM.

Conflict of interest statement. None declared.

References

1. Navarro, B., Gisel, A., Rodio, M., Delgado, S., Flores, R., and Di Serio, F. (2012) Viroids: How to infect a host and cause disease without encoding proteins. *Biochimie,* **94**, 1474–1480.
2. Palukaitis, P. (2014) What has been happening with viroids? *Virus Genes,* **49**, 175–184.
3. Gago-Zachert, S. (2015) Viroids, infectious long non-coding RNAs with autonomous replication. *Virus Res.,* **212**, 12–24.
4. Flores, R., Grubb, D., Elleuch, A., Nohales, M.-Á., Delgado, S., and Gago, S. (2011) Rolling-circle replication of viroids, viroid-like satellite RNAs and hepatitis delta virus: variations on a theme. *RNA Biol.,* **8**, 200–206.
5. Gago, S., Elena, S. F., Flores, R., and Sanjuán, R. (2009) Extremely high mutation rate of a hammerhead viroid. *Science,* **323**, 1308.
6. Eigen, M. (1971) Selforganization of matter and the evolution of biological macromolecules. *Naturwissenschaften,* **58**, 465–523.
7. Flores, R., Serra, P., Minoia, S., Di Serio, F., and Navarro, B. (2012) Viroids: from genotype to phenotype just relying on RNA sequence and structural motifs. *Front. Microbiol.,* **3**, 217.
8. Semancik, J., Szychowski, J., Rakowski, A., and Symons, R. (1993) Isolates of citrus exocortis viroid recovered by host and tissue selection. *J. Gen. Virol.,* **74**, 2427–2436.
9. Matoušek, J., Orctová, L., Ptáček, J., Patzak, J., Dědič, P., Steger, G., and Riesner, D. (2007) Experimental transmission of pospiviroid populations to weed species characteristic of potato and hop fields. *J. Virol.,* **81**, 11891–11899.
10. Elena, S., Gómez, G., and Daròs, J. (2009) Evolutionary constraints to viroid evolution. *Viruses,* **1**, 241–254.
11. Matoušek, J., Stehlík, J., Procházková, J., Orctová, L., Wullenweber, J., Füssy, Z., Kováčik, J., Duraisamy, G. S., Ziegler, A., Schubert, J., and Steger, G. (2012) Biological and molecular analysis of the pathogenic variant C3 of potato spindle tuber viroid (PSTVd) evolved during adaptation to chamomile (*Matricaria chamomilla*). *Biol. Chem.,* **393**, 605–615.
12. Papaefthimiou, I., Hamilton, A., Denti, M., Baulcombe, D., Tsagris, M., and Tabler, M. (2001) Replicating potato spindle tuber viroid RNA is accompanied by short RNA fragments that are characteristic of post-transcriptional gene silencing. *Nucleic Acids Res.,* **29**, 2395–2400.
13. Hammann, C. and Steger, G. (2012) Viroid-specific small RNA in plant disease. *RNA Biol.,* **9**, 809–819.
14. Navarro, B., Gisel, A., Rodio, M. E., Delgado, S., Flores, R., and Di Serio, F. (June, 2012) Small RNAs containing the pathogenic determinant of a chloroplast-replicating viroid guide the degradation of a host mRNA as predicted by RNA silencing. *Plant J.,* **70**, 991–1003.
15. Avina-Padilla, K., Martinez de la Vega, O., Rivera-Bustamante, R., Martinez-Soriano, J., Owens, R., Hammond, R., and Vielle-Calzada, J. (2015) In silico prediction and validation of potential gene targets for pospiviroid-derived small RNAs during tomato infection. *Gene,* **564**, 197–205.

8

16. Adkar-Purushothama, C., Brosseau, C., Giguère, T., Sano, T., Moffett, P., and Perreault, J. (2015) Small RNA derived from the virulence modulating region of the *Potato spindle tuber viroid* silences *callose synthase* genes of tomato plants. *Plant Cell,* **27**, 2178–2194.
17. Adkar-Purushothama, C. R., Perreault, J.-P., and Sano, T. (2015) Analysis of small RNA production patterns among the two potato spindle tuber viroid variants in tomato plants. *Genom. Data,* **25**, 65–66.
18. Owens, R. A., Tech, K. B., Shao, J. Y., Sano, T., and Baker, C. J. (2012) Global analysis of tomato gene expression during Potato spindle tuber viroid infection reveals a complex array of changes affecting hormone signaling. *Mol. Plant Micr. Int.,* **25**, 582–598.
19. Li, R., Gao, S., Hernandez, A., Wechter, W., Fei, Z., and Ling, K. (2012) Deep sequencing of small RNAs in tomato for virus and viroid identification and strain differentiation. *PLoS ONE,* **7**, e37127.
20. Zhang, Z., Qi, S., Tang, N., Zhang, X., Chen, S., Zhu, P., Ma, L., Cheng, J., Xu, Y., Lu, M., Wang, H., Ding, S., Li, S., and Wu, Q. (2014) Discovery of replicating circular RNAs by RNA-seq and computational algorithms. *PLoS Pathog.,* **10**, e1004553.
21. Seguin, J., Rajeswaran, R., Malpica-LÃşpez, N., Martin, R., Kasschau, K., Dolja, V., Otten, P., Farinelli, L., and Pooggin, M. (2014) De novo reconstruction of consensus master genomes of plant RNA and DNA viruses from siRNAs. *PLoS ONE,* **9**, e88513.
22. Tsibris, A. M. N., Korber, B., Arnaout, R., Russ, C., Lo, C. C., Leitner, T., Gaschen, B., Theiler, J., Paredes, R., Su, Z., Hughes, M. D., Gulick, R. M., Greaves, W., Coakley, E., Flexner, C., Nusbaum, C., and Kuritzkes, D. R. (2009) Quantitative deep sequencing reveals dynamic HIV-1 escape and large population shifts during CCR5 antagonist therapy in vivo. *PLoS One,* **4**, 1–12.
23. Rozera, G., Abbate, I., Ciccozzi, M., Presti, A. L., Bruselles, A., Vlassi, C., D'Offizi, G., Narciso, P., Giombini, E., Bartolini, B., Ippolito, G., and Capobianchi, M. R. (2012) Ultra-deep sequencing reveals hidden HIV-1 minority lineages and shifts of viral population between the main cellular reservoirs of the infection after therapy interruption. *J. Med. Virol.,* **84**, 839–844.
24. Timm, C., Akpinar, F., and Yin, J. (2013) Quantitative characterization of defective virus emergence by deep sequencing. *J. Virol.,* **88**, 2623–2632.
25. Astrovskaya, I., Tork, B., Mangul, S., Westbrooks, K., Măndoiu, I., Balfe, P., and Zelikovsky, A. (2011) Inferring viral quasispecies spectra from 454 pyrosequencing reads. *BMC Bioinformatics,* **12**, S1.
26. Andino, R. and Domingo, E. (2015) Viral quasispecies. *Virology,* **479-480**, 46–51.
27. Biebricher, C. and Eigen, M. (2005) The error threshold. *Virus Res.,* **107**, 117–127.
28. Schmieder, R. and Edwards, R. (2011) Quality control and preprocessing of metagenomic datasets. *Bioinformatics,* **27**, 863–864.
29. Bolger, A. M., Lohse, M., and Usadel, B. (2014) Trimmomatic: a flexible trimmer for Illumina sequence data. *Bioinformatics,* **30**, 2114–2120.
30. Hoffmann, S., Otto, C., Kurtz, S., Sharma, C. M., Khaitovich, P., Vogel, J., Stadler, P. F., and Hackermüller, J. (2009) Fast mapping of short sequences with mismatches, insertions and deletions using index structures. *PLoS Comput. Biol.,* **5**, e1000502.
31. Hoffmann, S., Otto, C., Doose, G., Tanzer, A., Langenberger, D., Christ, S., Kunz, M., Holdt, L., Teupser, D., Hackermüller, J., and Stadler, P. F. (2014) A multi-split mapping algorithm for circular RNA, splicing, trans-splicing, and fusion detection. *Genome Biol.,* **15**, R34.
32. Domingo, E., Biebricher, C., Eigen, M., and Holland, J., (eds.) (2001) Quasispecies and RNA virus evolution: principles and consequences, Landes Bioscience, Austin.
33. Li, H., Handsaker, B., Wysoker, A., Fennell, T., Ruan, J., Homer, N., Marth, G., Abecasis, G., and Durbin, R. (2009) The sequence alignment/map format and SAMtools. *Bioinformatics,* **25**, 2078–2079.
34. Rocheleau, L. and Pelchat, M. (2006) The Subviral RNA Database: a toolbox for viroids, the hepatitis delta virus and satellite RNAs research. *BMC Microbiol.,* **6**, 24.
35. Gozmanova, M., Denti, M., Minkov, I., Tsagris, M., and Tabler, M. (2003) Characterization of the RNA motif responsible for the specific interaction of potato spindle tuber viroid RNA (PSTVd) and the tomato protein Virp1. *Nucleic Acids Res.,* **31**, 5534–5543.
36. Kalantidis, K., Denti, M., Tzortzakaki, S., Marinou, E., Tabler, M., and Tsagris, M. (2007) Virp1 is a host protein with a major role in *Potato spindle tuber viroid* infection in *Nicotiana* plants. *J. Virol.,* **81**, 12872–12880.
37. Zhong, X., Leontis, N., Qian, S., Itaya, A., Qi, Y., Boris-Lawrie, K., and Ding, B. (2006) Tertiary structural and functional analyses of a viroid RNA motif by isostericity matrix and mutagenesis reveal its essential role in replication. *J. Virol.,* **80**, 8566–8581.
38. Lynch, M. (2010) Evolution of the mutation rate. *Trends Genet.,* **26**, 345–352.
39. Carey, L. (2015) RNA polymerase errors cause splicing defects and can be regulated by differential expression of RNA polymerase subunits. *Elife,* **4**, e09945.
40. Qi, Y. and Ding, B. (2003) Differential subnuclear localization of RNA strands of opposite polarity derived from an autonomously replicating viroid. *Plant Cell,* **15**, 2566–2577.
41. Góra-Sochacka, A., Kierzek, A., Candresse, T., and Zagórski, W. (1997) The genetic stability of potato spindle tuber viroid (PSTVd) molecular variants. *RNA,* **3**, 68–74.
42. Góra-Sochacka, A., Candresse, T., and Zagórski, W. (2001) Genetic variability of potato spindle tuber viroid RNA replicon. *Acta Biochim. Pol.,* **48**, 467–476.
43. Matoušek, J., Orctová, L., Steger, G., Škopek, J., Moors, M., Dědič, P., and Riesner, D. (2004) Analysis of thermal stress-mediated PSTVd variation and biolistic inoculation of progeny of viroid "thermomutants" to tomato and *Brassica* species. *Virology,* **323**, 67–78.
44. Matoušek, J., Orctová, L., Steger, G., and Riesner, D. (2004) Biolistic inoculation of plants with viroid nucleic acids. *J. Virol. Meth.,* **122**, 153–164.
45. Matoušek, J., Kozlova, P., Orctova, L., Schmitz, A., Pešina, K., Bannach, O., Diermann, N., Steger, G., and Riesner, D. (2007) Accumulation of viroid-specific small RNAs and increase in nucleolytic activities linked to viroid-caused pathogenesis. *Biol. Chem.,* **388**, 1–13.
46. Ameta, S., Winz, M.-L., Previti, C., and Jäschke, A. (2013) Next-generation sequencing reveals how RNA catalysts evolve from random space. *Nucleic Acids Res.,* **42**, 1303–1310.
47. Duran-Vila, N., Elena, S., Daròs, J.-A., and Flores, R. (2008) Structure and evolution of viroids. In Domingo, E., Parrish, C., and Holland, J., (eds.), *Origin and Evolution of Viruses*, pp. 43–64 Academic Press London 2nd edition.

Supplement material for "Viroid quasispecies revealed by deep sequencing"

Rajen J. J. Piernikarczyk [1], Robert A. Owens [2], Jaroslav Matoušek [3], and Gerhard Steger [1*]

[1]**Institut für Physikalische Biologie, Heinrich-Heine-Universität Düsseldorf, 40204 Düsseldorf, Germany**
[2]**United States Department of Agriculture, Agricultural Research Service, Molecular Plant Pathology Laboratory, Beltsville, MD 20705, USA**
[3]**Biology Centre, CAS, v. v. i., Institute of Plant Molecular Biology, Branišovská 31, 37005 České Budějovice, Czech Republic**

[*]To whom correspondence should be addressed. Tel: +49 211 8114597; Fax: +49 211 8115167; Email: steger@biophys.uni-duesseldorf.de

10

Table S1. Parameters used in different programs

(a) PRINSEQ

Variable	Value
-min_len	18
-max_len	36
-ns_max_n	0
-lc_method	entropy
-lc_threshold	60
-trim_tail_right	2
-trim_tail_left	6

(b) TRIMMOMATIC

Variable	Value
SE	True
-phred33	True
ILLUMINACLIP	5:5:5
LEADING	3
SLIDINGWINDOW	4:30
MINLEN	18
AVGQUAL	30

(c) SEGEMEHL

Variable	Value
H	1
m	100
A	80, 85, 90, 95, 100

Table S2. Number of reads mapping to PSTVd variants at 90% and 100% accuracy.

Dataset	Cultivar	PSTVd	Count (90%) / 10^5	Count (100%) / 10^5	Ratio	$\overline{\text{Ratio}}$
D_s	Heinz1706	AS1	7.57	7.25	1.04	1.05
		C3	9.46	8.93	1.06	
		QFA→KF5M5	1.88	1.80	1.04	
		QFA	1.77	1.46	1.22	
D_p	Rutgers	I	5.74	5.31	1.08	1.10
		M→Var	1.29	1.16	1.11	
		M	1.29	1.16	1.11	
D_o	Heinz1706	RG1	7.01	6.19	1.13	1.14
	Moneymaker		4.27	3.76	1.14	
	Rutgers		5.10	4.34	1.18	
	UC82B		3.26	2.97	1.10	

Count: number of reads mapping to the respective PSTVd variant at 90 and 100% accuracy, respectively.
Ratio: count (90%)/count (100%)
$\overline{\text{Ratio}}$: mean ratio values; the mean value of the nine ratios is 1.10 ± 0.03 .

Table S3. Error rate of two highly abundant *S. lycopersicum* miRNAs mapped with 90% accuracy. Only positions 3–17 were considered for calculation of P_{error} due to increased sequencing errors in the excluded positions.

Dataset	Condition	Variant	Cultivar	P_{error} / 10^{-4} sly-miR159	sly-miR162	
D_s	Healthy			7.00	1.00	4
	Infected	AS1	Heinz1706	14.8	4.84	7.94 ± 4.23
		C3		9.39	4.02	
		QFA		10.0	4.59	
D_p	Healthy			6.00	5.00	5.5
	Infected	I	Rutgers	6.14	3.97	4.69 ± 1.30
		M		5.36	3.27	
D_o	Healthy		Heinz1706	10.0	4.00	6.75 ± 2.55
			Moneymaker	10.0	4.00	
			Rutgers	8.00	5.00	
			UC82B	8.00	5.00	
	Infected	RG1	Heinz1706	6.81	4.99	6.14 ± 1.97
			Moneymaker	8.33	2.94	
			Rutgers	8.05	4.58	
			UC82B	8.04	5.41	

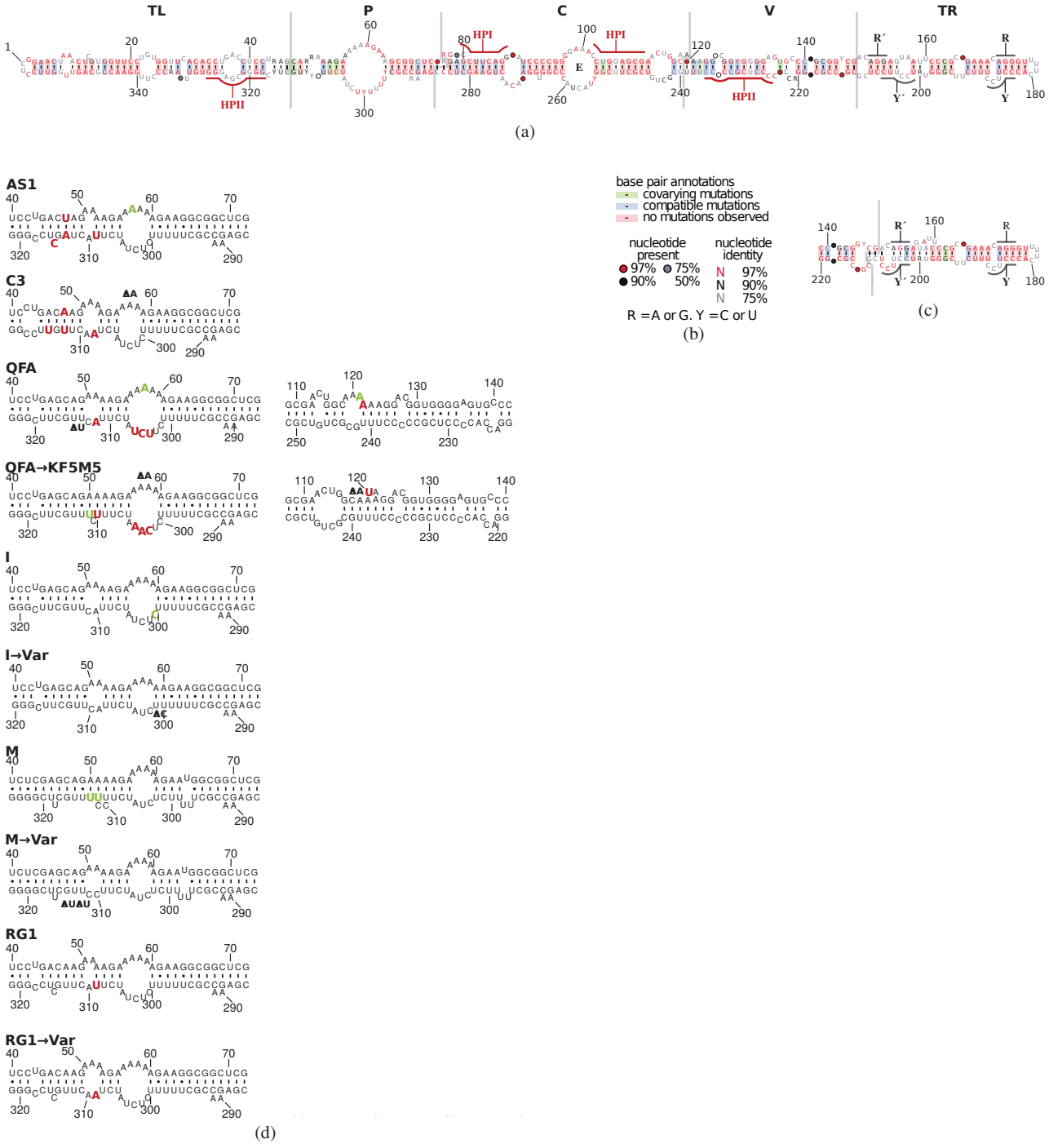

Figure S1. Structure of (+)-stranded PSTVd variants. (a) The consensus sequence and structure were predicted for an alignment of 234 variants with MAFFT/G-INS-1 (1) optimized in CONSTRUCT (2) at 37°C, excluding lonely base pairs, and drawn with R2R (3). Borders of the five domains (4) are marked by gray lines (TL, terminal left; P, pathogenicity-related; C, central; V, variable; TR, terminal right). Basepairs on green and blue background are supported by covarying and compatible mutations, respectively; no mutations are observed for basepairs on red background; for further nucleotide annotations see (b). Nucleotides forming the extra-stable hairpins I (HPI) and II (HPII) in thermodynamically metastable structures are outlined. The two RY motifs in the TR critical for binding of the viroid RNA-binding protein VirP1 are outlined and marked by R, R' and Y, Y', respectively (5). (c) This thermodynamically suboptimal structure of the TR domain emphasizes the similarity in sequence and structure of the two VirP1 binding sites. (d) Selected structural regions of PSTVd variants. Sequence differences between AS1 and C3, QFA and QFA→KF5M5, I and I→var, M and M→var, and RG1 and RG1→var, respectively, are marked in red (mutation), green (insertion), and by ΔN (deletion).

12

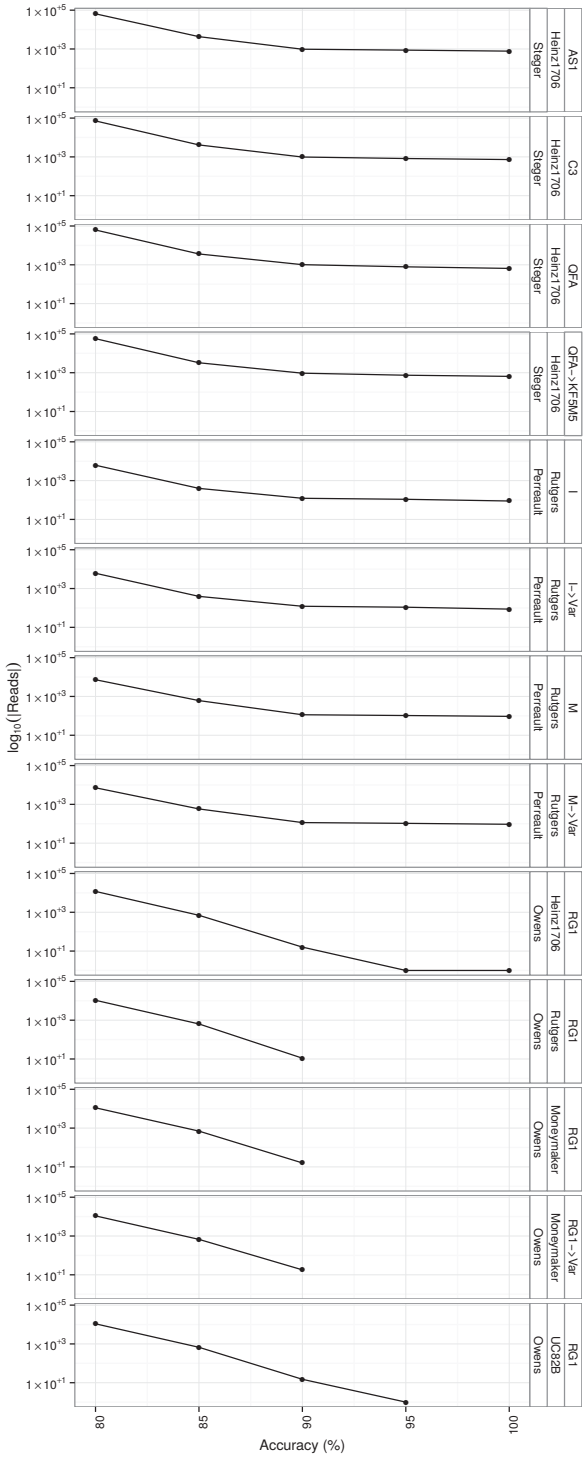

Figure S2. Mapping of small reads from mock-inoculated plants to the PSTVd variants at different accuracies.

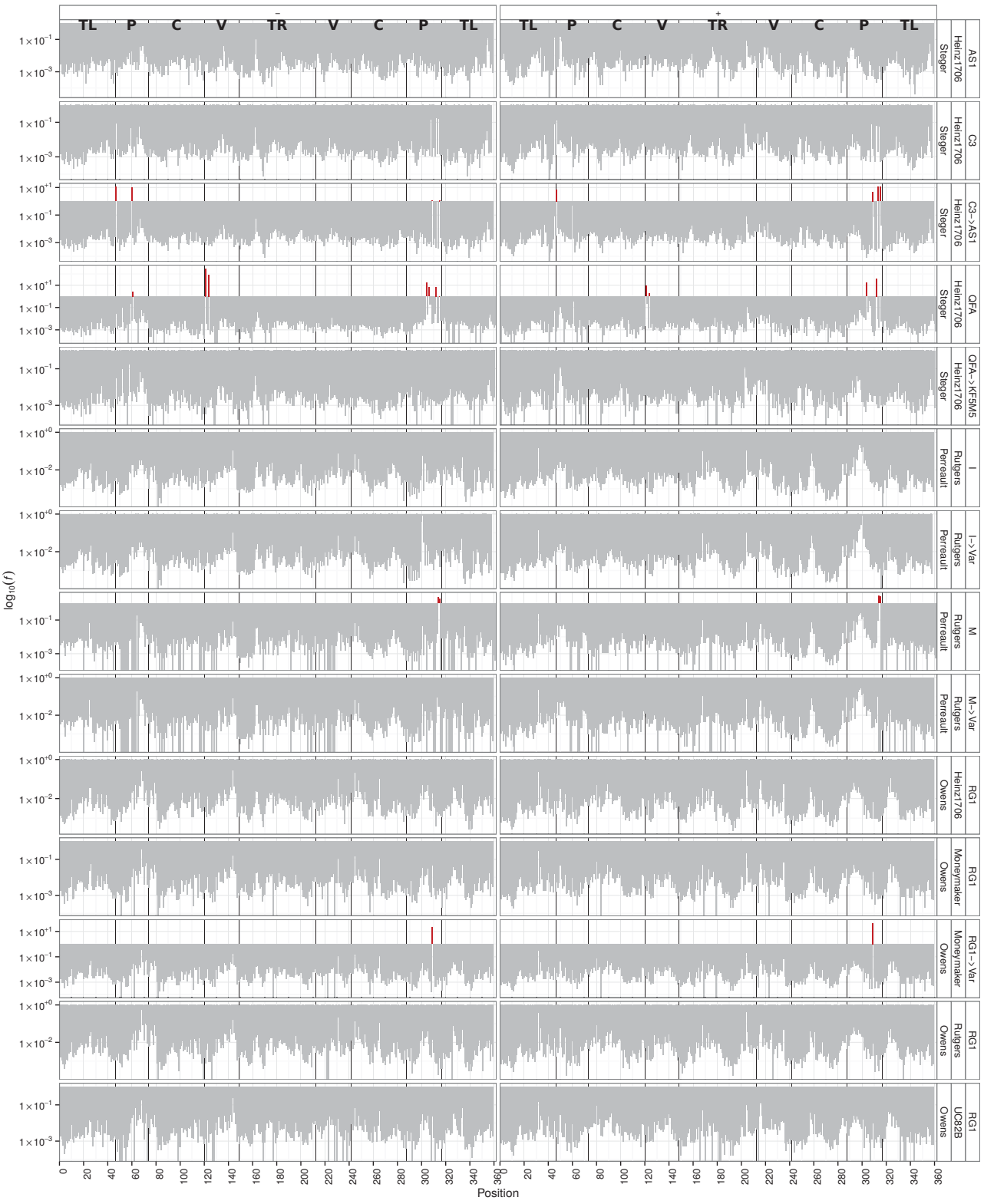

Figure S3. Ratio of read frequencies with a variant nucleotide relative to those with the reference nucleotide. Bars in red mark mutations that occur more often than the reference nucleotide, others are shown in gray. The y axis is in a logarithmic scale. Left and right columns show mappings to $(-)$- and $(+)$-stranded viroid sequences.

14

References

1. Katoh, K., Kuma, K., Miyata, T., and Toh, H. (2005) Improvement in the accuracy of multiple sequence alignment program MAFFT. *Genome Inform. Ser.,* **16**, 22–33.
2. Wilm, A., Linnenbrink, K., and Steger, G. (2008) ConStruct: Improved construction of RNA consensus structures. *BMC Bioinformatics,* **9**, 219.
3. Weinberg, Z. and Breaker, R. (2011) R2R—software to speed the depiction of aesthetic consensus RNA secondary structures. *BMC Bioinformatics,* **12**, 3.
4. Keese, P. and Symons, R. H. (1985) Domains in viroids: evidence of intermolecular RNA rearrangements and their contribution to viroid evolution. *Proc. Natl. Acad. Sci. U. S. A.,* **82**, 4582–4586.
5. Gozmanova, M., Denti, M., Minkov, I., Tsagris, M., and Tabler, M. (2003) Characterization of the RNA motif responsible for the specific interaction of potato spindle tuber viroid RNA (PSTVd) and the tomato protein Virp1. *Nucleic Acids Res.,* **31**, 5534–5543.

Eur J Plant Pathol (2014) 138:93–101
DOI 10.1007/s10658-013-0304-6

Characterization of *Potato spindle tuber viroid* (PSTVd) incidence and new variants from ornamentals

Jaroslav Matoušek · Rajen J. J. Piernikarczyk · Petr Dědič · Josef Mertelík · Kateřina Uhlířová · Ganesh S. Duraisamy · Lidmila Orctová · Kateřina Kloudová · Jiří Ptáček · Gerhard Steger

Accepted: 23 September 2013 / Published online: 19 October 2013

Abstract We analyzed the spreading and persistence of PSTVd variants in several ornamentals in the territory of the Czech Republic. The pool of PSTVd variants detected in *Solanum jasminoides*, *S. muricatum*, *Datura* sp. and *Brugmansia* sp. was biolistically transferred to *Matricaria chamomilla*, *Argyranthemum frutescens* and *Diascia* sp., species which we found as sensitive hosts for PSTVd from ornamentals. The PSTVd pool showed sequence changes and increased variation after its transfer to potato, suggesting a wide adaptation potential of PSTVd in this crop. Potato exhibited genotype-dependent leaf and spindle tuber symptoms, when inoculated with the sap from *S. jasminoides* infected with the predominant and sequence-stable PSTVd-S1.

J. Matoušek · K. Uhlířová · G. S. Duraisamy · L. Orctová
BC ASCR v.v.i., Institute of Plant Molecular Biology, Branišovská 31, 37005 České Budějovice, Czech Republic

P. Dědič · J. Ptáček
Potato Research Institute, Havlíčkův Brod, Czech Republic

J. Mertelík · K. Kloudová
Silva Tarouca Research Institute for Landscape and Ornamental Gardening, Průhonice, Czech Republic

R. J. J. Piernikarczyk · G. Steger (✉)
Institute of Physical Biology, Heinrich-Heine-Universität Düsseldorf, 40204 Düsseldorf, Germany
e-mail: steger@biophys.uni-duesseldorf.de

Keywords Viroid pathogenicity · Real-time PCR · Biolistic inoculation of plants · *Solanum jasminoides* · *Solanum tuberosum* · *Solanum lycopersicum*

Introduction

Potato spindle tuber viroid (PSTVd) is the type member of the family *Pospiviroidae* for which 29 species have been described (see the "Subviral RNA Database"; Rocheleau and Pelchat 2006). *Pospiviroidae* cause serious plant diseases in many crops of considerable economic importance (for reviews see e. g. Hadidi et al. 2003; Tabler and Tsagris 2004; Flores et al. 2005). Characteristics of PSTVd are a thermodynamically optimal, rod-like secondary structure (Steger and Riesner 2003), replication in an asymmetric rolling-circle mechanism (for review see e. g. Schmitz and Steger 2007) and cellular localization primarily in the nucleolus (Schumacher et al. 1983; Harders et al. 1989; Qi and Ding 2003). Because viroids are non-coding RNAs, their propagation, including reproduction and transport, is fully dependent on specific structural interactions with host factors. In general, viroids and in particular PSTVd, are endowed with fast adaptability and plasticity as rapidly evolving biological systems (Diener 1995; Gago et al. 2009). PSTVd forms quasispecies (Eigen 1993; Codoñer et al. 2006) that might serve as a source of adaptations to new hosts and life-cycle conditions, and their exposure to selective pressures can induce the

rapid emergence of new dominant variants within days or weeks (e. g. Qu et al. 1993; Góra-Sochacka et al. 1997, 2001; Matoušek et al. 2004a, b, 2007b, 2012).

Some newly adapted PSTVd variants were determined to be extremely pathogenic and caused sublethal developmental distortions in sensitive genotypes of cultured plants; examples are PSTVd-AS1 in tomato cv. Rutgers (Matoušek et al. 2007a) or the recently described PSTVd-C3 in cultured chamomile cv. Novbona (Matoušek et al. 2012). Clear examples of obvious danger represented by PSTVd were described recently by Soliman et al. (2012) documenting an invasion of PSTVd into the European Union. The predominant PSTVd-S1 variant (Verhoeven and Roenhorst 2010)—originally reported in the "symptomless" ornamental plant *Solanum jasminoides* (Verhoeven et al. 2008, GenBank accession code (AC) EF192393)—belongs to a viroid population that causes disease symptoms in important crops like tomato. This caused the European Commission to make a decision (2007/410/EC) on measures against the introduction and spread of PSTVd, as a quarantine pathogen listed in the phytosanitary Directive 2000/29/EC. The Commission decision obliges the EU member states to conduct official surveys and testing for PSTVd (e. g. Lemmetty et al. 2011). Recent analyses demonstrated spreading of a PSTVd population in ornamentals that included isolates from species like *Brugmansia* sp., *S. jasminoides*, *S. muricatum*, *S. pseudocapsicum*, *S. rantonnetii*, *Datura* sp., *Chrysanthemum* sp., *Cestrum* sp., *Dahlia* sp., and *Petunia* sp. (Di Serio 2007; Lemmetty et al. 2011; Mertelík et al. 2010; Tsushima et al. 2011; Verhoeven et al. 2010b; Luigi et al. 2011). The first report of PSTVd in *S. jasminoides*, *Brugmansia* spp., *S. muricatum* and *Petunia* sp. in the Czech Republic was published by Mertelík et al. (2010). Despite these studies on PSTVd incidence, outbreaks and infectivity, more detailed comparisons between pathogenic PSTVd variants from ornamentals with well-characterized PSTVd variants are missing.

In our previous work we characterized the pathogenic variant PSTVd-C3 that evolved within a single passage in cultured chamomile. In this work we analyzed variation of PSTVd variants in selected ornamentals and confirmed the dominant incidence and high fitness of PSTVd-S1. PSTVd-S1 also infects and causes severe symptoms in tomato and potato including induction of spindle tubers.

Material and methods

Plant material and cultivation conditions

If not otherwise stated, ornamental plants, *S. jasminoides*, *S. rantonnetii*, *S. muricatum*, *Datura* sp., *Brugmansia* sp. and *Petunia* x *hybrida* were grown either under glasshouse conditions or in private gardens. Samples from ornamental plants were collected in collaboration with State Phytosanitary Administration in various localities including plant growers, markets, private gardens, public greenery etc. all over the Czech Republic. Surveys were carried out in 2007–2011 and samples were collected from 56 *S. jasminoides*, 69 *Brugmansia* sp., six *Datura* sp., nine *S. muricatum* and six *S. rantonnetii* plants. *Diascia* sp. and *A. frutescens* plants were maintained after the biolistic inoculation in climate boxes at a temperature of 25 °C during the 12 h light and 20 °C during the 12 h dark period. Potato plants *S. tuberosum* cvs Vendula, Vlasta and Verne were propagated in greenhouse under natural light conditions and temperatures ranging from 20 to 30 °C. Potatoes infected with a PSTVd population from *S. jasminoides* were maintained in tissue culture conditions at 20 °C and 16/8 h light period. Tomato (*S. lycopersicum*) cv. Rutgers, cultured diploid chamomile (*M. chamomilla*, *Ch. recutita*) cv. Novbona (kindly provided by Prof. Miroslav Repčák, Department of Botany, P. J. Šafárik University in Košice, Slovakia) were used for inoculation. These plants were maintained in climate boxes at a temperature of 25±3 °C and grown under natural light with supplementary illumination (90 μmol m^{-2} s^{-1}) to keep a 16 h-day period.

Preparation of viroid inocula and plant inoculation by biolistic method

For plant inoculation with PSTVd the following viroids were used: S1 (AC: EF192393), AS1 (AC: AY518939), and QFA (AC: U23059). In addition to individual PSTVd variants, we prepared a complex population of PSTVd cDNAs from ornamentals: cDNAs were amplified from libraries established for isolates from *S. jasminoides*, *S. muricatum*, *Datura* sp. and *Brugmansia* sp. and mixed in equimolar quantities. *Sty*I-cleaved full-length cDNA fragments of PSTVd were prepared as inocula (Matoušek et al. 2004a). PSTVd fragments were immobilized on gold

microcarriers (1 μm) using a modified calcium-mediated precipitation protocol (Matoušek et al. 2004b). The Helios Gene Gun System from Bio-Rad (USA) was used for biolistic inoculation. Each plant was inoculated twice, each time with 200 ng DNA and a pressure of 120 psi at a distance of approximately 1 cm from the Gene Gun spacer. Plants were usually inoculated at the stage of 3–4 young expanded leaves. Attached leaves were inoculated while supported with thick cardboard paper. After inoculation, plants were immediately transferred into polyethylene bags to prevent drying-out of the wounded leaf area. Treated plants were further conditioned by shading them for 24 h and afterwards by cultivation in perforated bags for the next 2 days in the climate boxes under standard conditions as described above. In some experiments a carborundum method was used for plant inoculation: infected leaves were ground with a mortar and pestle, plants inoculated by sap, immediately rinsed by water and further kept in the greenhouse.

RNA isolation, PSTVd cloning and analysis of cDNA libraries by DNA heteroduplexes

For the RT-PCR total RNA was isolated from 100 mg of leaf tissue using CONCERT™ (Plant RNA Purification Reagent, Invitrogen, Darmstadt, Germany) followed by RNA purification and DNA cleavage on columns (RNeasy Plant Total RNA kit, Qiagen, Hilden, Germany). RT-PCR amplification for viroid detection and cloning was performed using the Titan One Tube RT-PCR (Roche, Mannheim, Germany) including a high fidelity *Pwo* polymerase (Roche). Primers PSTVds I (5′-aC_{337}CAAGGGCTAAACACCCTCGC-3′) and II (5′-aC_{343}CTTGGAACCGCAGTTGGTTC-3′) were used for full-length PSTVd amplification. The non-specific adenine in each primer (indicated by a small letter "a") was added to facilitate cleavage of cDNA fragments; the restriction sites in the primers are underlined; positions are numbered corresponding to the respective viroid sequence. RT was for 30 min at 52 °C, and after 2 min denaturation at 94 °C, the PCR was started with 36 cycles of 30 s at 94 °C, 30 s at 58 °C and 60 s at 68 °C. Full PSTVd copies were inserted into the vector pCR-Script SK(+) (Stratagene, La Jolla, CA, USA). A small cDNA library was established containing 100 positive bacterial clones verified by molecular hybridization with ^{32}PdCTP-labelled full-length viroid cDNA. Selected clones were sequenced.

To analyze cDNA variability by heteroduplexes (mismatch positions) cleavage, cDNA amplified from individual libraries or selected cDNAs, purified by Qiagen PCR purification protocol, were heated and allowed to form heteroduplexes in 1 mM Na cacodylate hybridization buffer (pH 6.8) containing 100 mM NaCl and 1 mM EDTA as previously described (Matoušek et al. 2004b). Subsequently, samples were cleaved with Surveyor nuclease (SURVEYOR™ Mutation Detection kit, Transgenomic, USA) according to manufacturer's instruction and analyzed in 2 % agarose gels for the cleavage products.

Sequence data analysis was carried out with the computer program DNASIS version 2.6 (Hitachi).

Results

PSTVd variation detected in ornamentals and experimental plant hosts

The first report of PSTVd in ornamentals (Mertelík et al. 2010) confirmed the identity of PSTVd-S1 in isolates of *S. jasminoides*. In order to quantify the PSTVd incidence and variation in ornamentals we analyzed samples from *S. jasminoides*, *S. rantonnetii*, *S. muricatum*, *Datura* sp., and *Brugmansia* sp. collected in 2007–2009. From 74 analyzed common localities, positive evidences were detected in 22, predominantly in *S. jasminoides*. From *S. jasminoides* 70 % of collected samples were positive, while only occasional infections were detected in other species; two isolates were collected from *Brugmansia* sp. and one from *S. muricatum* and *Datura* sp., respectively. No PSTVd infection was detectable in *S. rantonnetii*. Additionally, 60 annual ornamentals were tested for PSTVd: some limited positive signals were detected using reverse transcription real-time PCR (RT-PCR) in the species *Argyranthemum frutescens* and *Diascia* sp., suggesting occasional PSTVd infection of these plants. These infections, however, were not recurrently repeated. In contrast, recurrence was found in selected localities in 2011, especially in *S. jasminoides* and *Brugmansia* sp., suggesting long persistence of PSTVd in these ornamentals. Our results indicate a dominant incidence of PSTVd from *S. jasminoides* in the territory of Czech Republic that presumably spread from a common source of imported materials as an important reservoir of PSTVd infection. RT-PCR was performed on

selected samples from *S. jasminoides*, *S. muricatum*, *Datura*, *Brugmansia*, and the experimental host *Diascia* sp., and PSTVd cDNA libraries were prepared; we sequenced 12 clones from each library (Figs. 1 and 2). Sequence comparisons within this PSTVd pool from ornamentals and *Diascia* sp. revealed five new sequences with in total 23 point mutations including nucleotide changes, insertions and deletions that differed from the highly pathogenic PSTVd-AS1 variant (Matoušek et al. 2007a). The analyzed PSTVd isolates from ornamentals branched together with mild and intermediate PSTVd variants from tomato and potato, while a group of strongly pathogenic variants including PSTVd-AS1 formed a unique branch, as shown in Fig. 2.

To verify *A. frutescens* and *Diascia* sp. as potential hosts, we analyzed the infectivity of an experimental pool of PSTVd sequences isolated from *S. jasminoides*, *S. muricatum*, *Datura* sp. and *Brugmansia* sp. (see Materials and Methods) that was biolistically transferred to several experimental hosts including *Diascia* sp., *A. frutescens*, and *Matricaria chamomilla*, a newly described PSTVd host (Matoušek et al. 2012). PSTVd accumulated to a high level in certain (~33 %) viroid-inoculated *Diascia* samples (compare lanes 1, 4, and 7 in Fig. 3a). From *Diascia* sample 2, which showed the highest PSTVd level (see Fig. 3a, lane 4), a PSTVd cDNA library was established and screened; three dominant sequences were discovered (see individual nucleotide differences from PSTVd-S1 in Fig. 1): the PSTVd sequence Diascia1 was identical to the sequence Anthemis2 described earlier by Matoušek et al. (2007b); two other sequences from *Diascia* differed by several point mutations from Diascia1 including a C insertion in the upper central conserved region (UCCR). Samples of the experimental host *A. frutescens* accumulated much lower levels of PSTVd (Fig. 3a); the cDNA was not cloned. Our results suggest that both ornamentals are susceptible to infections with the described PSTVd pool.

Subsequently, the population of viroid variants from ornamental plants was biolistically inoculated also to potato to assay for possible changes in this important crop, for which the presence of a PSTVd reservoir in ornamentals potentially constitutes a threat, similar to the PSTVd reservoir formed by weed plant species (Matoušek et al. 2007b). The extent of PSTVd variability after biolistic inoculation of potato plants with infectious PSTVd cDNA was roughly assayed using heteroduplex analysis by means of Surveyor nuclease-mediated cleavage of mismatches within cDNA hybrids. The presence of cleavage products was detected by gel electrophoresis and staining (see Fig. 4). Changes were clearly detectable in the PSTVd population spectrum after only a short 40-day-propagation period in this species (Fig. 4a). On the one hand, this variation suggests a fast PSTVd adaptation towards potato; on the other hand, we found by sequencing that the majority of clones propagated for a longer period in potato were identical to the PSTVd-S1 sequence (data not shown). Consequently, this PSTVd sequence variant was analyzed in this work for variability and comparative pathogenicity. PSTVd-S1, originally isolated as a mixture of PSTVd-S1 isolates from various selections of *S. jasminoides*, was amplified from corresponding cDNA libraries and biolistically inoculated in tomato cv. Rutgers. We detected only minor sequence variations 18 dpi (see Fig. 4b, sample 2), which decreased after a more prolonged period of 40 dpi. This suggests that PSTVd-S1 has a high fitness and is well adapted to tomato. Similar results were found for long-time maintained PSTVd-S1 in potato after its subsequent transfer to tomato; also in this case, no variation was detectable (see Fig. 4c). In conclusion, the PSTVd-S1 variant seems to be well adapted to potato and tomato.

Comparative analyses of pathogenicity caused by PSTVd from ornamentals

According to reports describing PSTVd transfer from ornamentals to tomatoes (Verhoeven and Roenhorst 2010; Verhoeven et al. 2010b), these viroids induce to some extent the characteristic symptoms in tomato, while some ornamentals like *S. jasminoides* remain symptomless. In this study we determined that a PSTVd pool from ornamentals led to pathogenesis and, on later stages, to death of *Diascia* and of some *A. frutescens* plants. The same pool was strongly pathogenic to cultured chamomile (not shown), which was previously characterized as a very sensitive host to PSTVd-C3 and -AS1 (Matoušek et al. 2012). Pathogenic symptoms were also detected after biolistic transfer of this viroid pool to potato and tomato (not shown). According to our analyses, PSTVd from *S. jasminoides*, i. e. PSTVd-S1, inoculated with sap using the carborundum method, elicited the characteristic symptoms like spindle tubers on some potato cultivars, especially cv. Vendula. Two other cultivars, cv. Vlasta and Verne, remained

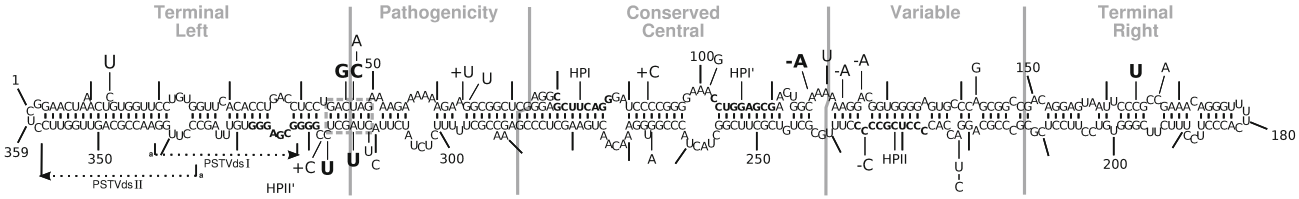

Fig. 1 Structural sequence comparison of PSTVd variants S1 and AS1. The shown consensus structure is based on 156 unique, full-length PSTVd variants from the "Subviral RNA Database" (Rocheleau and Pelchat 2006) and the newly found variants; the structure was predicted by ConStruct (Wilm et al. 2008) and drawn by R2R (Weinberg and Breaker 2011). Nucleotide changes in PSTVd-S1 in comparison to AS1 are shown by bold letters. Further changes found in the group of PSTVd-S1-related sequences isolated from *S. jasminoides*, *S. muricatum*, *Datura* sp., *Brugmansia* sp. and *Diascia* sp. are given by normal letters. The description of PSTVd domains is according to Keese and Symons (1985) in gray colour. The helix at the pathogenicity domain/terminal left domain boundary that represents significant structural differences between PSTVd-AS1, PSTVd-S1 and other isolates is framed. Regions forming hairpins (HP) I and II in metastable structures are marked (Steger and Riesner 2003). Primers used for cloning of mutants (PSTVdsI and PSTVdsII) are marked by dotted arrows

symptomless during primary infection although PSTVd was clearly detectable in their leaves. In contrast, we noticed the pathogenesis—the typical tuber symptoms—induced by viroid isolates from potato in all three tested potato genotypes already during primary infection. In some experiments, the symptoms mediated by PSTVd-S1 were only visible in plants grown from tubers (secondary infection; Fig. 5a). Besides the characteristic spindle shape of tubers, we observed clefts in tubers and specific changes in the shape of leaf blades

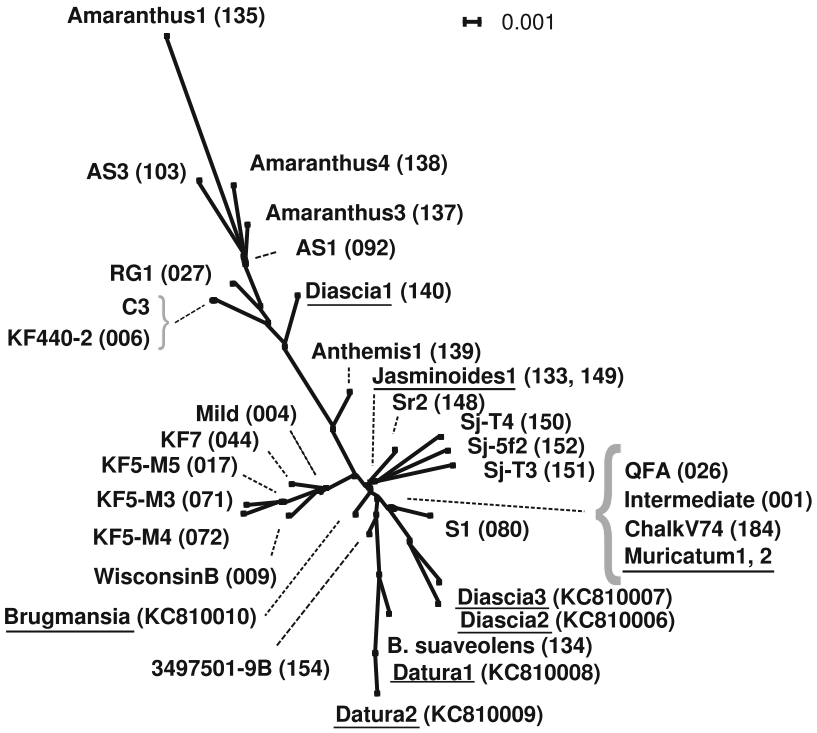

Fig. 2 Tree of similarities between PSTVd variants isolated from ornamentals (this work) and others including PSTVd-AS1 (Matoušek et al. 2007a) from tomato, PSTVd-C3 from chamomile (Matoušek et al. 2012), standard PSTVd variants, and PSTVd progenies that infect weed species (Matoušek et al. 2007b). Variants sequenced in this work are underlined and followed by GenBank AC KC810005-KC810010 in parenthesis. Numbers in parenthesis of other variants are accession codes of the "Subviral RNA Database" (Rocheleau and Pelchat 2006). The "phylogenetic" tree was produced by SplitsTree4 (Huson and Bryant 2006) using a "sequence+structure" alignment (Wilm et al. 2008) of the PSTVd sequences. Distances were calculated using the 'uncorrected P' model; the network was computed by the NeighborNet method. Despite the statistically low significance of the tree, no alternative topology was obtained using other distance, tree or network methods implemented in SplitsTree4

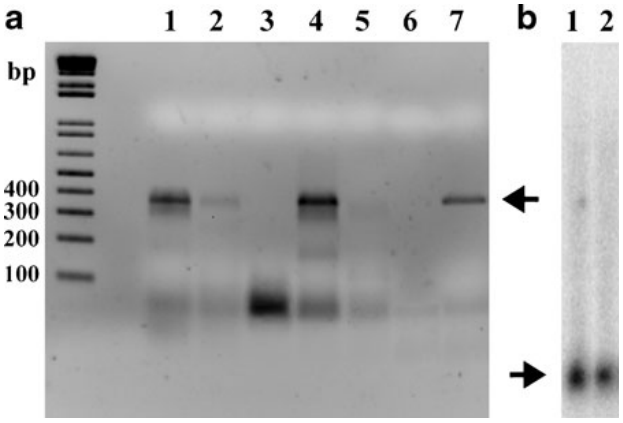

Fig. 3 Detection of full-length copies of PSTVd from ornamentals. Panel a, RT-PCR analysis of PSTVd infection in the following species: 1, *M. chamomilla* cv. Novbona; 2, *A. frutescens* sample 1; 3, *A. frutescens* sample 2; 4, *Diascia* sp. sample 1; 5, *Diascia* sp. sample 2; 6, control sample, without RNA; 7, *S. lycopersicum*. Plants were biolistically inoculated with the viroid population prepared from PSTVd isolates of ornamentals. RNA was isolated 5 weeks post inoculation (p. i.); full-length viroid cDNA copies were amplified using Titan One Tube RT-PCR reaction and analyzed in 2 % agarose gels (see Materials and Methods). No specific bands were detected in non-inoculated plants or in reactions without RNA templates as shown in sample 6. The left lane shows a 1 kb Plus DNA Ladder (Life Technologies). Panel b, levels of monomeric PSTVd-S1 (sample 1) and PSTVd-AS1 (sample 2) RNA corresponding to 359 nt in tomato 3 weeks p. i. as detected by northern blot analysis from 1.5 % agarose gels. PSTVd-specific bands are indicated by arrows. Total RNA (2 μg) were applied to the gels, blotted onto Nylon Biodine A membrane and hybridized against a PSTVd probe

and leaf edges (Fig. 5a). We conclude from our experiments that PSTVd from *S. jasminoides* elicits specific symptoms and developmental distortions in potato.

To precisely characterize the symptoms and extent of pathogenesis induced by the sequence-stable PSTVd-S1, a comparative inoculation of sensitive tomato cv. Rutgers with PSTVd-S1, -AS1 and -QFA, respectively, was performed using efficient biolistic transfer of defined quantities of these viroid cDNAs (Fig. 5b). This comparison confirmed that the impact of PSTVd-AS1 on tomato is more severe than that of PSTVd-S1, although levels of both viroids were similar as seen from northern blot analyses (see Fig. 3b). PSTVd-AS1 completely stopped tomato growth and caused collapse of leaf blade expansion. Developmental distortions induced by PSTVd-S1 were less pronounced, although symptoms were quite severe: note the leaf blade curling, rugosity and malformations shown in Fig. 5b. PSTVd-QFA caused no comparable symptoms (Fig. 5b).

Discussion

In this work we isolated PSTVd variants from ornamentals propagated in the territory of Czech Republic, confirming the expansion and persistence of PSTVd especially in *S. jasminoides*, and occasionally in *S. muricatum*, *Datura* sp. and *Brugmansia* sp. in Central Europe. This finding is also supported by our initial evidence of PSTVd in ornamentals including petunia (Mertelík et al. 2010). Thus, our results complement analyses performed by other authors describing PSTVd expansion in the Netherlands, Italy and even in northern European countries like Finland (Lemmetty et al. 2011). In addition, we showed here the adaptation of a PSTVd pool from ornamentals in *Diascia* sp. and *A. frutescens*, where some incidence of PSTVd was detected in commercially propagated plants, and in *M. chamomilla*. The adaptation of the PSTVd population in these ornamentals resulted in new PSTVd variants like Anthemis2 in *Diascia* sp. (family *Scrophulariaceae*) that independently appeared as dominant sequence in the different host *Anthemis arvensis* (family *Asteraceae*) described earlier (Matoušek et al. 2007b). In *Diascia* sp. we detected a further unusual mutant with a C insertion in the UCCR that should influence the formation of hairpin I. We observed several other adaptations including mutations in the CCR in experimentally infected weed plants like *Amaranthus retroflexus* and wild chamomile (*Chamomilla recutita*) (Matoušek et al. 2007b), where also other fast adaptational changes for example in the pathogenicity domain were observed (Matoušek et al. 2012), and in PSTVd-inoculated *Brassica* species (Matoušek et al. 2004b). On the one hand, very low PSTVd levels were maintained in some plant species, like *Veronica agrestis* (family *Scrophulariaceae*) (Matoušek et al. 2007b). On the other hand, high levels of PSTVd in some *Diascia* plants clearly showed that the family *Scrophulariaceae* contains species susceptible to PSTVd. In contrast, in our recent experiments the level of PSTVd in *A. frutescens* (family *Asteraceae*) was very low despite high levels of PSTVd in other species of this family (e. g. *Ch. recutita*, *Anthemis arvensis*, *Gynura aurantiaca*) (Matoušek et al. 2007b).

PSTVd from ornamentals is well transmissible to tomato and potato (as confirmed in the present work; see also Verhoeven et al. 2010a,b), where it causes—depending on physiological conditions like high temperature—significant economical losses as recently

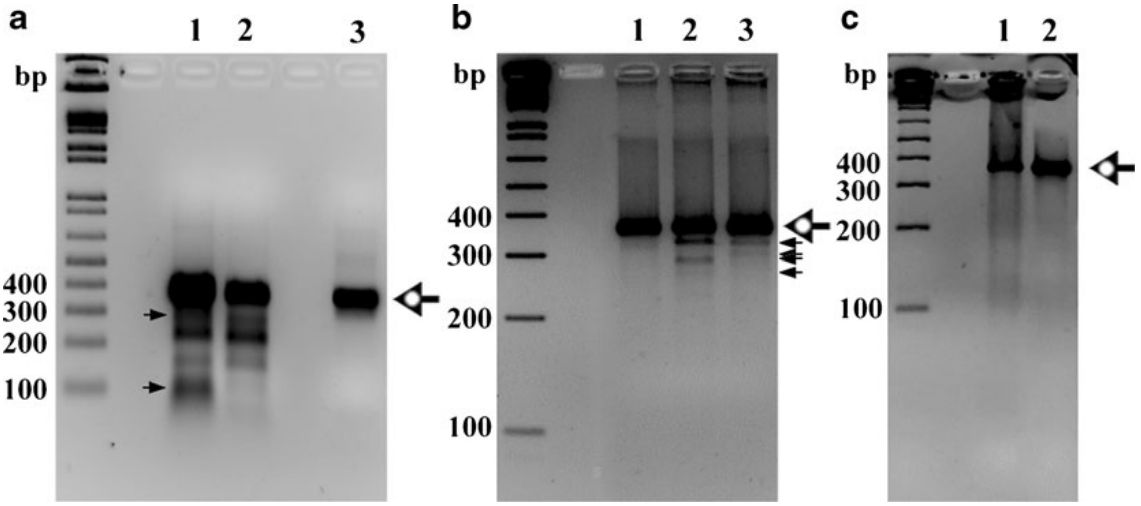

Fig. 4 Detection of PSTVd variability from ornamentals in experimentally infected potato and tomato by cleavage of cDNA heteroduplexes. cDNA was amplified from PSTVd libraries using high fidelity *Pwo* polymerase; the cDNA was hybridized and cleaved using a mismatch-specific nuclease (see Materials and Methods). Cleavage products were analyzed in agarose gels. Panel a, PSTVd population in potato; 1, PSTVd extracted 40 dpi.; 2, original PSTVd inoculum; 3, uncleaved library cDNA. Panel b, PSTVd population in tomato inoculated with the mixture of isolates from *S. jasminoides*; 1, uncleaved cDNA, 2, analysis 18 dpi.; 3, analysis 40 dpi. Panel c, PSTVd-S1 transferred to tomato after long-term maintenance in potato; 1, uncleaved library cDNA; 2, cleaved cDNA. The hollow arrows indicate positions of homoduplexes and cleavage products close to full lengths. The small black arrows indicate changes in the spectrum of cleavage products in panel A, lane 1, and products indicating viroid variants in panel B, lanes 2 and 3

calculated by Soliman et al. (2012). This fact is of particular interest because PSTVd causes a quarantine disease (Commission Decision 2007/410/EC of June 12, 2007) and has to be monitored to prevent its introduction and spreading. We isolated various PSTVd sequences from ornamentals that differed from strongly pathogenic viroids propagated in tomatoes; most of the viroid variants were clustering rather to mild or intermediate PSTVd variants. Among the analyzed PSTVd sequences from ornamentals, PSTVd-S1 was dominant and commonly distributed through infected *S. jasminoides* presumably from a common origin. Our analyses indicated that this viroid produces characteristic and severe morphological symptoms on potato tubers and specific morphological

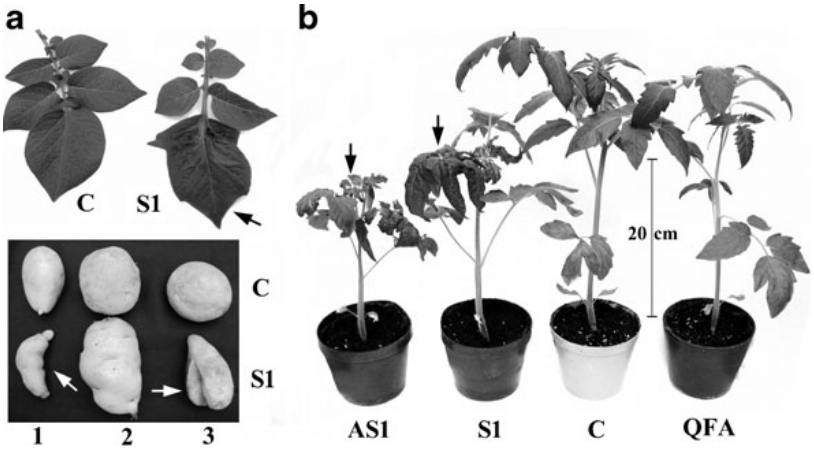

Fig. 5 Symptoms induced by PSTVd-S1 from *S. jasminoides* on potato and tomato, and symptom comparison between PSTVd-AS1, -S1 and -QFA on tomato. Panel a, upper part: C, control leaves from healthy cv. Vendula; S1, symptoms of the secondary infection on leaves of the same cultivar. Lower part: variability of symptoms on secondary-infected tubers of cvs Vendula (1), Verne (2) and Vlasta (3). Arrows indicate pathogenic changes in leaf shape, leaf malformations, tuber clefts and typical spindle shape of infected tubers. Panel b, symptoms on infected tomatoes 15 dpi. C, mock-inoculated control; AS1, S1 and QFA, plants infected with the corresponding viroid variant

symptoms on leaves of some potato cultivars. The PSTVd-S1 sequence is well adapted and stable in potatoes and tomatoes and shows high fitness, comparable to PSTVd-AS1 that has been described earlier as a lethal variant accumulating high levels of vsRNA and arresting tomato growth and development (Matoušek et al. 2007a). Similar results concerning PSTVd-S1 sequence stability in tomato and potato were published by Tsushima et al. (2011).

Acknowledgments The authors would like to acknowledge help and fruitful discussions with Dr. Csaba Koncz (Max-Planck-Institut für Züchtungsforschung, Cologne, Germany). The authors thank Mrs. Helena Matoušková, Ing. Olga Horáková and bc. Martin Selinger (BC v.v.i. IPMB, České Budějovice), Bernd Esters (Institute of Physical Biology, Heinrich-Heine-Universität Düsseldorf, Germany) for their help and excellent technical assistance. The project was supported by the Czech Science Foundation (GACR P501/10/J018), by the cooperative project FP7-REGPOT-2012-2013-1 MODBIOLIN No. 316304, by the project QH81262 (NAZV CR), and by institutional support (RVO:60077344) to J.M.

References

Codoñer, F. M., Darós, J. A., Solé, R. V., & Elena, S. F. (2006). The fittest versus the flattest: experimental confirmation of the quasispecies effect with subviral pathogens. *PLoS Pathogens, 2*, e136.

Di Serio, F. (2007). Identification and characterization of *Potato spindle tuber viroid* infecting *Solanum jasminoides* and *S. rantonnetii* in Italy. *Journal of Plant Pathology, 89*, 297–300.

Diener, T. O. (1995). Origin and evolution of viroids and viroid-like satellite RNAs. *Virus Genes, 11*, 119–131.

Eigen, M. (1993). Viral quasispecies. *Scientific American, 269*, 42–49.

Flores, R., Hernández, C., Martínez de Alba, A. E., Daròs, J. A., & Di Serio, F. (2005). Viroids and viroid-host interactions. *Annual Review of Phytopathology, 43*, 117–139.

Gago, S., Elena, S. F., Flores, R., & Sanjuán, R. (2009). Extremely high mutation rate of a hammerhead viroid. *Science, 323*, 1308.

Góra-Sochacka, A., Candresse, T., & Zagórski, W. (2001). Genetic variability of potato spindle tuber viroid RNA replicon. *Acta Biochimica Polonica, 48*, 467–476.

Góra-Sochacka, A., Kierzek, A., Candresse, T., & Zagórski, W. (1997). The genetic stability of potato spindle tuber viroid (PSTVd) molecular variants. *RNA, 3*, 68–74.

Hadidi, A., Flores, R., Randles, J. W., & Semancik, J. S. (Eds.). (2003). *Viroids*. Australia: CSIRO Publishing.

Harders, J., Lukács, N., Robert-Nicoud, M., Jovin, T. M., & Riesner, D. (1989). Imaging of viroids in nuclei from tomato leaf tissue by in situ hybridization and confocal laser scanning microscopy. *EMBO Journal, 8*, 3941–3949.

Huson, D. H., & Bryant, D. (2006). Application of phylogenetic networks in evolutionary studies. *Molecular Biology and Evolution, 23*, 254–267.

Keese, P., & Symons, R. H. (1985). Domains in viroids: Evidence of intermolecular RNA rearrangement and their contribution to viroid evolution. *Proc. Nat. Acad. Sci. U.S.A., 82*, 4582–4586.

Lemmetty, A., Laamanen, J., Soukainen, M., & Tegel, J. (2011). Emerging virus and viroid pathogen species identified for the first time in horticultural plants in Finland in 1997–2010. *Agricultural and Food Science, 20*, 29–41.

Luigi, M., Luison, D., Tomassoli, L., & Faggioli, F. (2011). Natural spread and molecular analysis of pospiviroids infecting ornamentals in Italy. *Journal of Plant Pathology, 93*, 491–495.

Matoušek, J., Kozlová, P., Orctová, L., Schmitz, A., Pešina, K., Bannach, O., Diermann, N., Steger, G., & Riesner, D. (2007a). Accumulation of viroid-specific small RNAs and increase in nucleolytic activities linked to viroid-caused pathogenesis. *Biological Chemistry, 388*, 1–13.

Matoušek, J., Orctová, L., Ptáček, J., Patzak, J., Dědič, P., Steger, G., & Riesner, D. (2007b). Experimental transmission of pospiviroid populations to weed species characteristic of potato and hop fields. *Journal of Virology, 81*, 11891–11899.

Matoušek, J., Orctová, L., Steger, G., & Riesner, D. (2004a). Biolistic inoculation of plants with viroid nucleic acids. *Journal of Virological Methods, 122*, 153–164.

Matoušek, J., Orctová, L., Steger, G., Škopek, J., Moors, M., Dědič, P., & Riesner, D. (2004b). Analysis of thermal stress-mediated PSTVd variation and biolistic inoculation of progeny of viroid "thermomutants" to tomato and *Brassica* species. *Virology, 323*, 67–78.

Matoušek, J., Stehlik, J., Procházková, J., Orctová, L., Wullenweber, J., Füssy, Z., Kováčik, J., Duraisamy, G., Ziegler, A., Schubert, J., et al. (2012). Biological and molecular analysis of the pathogenic variant C3 of potato spindle tuber viroid (PSTVd) evolved during adaptation to chamomilla (*Matricaria chamomilla*). *Biological Chemistry, 393*, 605–615.

Mertelík, J., Kloudová, K., Červená, G., Nečekalová, J., Mikulková, H., Levkaničová, Z., Dědič, P., & Ptáček, J. (2010). First report of *Potato spindle tuber viroid* (PSTVd) in *Brugmansia* spp., *Solanum jasminoides*, *Solanum muricatum* and *Petunia* spp. in the Czech Republic. *Journal of Plant Pathology, 59*, 392.

Qi, Y., & Ding, B. (2003). Differential subnuclear localization of RNA strands of opposite polarity derived from an autonomously replicating viroid. *Plant Cell, 15*, 2566–2577.

Qu, F., Heinrich, C., Loss, P., Steger, G., Tien, P., & Riesner, D. (1993). Multiple pathways of reversion in viroids for conservation of structural elements. *EMBO Journal, 12*, 2129–2139.

Rocheleau, L., & Pelchat, M. (2006). The Subviral RNA database: A toolbox for viroids, the hepatitis delta virus and satellite RNAs research. *BMC Microbiology, 6*, 24.

Schmitz, M., & Steger, G. (2007). Potato spindle tuber viroid (PSTVd). *Plant Viruses, 1*, 106–115.

Schumacher, J., Sänger, H. L., & Riesner, D. (1983). Subcellular localization of viroids in highly purified nuclei from tomato leaf tissue. *EMBO Journal, 2*, 1549–1555.

Soliman, T., Mourits, M. C. M., Oude Lansink, A. G. J. M., & van der Werf, W. (2012). Quantitative economic impact

assessment of an invasive plant disease under uncertainty - A case study for potato spindle tuber viroid (PSTVd) invasion into the European Union. *Crop Protection, 40*, 28–35.

Steger, G., & Riesner, D. (2003). Properties of Viroids: Molecular characteristics. In A. Hadidi, R. Flores, J. W. Randles, & J. S. Semancik (Eds.), *Viroids*. Australia: CSIRO Publishing.

Tabler, M., & Tsagris, M. (2004). Viroids: petite RNA pathogens with distinguished talents. *Trends in Plant Science, 9*, 339–348.

Tsushima, T., Murakami, S., Ito, H., He, Y., Raj, A. P. C., & Sano, T. (2011). Molecular characterization of *Potato spindle tuber viroid* in dahlia. *Journal of General Plant Pathology, 77*, 253–256.

Verhoeven, J., Hüner, L., Marn, M., Plesko, I., & Roenhorst, J. (2010a). Mechanical transmission of *Potato spindle tuber viroid* between plants of *Brugmansia suaveoles*, Solanum jasminoides and potatoes and tomatoes. *European Journal of Plant Pathology, 128*, 417–421.

Verhoeven, J. T. J., Jansen, C. C. C., Botermans, M., & Roenhorst, A. (2008). *Evidence that vegetatively-propagated solanaceous plant species act as sources of Potato spindle tuber viroid infection for tomato. Abstract at the International Conference on Viroids and Viroid-Like*. Berlin: RNAs.

Verhoeven, J. T. J., Jansen, C. C. C., Botermans, M., & Roenhorst, J. W. (2010b). Epidemiological evidence that vegetatively propagated, solanaceous plant species act as sources of *Potato spindle tuber viroid* inoculum for tomato. *Plant Pathology, 59*, 3–12.

Verhoeven, J. T., & Roenhorst, J. W. (2010). High stability of original predominant pospiviroid genotypes upon mechanical inoculation from ornamentals to potato and tomato. *Archives of Virology, 155*, 269–274.

Weinberg, Z., & Breaker, R. R. (2011). R2R-software to speed the depiction of aesthetic consensus RNA secondary structures. *BMC Bioinformatics, 12*, 3.

Wilm, A., Linnenbrink, K., & Steger, G. (2008). ConStruct: Improved construction of RNA consensus structures. *BMC Bioinformatics, 9*, 219.

Journal of Plant Physiology 183 (2015) 85–94

Contents lists available at ScienceDirect

Journal of Plant Physiology

journal homepage: www.elsevier.com/locate/jplph

Physiology

Expression of SANT/HTH Myb mRNA, a plant morphogenesis-regulating transcription factor, changes due to viroid infection

Jaroslav Matoušek[a], Rajen J.J. Piernikarczyk[b], Anna Týcová[a], Ganesh S. Duraisamy[a], Tomáš Kocábek[a], Gerhard Steger[b,*]

[a] BC ASCR v. v. i., Institute of Plant Molecular Biology, Branišovská 31, 37005 České Budějovice, Czech Republic
[b] Institute of Physical Biology, Heinrich-Heine-Universität Düsseldorf, D-40204 Düsseldorf, Germany

ARTICLE INFO

Article history:
Received 6 February 2015
Received in revised form 12 May 2015
Accepted 1 June 2015
Available online 9 June 2015

Keywords:
mRNA target
RNA decay
Biolistic plant inoculation
Transgenote
Nicotiana benthamiana
Solanum lycopersicum

ABSTRACT

Potato spindle tuber viroid (PSTVd) belongs to plant-pathogenic, circular, non-coding RNAs. Its propagation is accompanied by (mis)regulation of host genes and induction of pathogenesis symptoms including changes of leaf morphogenesis depending on the strength of viroid variant. We found strong genotype-dependent suppression of tomato morphogenesis-regulating transcription factor SANT/HTH-Myb (*Sl*Myb) due to viroid pathogenesis. Its relative mRNA level was found to be significantly decreased in PSTVd-sensitive tomato (cvs Rutgers and Heinz 1706) due to degradation processes, but increased in PSTVd-tolerant (cv. Harzfeuer). In heterologous system of *Nicotiana benthamiana*, we observed a *Sl*Myb-associated necrotic effect in agroinfiltrated leaf sectors during ectopic overexpression. Leaf sector necroses were accompanied by activation of nucleolytic enzymes but were suppressed by a strongly pathogenic PSTVd variant. Contrary to that, PSTVd's effect was inhibited by the silencing suppressor p19. It was found that in both, *Solanum lycopersicum* leaves and *N. benthamiana* leaf sectors, *Sl*Myb mRNA degradation was significantly stronger in viroid-infected tissues. Necroses induction as well as gene silencing experiments using the SANT/HTH-Myb homologues revealed involvement of this Myb in physiological changes like distortions in flower morphogenesis and growth suppression.

Introduction

Viroids are the smallest infectious pathogens known, consisting solely of circular, highly structured single-stranded RNA with small genomes ranging from 246 to 401 nucleotides. They do not encode proteins; that is, all their biological functions including replication are achieved by direct interaction of the genomic RNAs (or derivatives thereof) with host components. Potato spindle tuber viroid (PSTVd) is the type member of the family *Pospiviroidae*. Various viroids from *Pospiviroidae* cause plant developmental distortions, alter morphogenetic and physiological parameters, and thus cause serious plant diseases in numerous crops depending on plant species and viroid genotypes. Certain viroid–host combinations are accompanied by severe host symptoms, while in other combinations the same viroid variant is tolerated by the host and symptoms are weak or not detectable (Sänger, 1982; Hadidi et al., 2003).

Viroid infections are accompanied by the accumulation of viroid-specific small RNAs (vsRNAs) (Hammann and Steger, 2012). Like small interfering RNAs (siRNA), microRNAs (miRNA), or trans-acting siRNAs (ta-siRNA), vsRNAs influence expression of certain genes *via* posttranscriptional gene silencing (PTGS) or transcriptional silencing (TGS) (*e.g.* Itaya et al., 2007; Di Serio et al., 2009; Diermann et al., 2010; Wang et al., 2011; Owens et al., 2012; Matoušek et al., 2012). Recently, it has been shown by Navarro et al. (2012) and Eamens et al. (2014) that vsRNA can directly target plant mRNAs. Assays of mRNA levels provided evidence for an

Abbreviations: CIPK, Calcineurin B-Like (CBL)-Interacting Protein Kinase; dpi, days post infiltration; PSTVd, Potato spindle tuber viroid; PUF, Pumilio/Fem-3 mRNA binding factor; SANT/HTH-Myb, SANT for switching-defective protein 3 (Swi3), adaptor 2 (Ada2), nuclear receptor co-repressor (N-CoR), transcription factor (TF)IIIB, HTH for helix–turn–helix, MYB for myeloblastosis family of transcription factors; *Sl*Myb, tomato SANT/HTH-Myb; TCP3, TEOSINTE BRANCHED1, CYCLOIDEA, and PCF; VPE, vacuolar processing enzyme; VSF, vascular specificity factor; vsRNA, viroid-specific small RNA.

* Corresponding author. Tel.: +49 211 81 14597; fax: +49 211 81 15167.
E-mail addresses: jmat@umbr.cas.cz (J. Matoušek), Rajen.Piernikarczyk@uni-duesseldorf.de (R.J.J. Piernikarczyk), tycova@umbr.cas.cz (A. Týcová), gansels@umbr.cas.cz (G.S. Duraisamy), kocabek@umbr.cas.cz (T. Kocábek), steger@biophys.uni-duesseldorf.de (G. Steger).

http://dx.doi.org/10.1016/j.jplph.2015.06.001
0176-1617/

involvement of several pathways to misregulation and suppression of potential target and non-target mRNAs (Owens et al., 2012; Matoušek et al., 2012; Füssy et al., 2013) and stimulation of mRNA expression within the potential viroid-induced pathogenesis network (Matoušek et al., 2007).

Moreover, previous studies of the pathogenicity caused by *Pospiviroidae* indicated that expression of certain enzymes is altered in infected plants (*e.g.* Rodriguez and Flores, 1987; Vera and Conejero, 1988; Matoušek and Dědič, 1988; Trněná and Matoušek, 1991; Diener et al., 1993). Based on these observations, we concluded that viroid-induced pathogenesis is indeed a complex developmental process that depends on interaction between plant and viroid genotypes. In our previous study, we have reported the suppression of mRNA levels of several regulatory factors influencing the leaf morphogenesis of tomato (*Solanum lycopersicum*) infected with pathogenic viroid variants PSTVd-AS1 (Matoušek et al., 2012). In this study, we analyzed the expression level of another regulatory factor, SANT/HTH-Myb (*Sl*Myb) described as morphogenesis regulating factor "trifoliate" (Naz et al., 2013). Our investigation showed that infection with "lethal" symptoms-inducing PSTVd-AS1 leads to induction of rapid degradation of *Sl*Myb mRNA and to suppression of *Sl*Myb functions by a genotype-dependent process that differs from direct vsRNA-mediated degradation at the corresponding target sites. In addition, our study established the function previously unknown to *Sl*Myb and its a possible involvement in the PSTVd-induced pathogenesis network.

Materials and methods

Plant material and cultivation conditions

Tomato (*Solanum lycopersicum*) and *Nicotiana benthamiana* plants were used for inoculation. PSTVd (Potato spindle tuber viroid)-sensitive tomatoes cultivars Rutgers (USA) and Heinz 1706 (kindly provided by Heinz N. A., Ag. Research, Stockton, USA), PSTVd-tolerant tomato cv. Harzfeuer (kindly provided by Dr. J. Schubert, BAZ, Quedlinburg, Germany). Hybrids between cvs Rutgers × Harzfeuer were made by conventional crossings. Seeds of *N. benthamiana* transgenic line C16 GFP were kindly provided by Dr. D. C. Baulcombe (University of Cambridge, UK).Tomato and *N. benthamiana* plants were maintained in climate boxes at 25 ± 3 °C. Plants were grown under natural light with supplementary illumination [90 μmol m^{-2} s^{-1} PAR] to maintain a 16 h-day period.

Viroid variants, preparation of infectious vectors, biolistic inoculation, viroid agroinoculation, and detection

We used the following PSTVd variants for plant inoculations: mild QFA (AC U23059), severe C3 (AC HE575349), and lethal AS1 (AC AY518939). For biolistic inoculation of tomato, we prepared StyI-cleaved full-length cDNA fragments of PSTVd as inoculum using primers PSTVds I and PSTVds II (refer nos. 33 and 34, respectively, in Table S1 in Supplemental materials). The same primers were used for RT-PCR diagnosis of PSTVd. Biolistic inoculation was conducted with the Helios Gene Gun System (Bio-Rad, USA) as described previously (Matoušek et al., 2012). Each plant was inoculated twice, each time with 200 ng DNA. If not stated otherwise, plants were inoculated at the stage of three partly expanded true leaves. After inoculation, plants were immediately transferred into polyethylene bags to prevent drying-out of the wounded leaf areas. Treated plants were further conditioned by shading them for 24 h, and afterwards by cultivation in perforated bags for two days in the climate boxes under standard conditions. *N. benthamiana* plants were agroinfected by PSTVd AS1 or PSTVd QFA. For agroinoculation we constructed dimeric infectious vectors AS1(−) pLV07 and QFA(−) pLV07 as described in Fig. S2. In some experiments, conventional inoculation was performed in 0.04 M sodium phosphate buffer (pH 7.6) using Carborundum as abrasive. PSTVd infections were followed by Northern blots or dot-blots using full-length PSTVd [^{32}P]dCTP-labeled probes; the detection limit of the latter method is about 0.03 pg per mg of fresh material (Matoušek et al., 1994) (see Fig. S2).

Polyacrylamide gel electrophoretic analysis of circular and linear PSTVd RNAs was performed in 6% denaturing polyacrylamide gels containing 30:1 acrylamide:bisacrylamide (w/w), 89 mM Tris–borate buffer, 0.24 mM EDTA (1× TBE), pH 8.3, 0.1% TEMED, 8 M urea, 2% glycerol and 0.06% ammonium persulfate. Samples were electrophoresed at a constant voltage of 220 V at 60 °C. Separated RNA was transblotted on to a Nylon membrane Charge Modified 0.2 μm (Sigma) using a semi-dry blotting procedure in 1× TB (0.1 M Tris–borate, pH 8.3) buffer and hybridized to [α^{32}P]dCTP-labeled viroid cDNAs as described above.

RNA extraction, quantification of mRNA levels and Northern blots

For mRNA quantification, total RNA was isolated from 100 mg of leaf tissue using Concert™ Plant RNA Reagent (Invitrogen) followed by RNA purification and DNA cleavage on columns (RNeasy Plant Total RNA kit, Qiagen), if not stated otherwise. Contaminating DNA, especially in samples from agroinfiltrated leaf sectors, was removed from the total RNA using the DNA-free™ kit (Invitrogen); and further absence of DNA was verified by PCR without RT step. One μg of purified RNA was reverse transcribed using oligo dT18 primer and Superscript III reverse transcriptase (Invitrogen) at 42 °C for 60 min.

In some experimental variants of mRNA probing, as described in individual figure legends, either a mixture of oligo dT18 and random nonamers or specific RT primers (Table S1) were used. A total of 5 μL of 50× diluted cDNA was used for a 20 μL PCR reaction with IQ™ SYBR Green Supermix (0.6 units of Hot Start Ex Taq polymerase (TaKaRa Bio), Taq buffer 1×, dNTPs 200 μM each, SYBR Green 1:20,000 (Molecular Probes) and primers 375 nM each). All amplifications were carried out on a Bio-Rad IQ5 cycler for 40 cycles (94 °C for 20 s, 59 °C for 30 s, 72 °C for 30 s) following an initial denaturation/i-Taq activation step (94 °C for 3 min). The product size was confirmed by melting analysis and 2% agarose gel electrophoresis. Data were analyzed and quantified with the Bio-Rad IQ5 Optical System v. 2.0 software. Values were standardized to house keeping markers or 7SL RNA (Matoušek et al., 1999) as shown in individual figures using the "Delta–delta method" and normalized to the sample with highest expression (calibrator set to 100%) according to Pfaffl (2001). The data points show the mean ± S.D. of two replicates of each PCR reaction.

The levels of mRNAs from tomato were assayed using qRT-PCR with primers described in Table S1. For Virus-induced gene silencing (VIGS) analysis, levels of *N. benthamiana* Myb homologue were quantified using primers 44 and 45; for tomato SANT/HTH-Myb (*Sl*Myb) mRNA probing, four primer pairs were used listed as numbers 5–12 in Table S1.

Northern blot analysis of *Sl*Myb mRNA was performed as described earlier for TBN1 mRNA (Matoušek et al., 2007). For *Sl*Myb mRNA analysis, 35 μg of DNase-treated and Qiagen purified total RNA was applied per slot in the gel.

Analysis of mRNA degradation, 5′ RACE mapping of 5′P ends and Southern blots

For specific degradomes total RNA samples were isolated from 1–2 g of leaf tissues using Concert™ (Plant RNA Purification Reagent, Invitrogen). From total RNA either a mRNA fraction was

isolated using Oligotex Direct mRNA Mini Kit (Dynex) according to the batch protocol supplied by the manufacturer or a 2 M LiCl-soluble fraction was isolated. This fraction was prepared by mixing the total RNA samples 1:1 v/v with 4 M LiCl, the mixture was kept in ice for 2 h; precipitated nucleic acids were sedimented in the cold at 15×10^3 g for 30 min. RNA from the supernatant was precipitated with 3 v/v of ethanol, washed in the cold with pre-chilled 70% ethanol, dried and dissolved in appropriate volume of water. For specific 5′ RACE profiles of *Sl*Myb, the following procedure involving PCR amplification of samples immobilized on magnetic beads by biotin-streptavidin was used. For immobilization on Dynabeads M-280 Streptavidin (Invitrogen) the protocol supplied by the manufacturer was followed: 10 mM Tris–HCl (pH 7.5) containing 1 mM EDTA, 1 M NaCl and 0.05% Tween 20 was used as binding and washing buffer; purification and amplification was performed as individual steps as schematically shown in Fig S8. PARE RNA and DNA adaptors (for sequences Nos 35–37, Table S1) were used as described by German et al. (2009). The procedure (Fig S8) include ligation of RNA adaptors, a reverse transcription step using Superscript III reverse transcriptase (Invitrogen) at 42 °C for 60 min, PCR amplifications using a premix of Taq1 polymerase (Qiagen), electrophoretic analyses on native 6% polyacrylamide gels and silver-staining of DNA fragments (Schumacher et al., 1986). In some experiments, electroblotting and hybridization with [α^{32}P]dCTP-labeled cDNA probes or sequencing were performed as given in legends to individual experiments. Adaptor ligation was performed using miRCat™ RNA Cloning Kit (IDT); manufacturer's instructions were followed.

For *Sl*Myb degradome analysis, reverse transcriptions with 3′-specific primers (RII, RIV, Stop, and 3UTR; Nos 10, 12, 17, and 20 in Table S1) covering different mRNA regions were performed."Bi-nested" PCR reactions were performed for analyses of *Sl*Myb using primer 5′ ada in combination with primers with prefixes Nes1 and Nes2 (13–16, 18, 19, 21, 22; Table S1). PCR reactions were performed using denaturation at 94 °C for 3 min and the following cycle: 94 °C for 30 s, 52 °C for 30 s and 72 °C for 55 s. The number of cycles differed as described for individual experiments; see Fig S8.

Southern blot of PCR products was performed using capillary alkaline transfer from 2% agarose and electroblots from native 6% polyacrylamide gels onto Nylon membranes (Charge Modified 0.2 μm, Sigma) using a semi-dry blotting device of size 14 × 15 cm (OMNIBIO, Brno). Blotting was performed in 0.5× phosphate buffer, pH 6.8, with 0.5 A for 1 h. Afterwards the membranes were UV-irradiated using a Transilluminator and baked for 20 min at 80 °C. Hybridization was performed by cDNA probes labeled with [α^{32}P]dCTP using Rediprime™ II Random Prime Labeling System kit (Amersham Biosciences). Hybridization was performed in 50% formamide hybridization buffer at 32 °C overnight (Matoušek et al., 1995). The washing procedure included an incubation of membranes in 2× SSC for 10 min at 0 °C following incubation in 2× SSC buffer containing 0.1% SDS for 30 min at 32 °C.

Plant transformation and VIGS experiments

N. benthamiana plants were transformed with *Agrobacterium tumefaciens* LBA4404 bearing the plant expression pLV07 construct (Matoušek et al., 2006) (clone 3907) containing the *Sl*Myb gene driven by 35S promoter. *Sl*Myb was cloned from tomato cv. Heinz 1706 into vector pLV68 (Matoušek et al., 2006) using primers 1 and 2 listed in Table S1; subsequently, the expression cassette was re-cloned to pLV07 using restriction enzymes *Pac*I and *Asc*I (Fig. 5). Transformation was performed using the standard leaf disc method according to Horsch et al. (1985). Regenerated transformed plants were maintained on a medium containing 100 mg/L kanamycin and 200 mg/L Timentin.

For VIGS experiments, we cloned the cDNA fragments of TBN1/GFP (Fig. S5) and of *N. benthamiana* Myb homologue/GFP fusion (Fig. 5d) into the SmaI site of vector pTV00 (Ratcliff et al., 2001) kindly provided by Dr. D. C. Baulcombe (University of Cambridge, UK). Both, the Tobravirus replicase component (vector pBINTRA6) and coat protein-containing modified pTV00 were transformed separately by electroporation into *A. tumefaciens* strain GV3101 containing the helper plasmid pJIC SA_Rep (Hellens et al., 2000). VIGS vectors were applied as a mixture in ratio 1:1 by agroinfiltration into *N. benthamiana* plants with 3–5 expanded leaves.

Bioinformatic methods

Sequence data analysis was carried out with DNASIS v. 2.6 (Hitachi). Protein sequence analyses were performed using InterProScan module of Geneious v. 5.5.6. Degradome mapping was performed using Visual Cloning 2000 (Redasoft). The PSTVd consensus structure was based on a sequence alignment by mafft/Q-INS-i (Katoh and Toh, 2008) and ConStruct (Wilm et al., 2008); the structure was drawn by R2R (Weinberg and Breaker, 2011). PSTVd sequences were taken from GenBank. Viroid-specific small RNAs (vsRNAs) were identified in deep-sequencing data of small RNAs from PSTVd-infected tomatoes (Matoušek et al., 2012) using segemehl (Otto et al., 2014). Myb sequence was verified from mRNAs annotated in the genome data of PSTVd-sensitive tomato cv. Heinz 1706 (release ITAG2.3; Tomato Genome Consortium, 2012).

Other methods

cDNA *Sl*Myb probes were labeled with [α^{32}P]dCTP using the Redivue™ [α^{32}P]dCTP 3000 Ci/mmol Rediprime™ II random prime labeling system (Amersham Pharmacia Biotech, Freiburg, Germany). Autoradiograms from Northern blots, Southern blots and electroblots were scanned using the TYPHOON PhosphoImager (Amersham Biosciences, Sunnyvale, California, USA) and quantified using ImageQuant software (Molecular Dynamics, Sunnyvale, California, USA). Analysis of nucleolytic activities in gels was performed as described by Matoušek et al. (2007). Photographs of individual samples were analyzed with respect to the area of various tissue types by 'Lucia measurement on VGA' v. 5.0 (Laboratory Imaging, Prague). This software was also used to characterize necrotizing effects from negative images and the habitus of symptomatic *N. benthamiana* plants.

Results

Characterization of selected PSTVd variants that produce different levels of pathogenicity and levels of Sl*Myb in infected tomatoes*

In our previous work (Matoušek et al., 2012) we found suppression of several factors that may be connected to the induction of tomato leaf abnormalities due to viroid pathogenesis: examples are TCP3 (TEOSINTE BRANCHED1, CYCLOIDEA, and PCF), member of a protein family that regulate plant growth and development and tomato leaf morphogenesis, and VSF (vascular specificity factor), a bZip-like plant transcription factor that regulates development of the plant vascular system and could regulate leaf morphogenesis. During this preliminary analysis, we also found that *Sl*Myb, the transcription factor "trifoliate" regulating leaf morphogenesis, belongs to factors whose expression is significantly suppressed by viroid infection.

We selected three different PSTVd variants to characterize *Sl*Myb mRNA levels in response to viroid pathogenesis in detail: a mild (PSTVd-QFA), a severe (PSTVd-C3), and a so-called lethal symptom-inducing (PSTVd-AS1) variant. These variants differ from

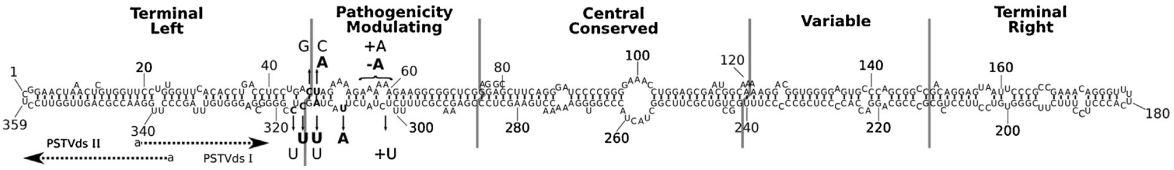

Fig. 1. The secondary structure of PSTVd-AS1. Base differences to PSTVd-C3 (in bold letters) and PSTVd-QFA (in normal letters) are marked. The shown consensus structure is based on a sequence alignment by mafft/Q-INS-i (Katoh and Toh, 2008) and ConStruct (Wilm et al., 2008) of 234 different PSTVd variants; the structure is drawn by R2R (Weinberg and Breaker, 2011). The domain boundaries of Pospiviroids are marked and named according to Keese and Symons (1985) in gray color. Position of primers used for PSTVd amplification (PSTVdsI and PSTVdsII) are marked by dotted arrows.

each other by four mutations and two insertions (AS1 → QFA) and by four mutations and a deletion (AS1 → C3), respectively, in the pathogenicity-modulating (P) domain and the boundary to the terminal-left (TL) domain (see Fig. 1). While PSTVd-QFA does induce only mild stunting and leaf epinasty but no leaf malformations, rugosity or necrosis on tomato (see supplementary Fig. S1) and no visible symptoms on *Nicotiana benthamiana* (not shown), PSTVd-AS1 leads to fast induction of developmental disorders like apex leaves malformations, rugosity, growth collapse, severe stunting (Fig. 2a and b), and appearance of necroses at later stages. PSTVd-C3 is a variant inducing lethal symptoms in chamomile (*Matricaria chamomilla*) plants, while in tomato and tobacco the distortions are severe (see Fig. S1). Thus, these three viroids induce a gradation of symptoms from mild to extraordinary strong.

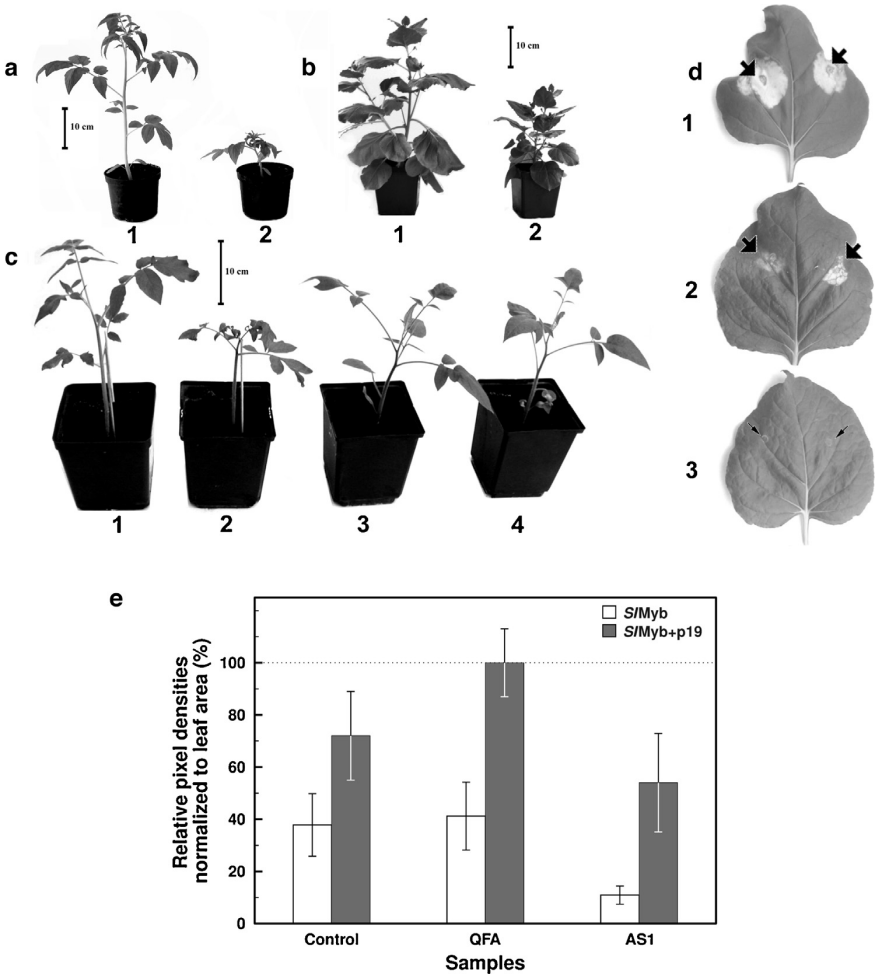

Fig. 2. Symptoms of PSTVd pathogenesis on tomato and *N. benthamiana*, and PSTVd suppression of necroses induced by *Sl*Myb. (a, b) Comparison of pathogenesis-associated symptoms on tomato cv. Heinz 1706 23 days post biolistic infection (a1, 2) and on *N. benthamiana* 25 days post agroinfiltration of a PSTVd-AS1 vector (b1, 2); (a1, b1), healthy control plants; (a2, b2) PSTVd-AS1-infected plants. (c) Comparisons of sensitive tomato cv. Rutgers (1, 2) and tolerant tomato cv. Harzfeuer (3, 4). (c1, c3) Healthy controls; (c2, c4) plants infected with PSTVd-AS1 19 days post biolistic inoculation. The scale bars in (a)–(c) have a length of 10 cm. (d) Necroses on *N. benthamiana* leaves 3.5 days post *Sl*Myb infiltration without PSTVd infection (d1), with PSTVd-QFA infection (d2), and with PSTVd-AS1 infection (d3). (e) Comparative image analysis of necrotizing effects; spots were quantified and normalized to tissue areas using Lucia v. 5.0. The lowest and highest color value was set to 100 and 0%, respectively. Variation is given from five independent experimental measurements. Control, infiltration of healthy leaves; QFA and AS1, leaves infected with PSTVd-QFA and AS1, respectively. White columns, infiltration with *Sl*Myb vector only; gray columns, leaves infiltrated with combination of *Sl*Myb and silencing suppressor p19.

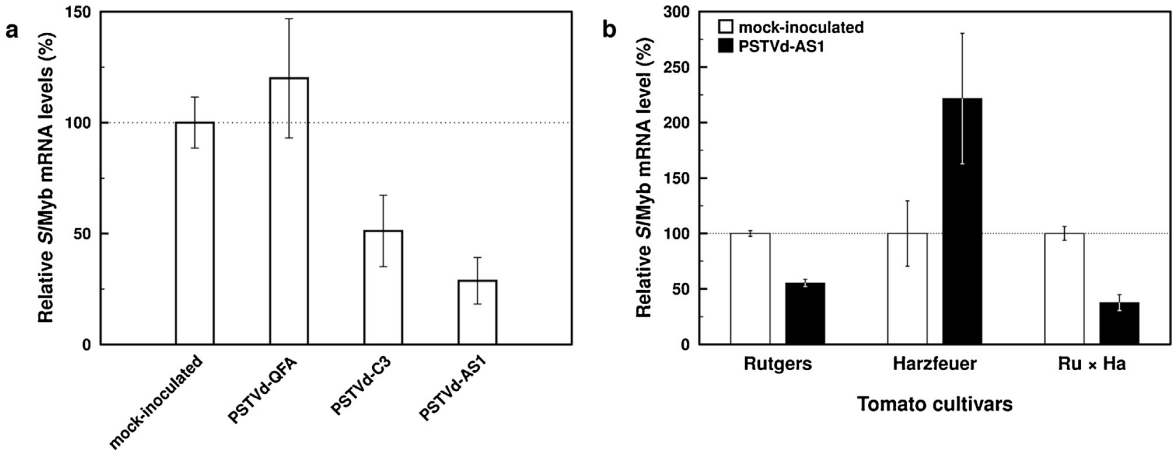

Fig. 3. Real time PCR analysis of *Sl*Myb mRNA levels in PSTVd-infected tomato genotypes. (a) Tomato plants (cv. Rutgers) were infected with PSTVd variants QFA, C3 and AS1 that induce mild, severe and lethal symptoms, respectively. RNA samples were collected from upper leaves 19 dpi with the Carborundum method. (b) *Sl*Myb mRNA levels in healthy and PSTVd-AS1-infected tomato genotypes, PSTVd-sensitive tomato cv. Rutgers (Ru), tolerant Harzfeuer (Ha) and the F1 hybrid Ru × Ha. RNA samples were collected 22 dpi from upper leaves. Relative levels in PSTVd-infected tissues are shown in comparison to controls (100%) and were normalized to UBI3 and to tomato 7SL RNA.

The quantification of the leaf-morphogenesis regulator *Sl*Myb mRNAs showed strong correlation with symptom expression: no suppression was seen in the mild PSTVd-QFA-infected tomato in comparison to controls; the strongest suppression was induced by PSTVd-AS1 (Fig. 3a).

*Sl*Myb was strongly suppressed in PSTVd-AS1-infected tissues in PSTVd-sensitive tomato cultivars Rutgers and Heinz 1706 showing pathogenicity-related symptoms. PSTVd-tolerant cultivars like Harzfeuer accumulate PSTVd to similar levels as sensitive cultivars, but lack significantly visible morphological symptoms; for an example with PSTVd-AS1 see Fig. 2c (compare plants 3 and 4). We described earlier that morphology and symptom appearance in the sensitive tomato Rutgers (Ru) dominated over the symptomless Harzfeuer (Ha) phenotype; hence Ha × Ru or Ru × Ha F1 hybrids are sensitive (Matoušek et al., 2007). We used these genotypes to compare levels of *Sl*Myb expression upon viroid pathogenesis (Fig. 3b). While *Sl*Myb mRNA levels significantly decreased in cv. Rutgers and the F1 hybrid Ru × Ha, an increase was detected in cv. Harzfeuer (Fig. 3b). These results strongly suggest unique genotype-dependent differences in mRNA expression of *Sl*Myb upon PSTVd infection and confirmed association with viroid pathogenesis.

Because suppression of a leaf morphogenesis regulator could contribute to the typical PSTVd symptoms, we analyzed *Sl*Myb in detail. At about 19 dpi (days post infiltration) after biolistic inoculation of PSTVd-AS1, the first visible symptoms like mild apex malformation appeared in our experimental conditions; during the next two days, symptoms rapidly developed including a stop of plant apex growth and leaf development. Simultaneously *Sl*Myb mRNA levels significantly decreased (Fig. 4). Within the interval of 19 to 23 dpi, the *Sl*Myb signal declined to 8%; at 23 dpi, the *Sl*Myb mRNA was no longer detectable in upper leaves by Northern blot analysis and by molecular hybridization.

Analysis of the Sl*Myb gene during overexpression in heterologous system of* N. benthamiana *and upon PSTVd pathogenesis*

The relatively low levels of *Sl*Myb mRNA in tomato after PSTVd infection allowed for us no detailed analyses. To increase *Sl*Myb mRNA levels, we constructed a plant vector containing a *Sl*Myb expression cassette driven by a 35S CaMV promoter (Fig. 5c) for agrobacterium infiltration into *N. benthamiana*, which is a plant enabling leaf infiltration. Furthermore we constructed an infectious vector for PSTVd agroinfection (Fig. S2). Then we were able to analyze *Sl*Myb expression in PSTVd-infected leaf sectors after agrobacterium infiltration into *N. benthamiana*.

We observed *Sl*Myb-induced leaf necroses if the mRNA was overexpressed in *N. benthamiana* leaves (Fig. 2d1 and Fig. S6I, sample D). Within three dpi with the Myb vector only, leaf sectors turned brown loosing chlorophyll, and later dried due to loss of cells devoid of chloroplast (Fig. S3, panel I, compare sectors A and B, C and D). This reaction was significantly stronger upon co-application of *Sl*Myb and silencing suppressors like p19 (see Fig. 2e and Fig. S3I) or p38 (not shown). With p19, the necrotizing reaction started after 2.5 days of application. This result might point to a regulation of *Sl*Myb mRNA *via* degradation by siRNA or miRNA, but does not exclude other nucleolytic degradation.

At the step of necroses formation, three dpi, an enhanced activity of RNases and nucleases towards RNA was observed in affected tissues (Fig. S4, compare lanes 1–4). Therefore, a nuclease that degrades both, RNA and DNA was further investigated using a VIGS vector with the tomato nuclease TBN1 sequence (Fig. S5).

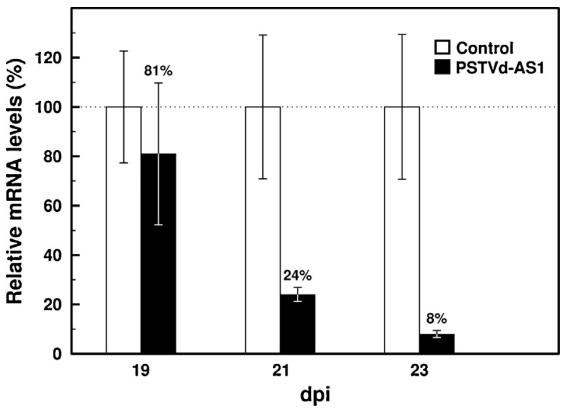

Fig. 4. Real time PCR analysis of *Sl*Myb mRNA levels in infected tomato cv. Rutgers at different intervals post biolistic inoculation. Early symptoms were detectable 19 dpi, while strong leaf malformations, apex collapse and first stem necroses appeared 23 dpi. Relative levels in AS1-infected tomatoes are shown in comparison to controls (100%); levels were normalized to UBI3 and to tomato 7SL RNA.

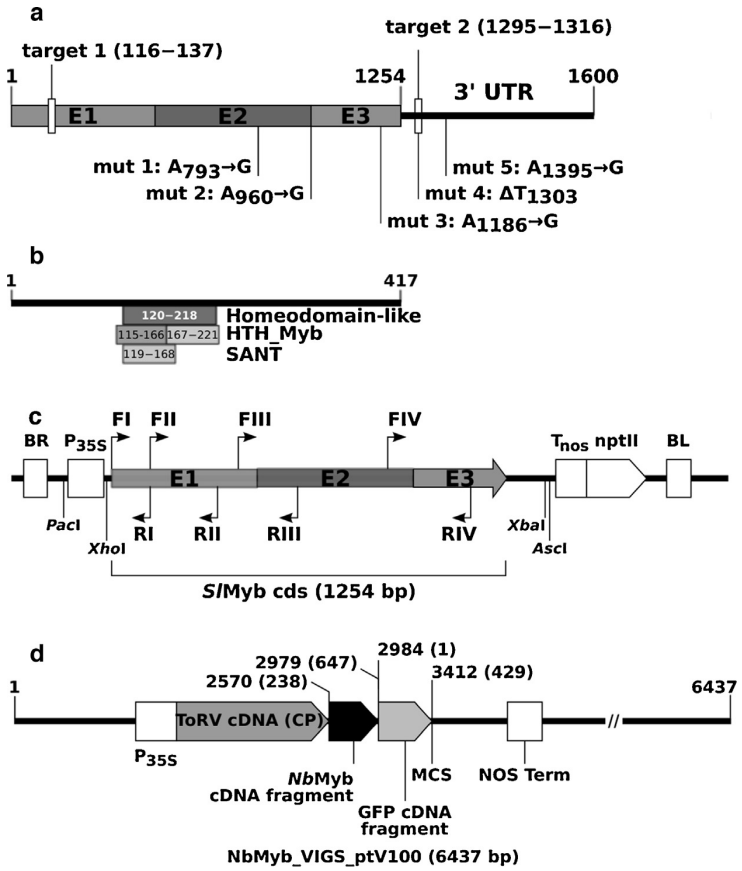

Fig. 5. Sequences of *Sl*Myb and of *Sl*Myb vector cassettes for overexpression and VIGS. (a) mRNA with positions of exons, 3′ UTR, potential vsRNA complementarity sites, and sequence differences between PSTVd-sensitive (Heinz 1706) and tolerant (Harzfeuer) tomato cultivars. (b) Protein domains in *Sl*Myb as annotated by the InterProScan module of Geneious software. (c) Plant vector cassette constructed for *Sl*Myb overexpression with localization of forward (F) and reverse (R) primers I–IV for qPCR probing; BR and BL, right and left T-DNA borders, respectively; P, promoter sequences; nptII, kanamycin resistance gene; restriction sites used for cassette cloning are marked. (d) VIGS vector cassette used for silencing of Myb homologue from *N. benthamiana*. Numbers in brackets give positions of fragments within *Nb*Myb and GFP genes. MCS, multiple cloning site; ToRV CP, Tobacco rattle virus coat protein.

Silencing of the *N. benthamiana* nuclease led to delay and suppression of necroses (Fig. S3, panel II, compare sectors A, B and C). Thus, we concluded that the necrotic reaction is accompanied by an increase in RNase activity and involves nucleases in some step. The induction of necroses is a previously unknown effect of *Sl*Myb that also propagates to leaf sectors not infiltrated by *Agrobacterium tumefaciens*. Additionally, we observed deviations in flower development, sterility, and dwarfism (Fig. S6, panel I, A–D) in some transgenic *N. benthamiana* plants.

The necroses induction upon ectopic overexpression of *Sl*Myb without application of silencing suppressors was fully suppressed in PSTVd-AS1-infected leaf tissues. In contrast, no significant suppression was observed in PSTVd-QFA-infected tissue (Fig. 2d, compare 1, 2 and 3; Fig. 2e and Fig. S3). This suppression of the "necrotic" Myb function, which is inhibitable by silencing suppressors, could be caused by the impact of PSTVd-induced pathogenesis on *Sl*Myb levels in *N. benthamiana*, which is in accordance with our observation of decreased *Sl*Myb mRNA levels in PSTVd-infected tomato (see previous section). Thus, we analyzed expression levels of *Sl*Myb in *N. benthamiana* leaf sectors.

PSTVd-AS1 pathogenesis caused fast degradation of Sl*Myb mRNA*

The *Sl*Myb overexpression in infiltrated leaves sectors enabled us to use Northern blots to compare mRNA levels in control and PSTVd-infected tissues. This analysis showed that decrease of *Sl*Myb mRNA in PSTVd-AS1-infected sectors was 20% compared to controls. In contrast, we observed no suppression in PSTVd-QFA-infected tissues (data not shown). Some smear of small hybridizing fragments, however, was visible in all samples suggesting a complex degradation process of *Sl*Myb mRNA (Fig. 6). Taking these experiments together, it follows that *Sl*Myb mRNA degradation mode and degradation rate depended on the pathogenic strength of the infecting PSTVd variant, but demonstrated no PSTVd-specific degradation.

We probed four mRNA regions of the Myb transgene by qPCR to assay this degradation (Fig. 7a). Total RNA was reverse transcribed using a mixture of oligo(dT) primers and random nonamers. We detected similar profiles for both, control and PSTVd-AS1 samples (Fig. 7a); significantly lower levels of Myb, however, were detected in PSTVd-AS1-infected tissues (Fig. 7b) in line with the preceding experiment. The qPCR signal differed between the regions: we detected higher levels in the 5′ region in contrast to the 3′ parts. This indicates a more intensive degradation from 3′ ends and/or more stable products derived from the 5′ end.

Different profiles, however, appeared when we used Oligotex-isolated mRNA as template and *Sl*Myb-specific reverse primers for RT steps. Comparison of profiles from Oligotex-isolated RNA and total RNA showed that cleavage proceeds also from 5′ ends where signals were minor compared to the 3′ region (Fig. S7).

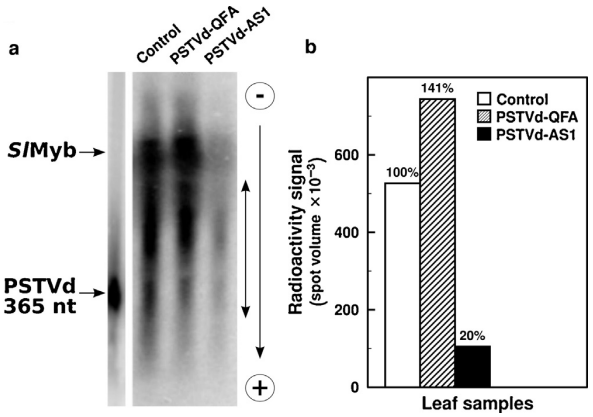

Fig. 6. Northern blot analysis of *Sl*Myb mRNA in leaf sectors of *N. benthamiana* co-agroinoculated with PSTVd and *Sl*Myb expression vectors. *N. benthamiana* leaves were co-agroinfiltrated with PSTVd and *Sl*Myb vectors (for expression cassette details see Fig. 5d and Fig. S2), or agroinoculated with the *Sl*Myb vector alone (C, control). Total RNA was isolated 2.5 dpi and purified as described in Material and Methods; 32 μg of total RNA samples were analyzed in an denaturing agarose gel and hybridized to [^{32}P]dCTP-labeled *Sl*Myb cDNA probe. Position of PSTVd RNA, from a 2 M LiCl-soluble fraction, is indicated on the side of the gel; the double arrow on the side indicates hybridizing smear.

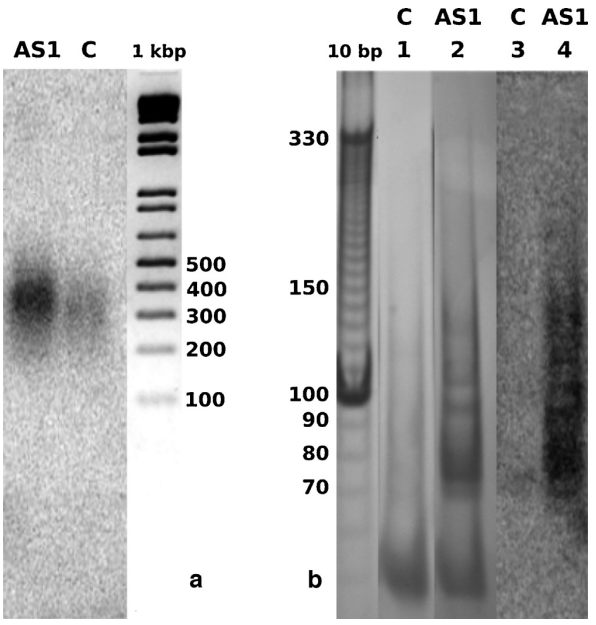

Fig. 8. Analysis of *Sl*Myb mRNA degradome. Southern blots of 5′ RACE fragments of *Sl*Myb mRNA degradome from co-agroinfiltrated leaf sectors of *N. benthamiana* (a) and 2 M LiCl-soluble RNA degradome of native *Sl*Myb from tomato cv. Heinz 1706 (b). (a) The 5′ region of *Sl*Myb mRNA was probed at an early stage, two days post co-infiltration with *Sl*Myb and PSTVd-AS1 vectors. Fragments were amplified with primers 5′ ada (Table S1, 36) and Rev I (Table S1, 10) and, in a nested reaction, with primers 5′ ada and Nes1 Rev I (Table S1, 13). Lanes AS1 and C show PCR products amplified from PSTVd-AS1-infected and from healthy leaves, respectively, transblotted from agarose gel and hybridized to [^{32}P]dCTP-labeled *Sl*Myb cDNA. (b) The 3′ UTR was probed by 5′ RACE (Fig. S8). Fragments were finally amplified with 5′ ada and Nes2 Myb 3UTR (Table S1, 22). Lanes 1 and 2 show silver-stained 3′ UTR PCR products in polyacrylamide gels corresponding to healthy and PSTVd-infected samples, respectively; lanes 3 and 4 show 3′ UTR PCR fragments from healthy and PSTVd-AS1 infected samples, respectively, electroblotted from 6% polyacrylamide gel and hybridized to [^{32}P]dCTP-labeled *Sl*Myb cDNA probe. Lengths of 1 kbp ladder in the agarose gel and 10 bp DNA ladder in the acrylamide gel are marked on the gel sides.

By 5′ RACE using miRCat^{TM} RNA Cloning Kit for 5′ RNA adaptor ligation to mRNA isolated from a very early stage, two days post *Sl*Myb agroinfiltration, we determined that the size of the 5′ RACE adaptor-containing fragment corresponds just to the mRNA 5′ end, suggesting either uncapped or partly cleaved mRNA fragments with 5′P ends (Fig. 8a). Such fragments were more abundant in PSTVd-AS1-infected tissues according to the radioactivity signals.

To explain the mode of "native" *Sl*Myb mRNA degradation, we wanted to analyze corresponding degradomes from tomato tissues. The *Sl*Myb mRNA is not abundant in tomato leaves and was not detectable in the mRNA fraction purified from PSTVd-AS1-infected leaves. Thus, we analyzed a 2 M LiCl-soluble RNA fraction for *Sl*Myb mRNA degradation fragments in tomato tissues. This LiCl fraction predominantly contained small RNAs and short degradation products while ribosomal RNA and long mRNA were precipitated. We modified the 5′ RACE system to increase sensitivity and specificity by use of streptavidin-coated magnetic beads with biotinylated adaptor primer and primer nesting (see Fig. S8). Mapping results of 5′ RACE products from the LiCl-fraction revealed a plethora of fragments covering the analyzed *Sl*Myb mRNA regions (Fig. 9).

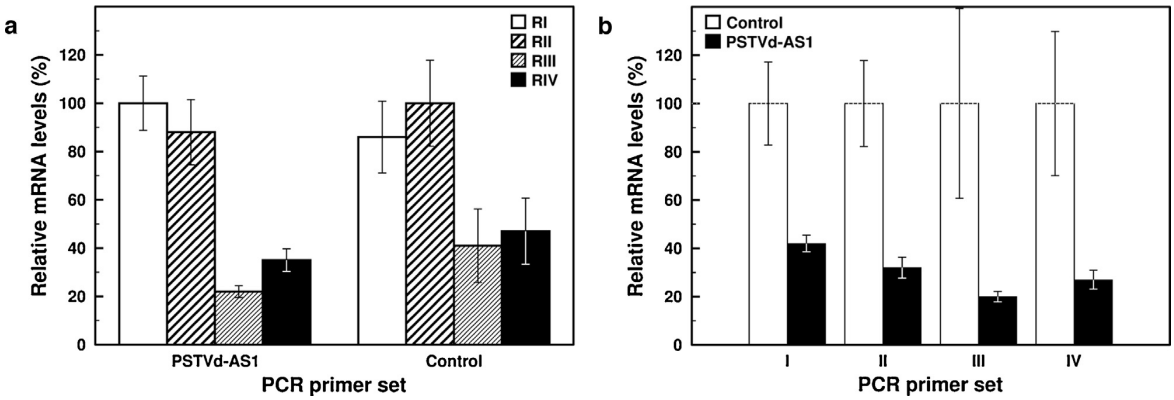

Fig. 7. Real time PCR "probing" of *Sl*Myb mRNA ectopically overexpressed in *N. benthamiana* leaf sectors. (a) Comparison of individual mRNA regions RI–RIV (Fig. 5c, Table S1) within sectors. (b) Comparison of *Sl*Myb mRNA levels in healthy and PSTVd-AS1-infected leaf sectors. Control or PSTVd-AS1(−) pLV07-agroinfected (AS1) leaves (see Fig. S2 for the vector cassette) of *N. benthamiana* were agroinfiltrated 25 days post agroinfection with a plant vector bearing the *Sl*Myb cassette (Fig. 5c); samples of total RNA were collected 2.5 dpi, treated with RNase-free DNase, reverse transcribed using a mixture of oligo(dT) primers and random nonamers, and analyzed for mRNA levels using sets of qPCR primers I–IV distributed at different positions along the mRNA sequence (Fig. 5c, Table S1). Relative levels are shown in comparison to the samples with the highest levels.

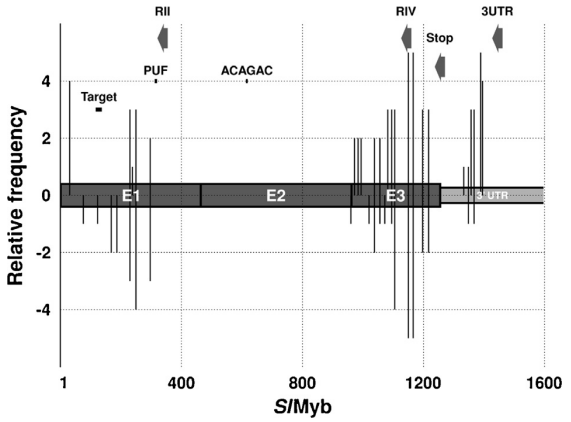

Fig. 9. Degradome plots of 5′P fragments of *Sl*Myb. Positions of primers are shown by arrows; letters E denote positions of exons; the gray bar indicates the open reading frame. The y-axes show relative frequency of individual fragments with free 5′ phosphates. Values range from 1 (barely detectable signal) up to 5 (strong); positive and negative values are for PSTVd-AS1-infected and control samples, respectively; Target, site of limited complementarity to PSTVd; PUF, PUF-binding site (with sequence CUGUAAUG that fits to the degradome site HTGTAMWK; Hou et al., 2014); ACAGAC, degradome site MCAGAC (Hou et al., 2014). Two M-LiCl-soluble RNA was extracted from symptomatic leaves of cv. Heinz 1706 23 dpi; for 5′ adaptor ligation, purification and amplification by "bi-nested" PCR see Fig. S8 and the 'Materials and methods' section. mRNA was isolated from symptomless infected leaves of tomato at early stage (12 dpi). Gels were silver-stained and visualized fragments were mapped according to position of nested primers.

Comparison of degradation patterns showed significant differences between controls and PSTVd-AS1-infected tissues especially in the 3′ UTR, where PSTVd pathogenesis led to induction of massive degradation already in the beginning of pathogenesis; we only detected a strong hybridization signal for young infected leaf tissues (Fig. 8b). Since our results showed a strong dependency of mRNA degradation on PSTVd-AS1, we performed bioinformatic analyses of *Sl*Myb for possible vsPSTVd target sites. Although our analyses revealed two vsRNA complementarity sites (Fig. 5a), these loci did not fulfill standard criteria for cleavable targets (Fahlgren and Carrington, 2010; Sun et al., 2011). This is consistent with our finding that no vsRNA complementarity site on *Sl*Myb mRNA mapped to a 5' P degradome position, suggesting indirect degradation associated to viroid pathogenesis.

Because of the different response to *Sl*Myb RNA levels in sensitive and tolerant tomatoes, we cloned the *Sl*Myb gene from cv. Harzfeuer to clarify differences on the molecular level. Sequence comparison between PSTVd-sensitive cv. Heinz 1706 and PSTVd-tolerant cv. Harzfeuer showed a conserved proximal promoter sequence 50 nt upstream of the start codon, but identified four A → G base changes and a T deletion in the coding region and 3′ UTR (Fig. 5a). The mutation at position 1395 perfectly matches the dominant 5′ P ends at positions 1389 and 1395 (compare Figs. 5a and 9). Therefore, we assume that at least partly the *Sl*Myb expression difference between Heinz 1706 and Harzfeuer genotypes is influenced by this A → G mutation on the 3′ UTR degradation process.

VIGS of SlMyb *homologue from* N. benthamiana *and observed effects of Myb downregulation*

The suppression of *Sl*Myb mRNA levels in PSTVd-infected tissues is correlated to symptoms development, while its level was unaffected in the PSTVd-tolerant tomato in comparison to controls. This suggests the possible involvement of *Sl*Myb suppression in pathogenesis-related symptoms development or modification. We constructed a Tobravirus VIGS vector with the *N. benthamiana* Myb homologue (*Nb*Myb; 80% aa homology; Niben.v0.4.2.Scf537) containing a *Nb*Myb/GFP fusion to investigate this possibility (Fig. S10a). The *Nb*Myb sequence shares the conserved domains R2R3Myb, homeodomain-like and SANT/HTH with *Sl*Myb (98% identity; see Fig. 5b). The VIGS-associated overexpression of the *Nb*Myb cDNA fragment of 400 nt led to significant *Nb*Myb suppression in GFP-silenced leaf sectors of *N. benthamiana* C16 plant transgenotes (Fig. S10b). About 20% of plants appeared weaker and stunted, and exhibited disorders of flower development (shortening of flower tubes, flower and anther degeneration; Fig. S6, panel IIE). We observed a strong growth suppression in *Nb*Myb-VIGS plants reaching 58% plant fresh weight compared to VIGS vector controls (27 dpi), similar to effects observed with AS1-infected symptomatic *N. benthamiana* at the same stage that also reached 58% fresh weight. In contrast, PSTVd-QFA-infected *N. benthamiana* reached 93.5% of the overall mass compared to controls.

According to qRT-PCR, PSTVd-AS1 induced significant *Nb*Myb suppression, reaching 36% of the mRNA levels in Tobravirus vector-infected *N. benthamiana* (not shown). This suggests that mixed virus and PSTVd infection leads to significant Myb degradation in this species. Simultaneously, such doubly infected plants were severely stunted and showed strong developmental distortions of flowers. These results showed that the same previously unknown functions of SANT/HTH-Myb homologues in plant development, and their possible contribution to a PSTVd-induced pathogenesis network.

Discussion

Suppression of SlMyb *and degradation processes upon PSTVd pathogenesis*

Several reports describe that viroid pathogenesis led to suppression of gene expression (*e.g.* Itaya et al., 2002; Wang et al., 2011; Owens et al., 2012). In our previous studies we described four "expression markers" that were strongly downregulated due to lethal PSTVd-AS1 infection that could be connected to the induction of leaf abnormalities (Matoušek et al., 2012). These four expression markers are as follow: TCP3 as a family member of proteins regulating plant growth, development and tomato leaf morphogenesis (*e.g.* Cubas et al., 1999; Ori et al., 2007); VSF, a bZip-like plant transcription factor regulating development of the plant vascular system (*e.g.* Torres-Schumann et al., 1996); CIPK (for 'Calcineurin B-Like (CBL)-Interacting Protein Kinase'), a kinase involved in interactions with calcium sensors and regulation of potassium channels (*e.g.* Kim et al., 2000; Lee et al., 2007), and VPE (for 'vacuolar processing enzyme'), a vacuolar processing protease with metacaspase activity and signaling function (Woltering, 2004; Kuroyanagi et al., 2005). Furthermore, we proposed a dual mode of hop chalcone synthase CHS_H1 suppression by Hop stunt viroid (HSVd) pathogenesis. First, *chs*_H1 contains a predicted vsRNA target site and could be directly suppressed by vsRNA and second, its expression could be suppressed by misbalancing of HlMyb2/3/HlbHLH2/HlWDR1 (MBW) complexes that activate the chs_H1 promoter. This imbalance was experimentally shown by downregulation of the HlbHLH2 component in MBW complexes according to levels observed in HSVd-infected plants (Füssy et al., 2013). In addition to the indirect influence of viroid infection on mRNA suppression, there is recent evidence of direct vsRNA-targeting of endogenous host mRNA (Navarro et al., 2012; Eamens et al., 2014).

In this work we found that *Sl*Myb mRNA shows expression alterations that correlate to symptoms induced by PSTVd variants of different severity in PSTVd-sensitive tomato; *i.e.*, these mRNAs were not suppressed due to mild symptom-inducing PSTVd-QFA but strongly suppressed in response to severe- and lethal symptom-inducing PSTVd-C3 and PSTVd-AS1, respectively. This transcription regulator showed strong dynamic suppression tightly bound to the

appearance of symptoms in tomato. The severity of PSTVd-induced pathogenesis was dependent on tomato genotypes. Even severe pathogenic PSTVd-AS1 induces no visible symptoms in the PSTVd-tolerant tomato cv. Harzfeuer (Matoušek et al., 2007), whereas *Sl*Myb mRNA levels showed some increase. These results suggested the involvement of PSTVd-induced alterations in mRNA expression in the tolerant Harzfeuer genotype. However, the induced changes did not led to marked visible morphological symptoms. In addition, we showed sequence differences in *Sl*Myb between cvs Harzfeuer and Heinz 1706. The mutation at position 1395, which perfectly matches the dominant 5′P ends at positions 1389 and 1395 from PSTVd-AS1-infected tissues of cv. Heinz 1706, might be responsible for the *Sl*Myb expression difference between sensitive and tolerant tomato genotypes.

We found that rapid *Sl*Myb mRNA degradation is associated with PSTVd pathogenesis. In the native *Sl*Myb mRNA, the 3′ UTR-directed degradation (Fig. 9a) was the dominant process. A similar degradation process was detectable in older and more senescent control leaf tissues (not shown). Thus, we speculate that the degradation process is coupled to a senescence network prematurely induced by viroid pathogenesis. We measured mRNA levels of the tomato homologue of leaf senescence marker SEN3, polyubiquitin (Park et al., 1998). Indeed, SlSEN3 mRNA was almost twice as abundant in young PSTVd-AS1-infected leaf tissues (208%) at the beginning of symptom development in PSTVd-sensitive cv. Rutgers compared to controls.

We expected in our analyzed LiCl-soluble fraction various fragments of *Sl*Myb mRNA processed by 5′ to 3′ exoribonucleases of the XRN class (Nagarajan et al., 2013) or by combination of XRNs with additional factors. Recently, Hou et al. (2014) recovered seven sequence motifs associated with uncapped 5′ ends from degradome data sets that are a mixture of the randomly and specifically degraded products of various degradation pathways. Two of these motifs (HTGTAMWK and MCAGAC) are present in the *Sl*Myb mRNA sequence. HTGTAMWK (see Fig. 9a) is a binding site for Pumilio/Fem-3 mRNA binding factor (PUF) proteins; PUF binding may result in the production of uncapped 5′ ends and deadenylation; MCAGAC is described as a further motif overrepresented close to mRNA degradation sites (Hou et al., 2014). The first motif is close to our mapped degradation fragments. One explanation of the general mRNA imbalance within the pathogenesis network mediated by lethal PSTVd variants might involve a change in specificity of some factors and also some motifs of degradation pathways upon viroid pathogenesis.

In addition, we observed that PSTVd-AS1-induced suppression of necrotic leaf-tissue reactions in *N. benthamiana* is mediated by Myb overexpression. The high Myb level, if supported by silencing suppressors, led to a more intensive necrosis in a shorter time interval. The necrotic reaction is inhibited in AS1-infected tissue; contrary to that, application of silencing suppressors clearly suppresses the inhibition mediated by AS1, which confirmed that *Sl*Myb is rapidly degraded in infected plant tissues. *Sl*Myb mRNA fragments with free 5′ phosphates were detected in 5′ and 3′ regions and 3′ UTR, as shown by our mRNA quantitative probing, modified RACE technology, Northern and Southern blot analyses. Although this degradation appeared in absence of cleavable vsRNA targets in *Sl*Myb mRNA, the process was influenced by silencing suppressors. In conclusion, we propose that intensive *Sl*Myb degradation is interconnected with PSTVd-AS1-induced pathogenesis that might be caused by silencing mechanism(s) due to action of vsRNAs upon other targets (Navarro et al., 2012). Although it does not follow from our results which vsRNAs, either primary or secondary, are involved in the pathogenesis network mediating *Sl*Myb degradation, our results are consistent with the role of p19 as silencing suppressor that interferes with the role of small RNAs and presumably vsRNAs (Fig. S10). An application of p19 stabilizes *Sl*Myb expression and leads to a quick necrotic response. The same seems to be true for p19-mediated inhibition of PSTVd AS1. In this case, p19-mediated suppression of some vsRNAs or secondary small RNAs abolishes PSTVd-mediated degradation at an early stage and leads to stabilized *Sl*Myb expression subsequently initiating the necrotic reaction. This assumption remains to be elucidated in the future.

Functions of SANT/HTH-Myb and a possible role of the Myb deficiency in PSTVd-induced pathogenesis network

We found that *Sl*Myb induced necroses if overexpressed in *N. benthamiana* leaf sectors or during ectopic 35S CaMV promoter-driven expression in *N. benthamiana* transgenotes. This deleterious effect was suppressed by lethal PSTVd-AS1 and is accompanied by nucleolytic activities; this reveals a connection to apoptotic reactions, which was not further studied in this work. Simultaneously, the induction of necroses manifests the polyfunctionality of this protein. This is also consistent with the ectopic overexpression that led to malformation of flower corollae, shortening of corolla tubes and plant stunting in some transgenic lines; mutual silencing of the homologous internal Myb gene of *N. benthamiana* and the *Sl*Myb transgene explains this phenomenon. Furthermore, this is consistent with the same morphological symptoms induced by VIGS of the Myb homologue in *N. benthamiana* (see Fig. S6, panel II, E and G). The SANT domains of Myb might participate in chromatin re-modeling (for review see e. g. Fisher and Franklin, 2011). Additionally, *Sl*Myb overexpression led to plant weakness and stunting (Fig. S6, panel II). These symptoms of Myb deficiency were much stronger in VIGS-treated, PSTVd-AS1-infected plants due to the synergism between the modified virus component and PSTVd (not shown).

Finally one can address the question whether deficiency of *Sl*Myb could contribute to the pathogenesis network. The character of some symptoms like collapsing of leaf development, leaf malformation, reduction of flowering, flower size and malformation, and plant stunting is consistent with this assumption. In addition, *Sl*Myb deficiency was not observed in the tolerant, symptomless tomato genotype cv Harzfeuer, suggesting its possible role in the pathogenesis network in dominating sensitive genotypes.

Acknowledgments

Authors acknowledge significant support by Dr. Csaba Koncz (Max Planck Institute for Plant Breeding Research, Köln), for fruitful discussions and for providing some materials for degradome analyses. We thank Prof. em. Detlev Riesner (Institute of Physical Biology, Heinrich-Heine-Universität Düsseldorf) for fruitful consultations and for providing some materials. We thank Helena Matoušková, Lidmila Orctová, and Olga Horáková (BC v. v. i. ASCR IPMB) for excellent technical assistances, Mgr. Kateřina Uhlířová (BC v. v. i. ASCR IPMB) for her help with quantitative mRNA analyses, and Martin Selinger and Jaroslav Ondruš, students of the South Bohemian University, for their assistances, laboratory work and help with preparation of transgenic materials. The project was supported by the Alexander von Humboldt Foundation, Research Group Linkage Programme, by the Czech Science Foundation (GACR P501/10/J018), by the cooperative project FP7-REGPOT-2012-2013-1 MODBIOLIN no. 316304, and by institutional support RVO:60077344 to JM. JP was supported by the graduate school E-Norm (HHUD). All authors have no conflict of interest to declare.

Appendix A. Supplementary data

Supplementary data associated with this article can be found, in the online version, at http://dx.doi.org/10.1016/j.jplph.2015.06.001

References

Cubas, P., Lauter, N., Doebley, J., Coen, E., 1999. The TCP domain: a motif found in proteins regulating plant growth and development. Plant J 18, 215–222.

Di Serio, F., Martínez de Alba, A.E., Navarro, B., Gisel, A., Flores, R., 2009. RNA-dependent RNA polymerase 6 delays accumulation and precludes meristem invasion of a viroid that replicates in the nucleus. J Virol 84, 2477–2489.

Diener, T.O., Hammond, R.W., Black, T., Katze, M.G., 1993. Mechanism of viroid pathogenesis: differential activation of the interferon-induced, double-stranded RNA-activated, M 68,000 protein kinase by viroid strains of varying pathogenicity. Biochimie 75, 533–538.

Diermann, N., Matoušek, J., Junge, M., Riesner, D., Steger, G., 2010. Characterization of plant–miRNAs and small RNAs from potato spindle tuber viroid (PSTVd) in infected tomato. Biol Chem 391, 1379–1390.

Eamens, A.L., Smith, N.A., Dennis, E.S., Wassenegger, M., Wang, M.B., 2014. In *Nicotiana* species, an artificial microRNA corresponding to the virulence modulating region of Potato spindle tuber viroid directs RNA silencing of a soluble inorganic pyrophosphatase gene and the development of abnormal phenotypes. Virology 450–451, 266–277.

Fahlgren, N., Carrington, J.C., 2010. miRNA target prediction in plants. Methods Mol Biol 592, 51–57.

Fisher, A.J., Franklin, K.A., 2011. Chromatin remodelling in plant light signalling. Physiol Plant 142, 305–313.

Füssy, Z., Patzak, J., Stehlík, J., Matoušek, J., 2013. Imbalance in expression of hop (*Humulus lupulus*) chalcone synthase H1 and its regulators during hop stunt viroid pathogenesis. J Plant Physiol 170, 688–695.

German, M.A., Luo, S., Schroth, G., Meyers, B.C., Green, P.J., 2009. Construction of Parallel Analysis of RNA Ends (PARE) libraries for the study of cleaved miRNA targets and the RNA degradome. Nat Protoc 4, 356–362.

Hadidi, A., Flores, R., Randles, J., Semancik, J. (Eds.), 2003. Viroids. CSIRO Publishing, Australia.

Hammann, C., Steger, G., 2012. Viroid-specific small RNA in plant disease. RNA Biol 9, 809–819.

Hellens, R.P., Edwards, E.A., Leyland, N.R., Bean, S., Mullineaux, P.M., 2000. pGreen: a versatile and flexible binary Ti vector for *Agrobacterium*-mediated plant transformation. Plant Mol Biol 42, 819–832.

Horsch, R.B., Fry, J.E., Hoffman, N.L., Eichholtz, D., Rogers, S.G., Fraley, R.T., 1985. A simple and general method for transferring genes into plants. Science 227, 1229–1231.

Hou, C.Y., Wu, M.T., Lu, S.H., Hsing, Y.I., Chen, H.M., 2014. Beyond cleaved small RNA targets: unraveling the complexity of plant RNA degradome data. BMC Genomics 15, 15.

Itaya, A., Matsuda, Y., Gonzales, R.A., Nelson, R.S., Ding, B., 2002. Potato spindle tuber viroid strains of different pathogenicity induces and suppresses expression of common and unique genes in infected tomato. Mol Plant Micr Int 15, 990–999.

Itaya, A., Zhong, X., Bundschuh, R., Qi, Y., Wang, Y., Takeda, R., et al., 2007. A structured viroid RNA serves as substrate for Dicer-like cleavage to produce biologically active small RNAs but is resistant to RISC-mediated degradation. J Virol 81, 2980–2994.

Katoh, K., Toh, H., 2008. Improved accuracy of multiple ncRNA alignment by incorporating structural information into a MAFFT-based framework. BMC Bioinformatics 9, 212.

Keese, P., Symons, R.H., 1985. Domains in viroids: evidence of intermolecular RNA rearrangement and their contribution to viroid evolution. Proc Natl Acad Sci USA 82, 4582–4586.

Kim, K.N., Cheong, Y.H., Gupta, R., Luan, S., 2000. Interaction specificity of Arabidopsis calcineurin B-like calcium sensors and their target kinases. Plant Physiol 124, 1844–1853.

Kuroyanagi, M., Yamada, K., Hatsugai, N., Kondo, M., Nishimura, M., Hara-Nishimura, I., 2005. Vacuolar processing enzyme is essential for mycotoxin-induced cell death in *Arabidopsis thaliana*. J Biol Chem 280, 32914–32920.

Lee, S.C., Lan, W.Z., Kim, B.G., Li, L., Cheong, Y.H., Pandey, G.K., et al., 2007. A protein phosphorylation/dephosphorylation network regulates a plant potassium channel. Proc Natl Acad Sci USA 104, 15959–15964.

Matoušek, J., Dědič, P., 1988. Acid nucleases in PSTV-infected tomato (*Lycopersicon esculentum* L.) I. Levels of acid nuclease activity in healthy and PSTV-infected tomato leaves and callus tissues. J Plant Physiol 133, 340–344.

Matoušek, J., Junker, V., Vrba, L., Schubert, J., Patzak, J., Steger, G., 1999. Molecular characterization and genome organization of 7 SL RNA genes from hop (*Humulus lupulus* L.). Gene 239, 173–183.

Matoušek, J., Kozlová, P., Orctová, L., Schmitz, A., Pešina, K., Bannach, O., et al., 2007. Accumulation of viroid-specific small RNAs and increase of nucleolytic activities linked to viroid-caused pathogenesis. Biol Chem 388, 1–13.

Matoušek, J., Schröder, A.R.W., Trněná, L., Reimers, M., Baumstark, T., Dědič, P., et al., 1994. Inhibition of viroid infection by antisense RNA expression in transgenic plants. Biol Chem 375, 765–777.

Matoušek, J., Stehlík, J., Procházková, J., Orctová, L., Wullenweber, J., Füssy, Z., et al., 2012. Biological and molecular analysis of the pathogenic variant C3 of potato spindle tuber viroid (PSTVd) evolved during adaptation to chamomile (*Matricaria chamomilla*). Biol Chem 393, 605–615.

Matoušek, J., Trněná, L., Svoboda, P., Oriniaková, P., Lichtenstein, C.P., 1995. The gradual reduction of viroid levels in hop mericlones following heat therapy: a possible role for a nuclease degrading dsRNA. Biol Chem 376, 715–721.

Matoušek, J., Vrba, L., Škopek, J., Orctová, L., Pešina, K., Heyerick, A., et al., 2006. Sequence analysis of a "true" chalcone synthase (*chs*_H1) oligofamily from hop (*Humulus lupulus* L.) and PAP1 activation of *chs*_H1 in heterologous systems. J Agric Food Chem 54, 7606–7615.

Nagarajan, V.K., Jones, C.I., Newbury, S.F., Green, P.J., 2013. XRN 5′ 3′ exoribonucleases: structure, mechanisms and functions. Biochim Biophys Acta 1829, 590–603.

Navarro, B., Gisel, A., Rodio, M.E., Delgado, S., Flores, R., Di Serio, F., 2012. Small RNAs containing the pathogenic determinant of a chloroplast-replicating viroid guide the degradation of a host mRNA as predicted by RNA silencing. Plant J 70, 991–1003.

Naz, A.A., Raman, S., Martinez, C.C., Sinha, N.R., Schmitz, G., Theres, K., 2013. *Trifoliate* encodes an MYB transcription factor that modulates leaf and shoot architecture in tomato. Proc Natl Acad Sci USA 110, 2401–2406.

Ori, N., Cohen, A.R., Etzioni, A., Brand, A., Yanai, O., Shleizer, S., et al., 2007. Regulation of *LANCEOLATE* by miR319 is required for compound-leaf development in tomato. Nat Genet 39, 787–791.

Otto, C., Stadler, P.F., Hoffmann, S., 2014. Lacking alignments? The next generation sequencing mapper segemehl revisited. Bioinformatics 30, 1837–1843.

Owens, R.A., Tech, K.B., Shao, J.Y., Sano, T., Baker, C.J., 2012. Global analysis of tomato gene expression during *Potato spindle tuber viroid* infection reveals a complex array of changes affecting hormone signaling. Mol Plant Mic Int 25, 582–598.

Park, J.H., Oh, S.A., Kim, Y.H., Woo, H.R., Nam, H.G., 1998. Differential expression of senescence-associated mRNAs during leaf senescence induced by different senescence-inducing factors in *Arabidopsis*. Plant Mol Biol 37, 445–454.

Pfaffl, M.W., 2001. A new mathematical model for relative quantification in real-time RT-PCR. Nucleic Acids Res 29, e45.

Ratcliff, F., Martin-Hernandez, A.M., Baulcombe, D.C., 2001. Tobacco rattle virus as a vector for analysis of gene function by silencing. Plant J 25, 237–245.

Rodriguez, J.L., Flores, F., 1987. Effects of citrus exocortis viroid infection on the peroxidase/IAA-oxidase system of *Gynura aurantiaca* and *Lycopersicon esculentum*. Biochem Pflanzen 182, 449–457.

Sänger, H.L., 1982. Biology, structure, functions and possible origin of viroids. In: Parthier, B., Boulter, D. (Eds.), Nucleic acids and proteins in plants II, structure, biochemistry and physiology of nucleic acids. Encyclopedia of plant physiology, Vol. 14B. Springer, Berlin, pp. 368–454.

Schumacher, J., Meyer, N., Riesner, D., Weidemann, H.L., 1986. Diagnostic procedure for detection of viroids and viruses with circular RNAs by "return"-gel electrophoresis. J Phytopath 115, 332–343.

Sun, Y.H., Lu, S., Shi, R., Chiang, V.L., 2011. Computational prediction of plant miRNA targets. Methods Mol Biol 744, 175–186.

Tomato Genome Consortium, 2012. The tomato genome sequence provides insights into fleshy fruit evolution. Nature 485, 635–641.

Torres-Schumann, S., Ringli, C., Heierli, D., Amrhein, N., Keller, B., 1996. *In vitro* binding of the tomato bZIP transcriptional activator VSF-1 to a regulatory element that controls xylem-specific gene expression. Plant J 9, 283–296.

Trněná, L., Matoušek, J., 1991. Aminopeptidase activity in potato spindle tuber viroid-infected tomato leaves. Arch Phytopathol Plant Prot 27, 117–125.

Vera, P., Conejero, V., 1988. Pathogenesis-related proteins of tomato: p-69 as an alkaline endoproteinase. Plant Physiol 87, 58–63.

Wang, Y., Shibuya, M., Taneda, A., Kurauchi, T., Senda, M., Owens, R.A., et al., 2011. Accumulation of *Potato spindle tuber viroid*-specific small RNAs is accompanied by specific changes in gene expression in two tomato cultivars. Virology 413, 72–83.

Weinberg, Z., Breaker, R.R., 2011. R2R—software to speed the depiction of aesthetic consensus RNA secondary structures. BMC Bioinformatics 12, 3.

Wilm, A., Linnenbrink, K., Steger, G., 2008. ConStruct: improved construction of RNA consensus structures. BMC Bioinformatics 9, 219.

Woltering, E.J., 2004. Death proteases come alive. Trends Plant Sci 9, 469–472.

Characterization of a viroid-induced tomato degradome.

Preface

In the following manuscript we describe viroid-driven degradation of endogenous transcripts of host plants. We observed the differential degradation of key transcripts related to the host defense. Because experimental quantitative polymerase chain-reactions (qPCR) are missing, we are unable to conclude if host transcript degradation results from overexpression, increasing random degradation, or from viroid-orchestrated host reprogramming. In the latter framework, degradation intensities and dynamics are due to infecting viroid variants that pursue to reprogram host pathways by giving rise to pathogenesis networks of exogenous and endogenous small RNAs like vsRNAs, siRNAs, miRNAs, and phasiRNAs.

Introduction

Plants constitute the primary source of energy for the biosphere by transforming light into biological utilizable energy via photosynthesis. The existence of many organisms from all kingdoms of life and pathogens like viroids, viruses and bacteria depend primarily or secondarily on this synthesis. Plant pathogens constantly threaten crop yield and consequently existential needs of modern civilizations. Plants are targeted with distinct modes of action by diverse classes of pathogens that range in size between viroids (single-stranded, non-coding, and circular RNAs of 250-400 nucleotides length) to insects and mammals. In response to this broad range of threats, plants evolved diverse defense systems that recognize the class of pathogen and direct a pathogen-specific response against them. One integral defense system is the systemic acquired resistance (SAR). Within this pathway, mobile signals like hormones or small RNAs are generated in infected tissues and are transported to healthy tissues. Upon sensing these mobile signals, cells induce the expression of defense-related RNAs and proteins. Plant pathogens are classified into the following three categories: biotrophic, necrotrophic, and hemi-biotrophic. Biotrophic plant pathogens exploit resources from living tissue. In higher plants mobile signals like salicylic acid (SA) activate a biotrophic pathogen-specific SAR response inducing the transcription of Pathogenesis-related proteins 1 (PR-1; Pieterse et al., 2009). The SA pathway mediates the hypersensitive response (HR; Loake and Grant, 2007) leading to programmed cell death (PCD; Heath, 2000). The plant HR induces reactive oxidative species (ROS) that reinforce cell walls (for review see Torres et al., 2006), effectively denying access to resources which are required by the pathogen for systematic infections and propagation. In contrast, necrotrophic plant pathogens exploit host resources in the form of necrotic tissue. In response to this class, the plant defense keeps infected tissue alive as long as possible mediated by jasmonic acid (JA) and ethylene (ET) signaling to block resources for the pathogens growth (Glazebrook, 2005). Hemi-biotrophic pathogens switch between biotrophic and necrotrophic life styles (Mendgen and Hahn, 2002). In an arms race with this pathogen class, host plants rely on the biotrophic SA-mediated defense (Glazebrook et al., 1996). It is critical for plants to classify infecting pathogens and modulate an appropriate defensive response. The responses effectively revoke pathogen-required resources for growth; f. e. in the case of necrotrophic pathogens a HR response, including the induction of ROS, would support the infecting pathogen.

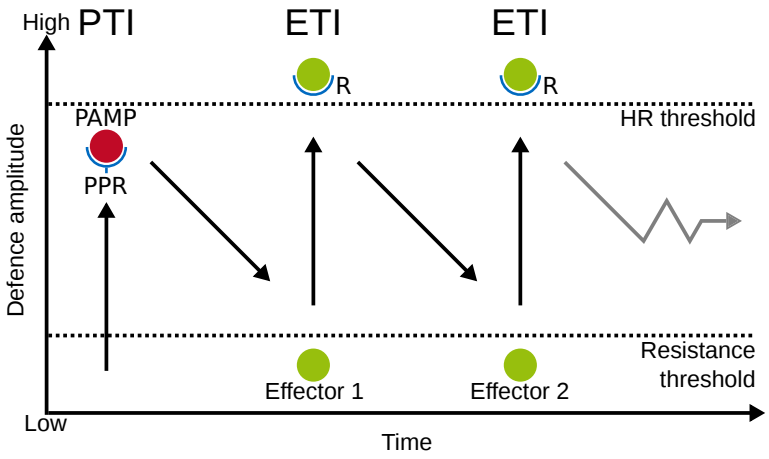

Figure 3.1: Zigzag model of plant-pathogen interactions. Pathogen-challenged hosts recognize pathogen-associated molecular patterns (PAMPs) (red dot) with Toll-like receptors (TLRs) or pattern-recognition receptors (PRRs) within the innate PAMP/pattern-triggered immunity (PTI) response; this response is countered by a pathogen-induced effectors (green dots). The plant host employs *R* genes and proteins to recognize pathogen-induced effectors within the adaptive effector-triggered immunity (ETI) response. The zigzag-model forces plant-pathogens into a complex interaction network with their host and to balance their pathogenesis between hypersensitive response (HR), adaptive and innate host defense system. Pathogens have to constantly suppress the plant defense system and balance their pathogenesis. Figure adapted from Jones and Dangl (2006).

Plants revoke resources and combat pathogens by a two-layered and interconnected (Tsuda and Katagiri, 2010; Thomma et al., 2011) pathogen defense system that results in the so-called "zigzag model" (see Fig. 3.1; Jones and Dangl, 2006).

In the first layer, plants integrate plasma membrane-localized pattern-recognition receptors (PRRs) as activators of innate immune signaling. These are triggered upon detection of microorganism-associated molecular patterns (MAMPs) or pathogen-associated molecular patterns (PAMPs) (for review see Macho and Zipfel, 2014). The phenylpropanoid pathway (PPP; Ferrer et al., 2008) is highly transcriptionally regulated during PTI and leads to the production of several toxic compounds (Vogt, 2010). Frequently, Receptor-like kinases (RLK) mediate a signal cascade as PRRs to initiate a PAMP-triggered immune response (PTI; Boller and He, 2009; Zipfel, 2014). The PTI response counters biotrophic pathogens by the induction of HR. Pathogens in turn counter the PTI response with effector molecules including RNAs, peptides and proteins (Pumplin and Voinnet, 2013), f. e. RNA silencing suppressors seen in viruses (Kasschau and Carrington, 1998), bacteria (Navarro et al., 2008) or oomycetes (Qiao et al., 2015). The Phenylalanine lyase (PAL) is the central regulatory component of the PPP and other downstream pathways (Vogt, 2010). Upon pathogen infection PAL is differentially expressed through land plants (Oliva et al., 2015). Consequently, the suppression of PTI by pathogens enhances the pathogenicity by breaking the imminent threat by HR.

In the second layer, plants integrate RNAs, peptides, and proteins as an effector-triggered susceptibility (ETS). Plants evolved resistance genes (*R* genes) that encode resistance proteins (R) recognizing and combating pathogen PTI suppressors. If pathogens fail to counter the induction of R, a PCD response is imminent upon recognition. *R* genes are part of the innate host immune system. Frequently, plant pathogen infections induce small RNAs that derive from *R* gene transcripts and other genomic sources (for review see Voinnet, 2009). Exogenous and endogenous small RNAs are 20–24 nt single-stranded RNAs that guide (post-)transcriptional gene silencing ((P)TGS) as guide RNAs to

host transcripts and the genome, a regulatory pathway mediated by ARGONAUTE proteins (AGO; for review see Vaucheret, 2008) and others. The plant adaptive immune system is able to target foreign RNAs like viruses to produce pathogen-derived small interfering RNAs (siRNA) from their genomes. Based on extensive sequence homology, siRNAs are directed against their originating pathogenic genome by the plant defense (Fei et al., 2016).

Both defense layers instruct major and partially distinct transcriptional reprogramming of the host plants (Etalo et al., 2013; Seyfferth and Tsuda, 2014). Plant pathogens are constantly conflicted to balance their pathogenicity to the plant defensive response. While molecular pathways involved in immunity are very well characterized for interactions with pathogens such as viruses, bacteria, fungi, and oomycetes, interactions with viroids are still scarcely described.

Viroids are minimalistic plant pathogens, as described above, composed of a small, unencapsulated, single-stranded and circular RNA of about 250–400 nucleotides (nt). Viroids are non-coding, thus they orchestrate systematic infections and reprogram diverse host plants (Hadidi et al., 2003) based on their primary structure. Here, we study the type-strain of the *Pospiviroidae* family, the Potato spindle tuber viroid (PSTVd). The pathogenesis of symptoms and severity in PSTVd infected *S. lycopersicum* (tomato) range from mild to "lethal" and depend on the infecting PSTVd variant as well as on the host cultivar genotype. Viroid infections are accompanied by viroid-specific small RNAs (vsRNA) that are about 20–24 nt in length (Papaefthimiou et al., 2001). One pathogenicity theorem postulates that vsRNAs exploit the host plant to establish and maintain a viroid-favorable environment by misguiding PTGS to host transcripts (see Fig. 3.2; for review see Hammann and Steger, 2012). Likewise, viruses like members of *Geminiviridae* reshape their hosts by inducing proteins and small RNAs (Hanley-Bowdoin et al., 2013). Recently, vsRNA-mediated cleavage of host transcripts was reported for Peach latent mosaic viroid (PLMVd; Navarro et al., 2012), Tomato planta macho viroid (TPMVd; Avina-Padilla et al., 2015), and PSTVd (Adkar-Purushothama et al., 2015). Viroid infections trigger a defensive response by plants and induce a plant defense-related protein expression (Domingo et al., 1994). The Pathogenesis-related protein PR-1a1, central to the PTI pathway, is induced upon infection by the Citrus exocortis viroid (CEVd; Vera et al., 1993). The highly self-complementary secondary structure of viroids seems to protect the genome from PTGS (Itaya et al., 2007).

We followed the pathogenicity theorem and infected tomato 'Heinz1706' plants (Tomato Genome Consortium, 2012) with two PSTVd variants that induce characteristic symptoms in this cultivar. The mild and "lethal" symptoms inducing QFA and AS1, respectively, were inoculated biolistically (Matousek et al., 2004) to elucidate whether host transcripts are directly targeted by vsRNAs. We describe the viroid-induced degradation regime in hosts by sequencing the host degradome.

Material and Methods

Plant Material

We biolistically inoculated *S. lycopersicum* cv. Heinz 1706 plants with mock, PSTVd variants QFA (mild, GenBank AC U23059.1) and AS1 ("lethal", AY518939.1), respectively. We collected samples for degradome sequencing at 20 days post inoculation (dpi). Additionally, we collected AS1 samples 10 dpi. This resulted in the sets M_{20}, QFA_{20}, $AS1_{10}$, $AS1_{20}$; dpi are indicated by indices.

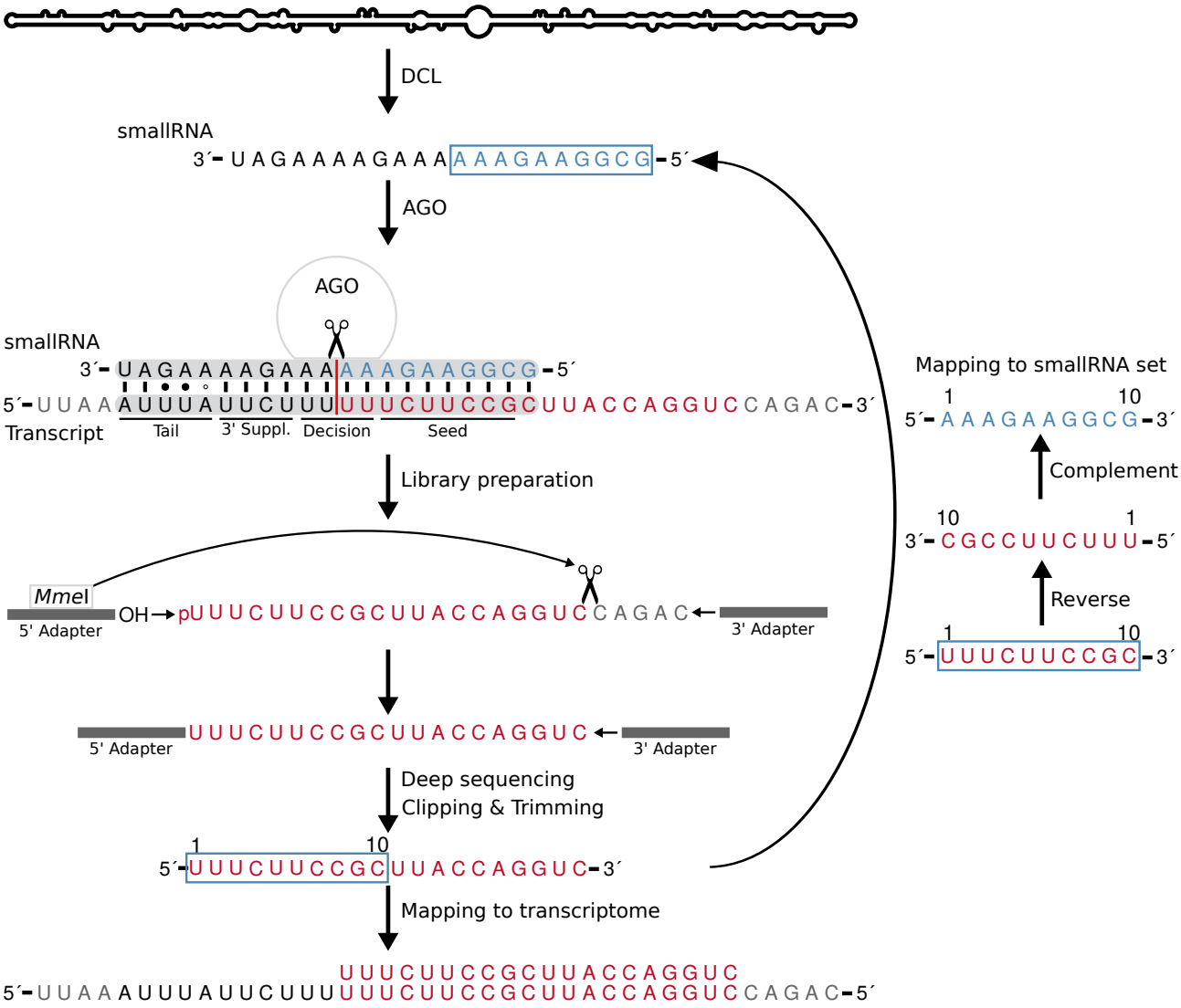

Figure 3.2: Pathogenesis theorem and degradome sequencing. From the viroid genome vsRNAs are excised by DCL (Itaya et al., 2007). Cleavage-competent AGO binds small RNAs like vsRNA forming a binary complex. This complex scans host transcripts for accessible target sites (Tafer et al., 2008), which are identified by extensive sequence complementarity (for review see Ameres and Zamore, 2013). Upon binding a ternary complex is formed and the transcript is cleaved between pos. 10 and 11 relative to the small RNA. Based on the cleavage the original transcript is lost. In degradome sequencing, 5′-adapters and 3′-adapters are ligated to the emerging 3′ fragment. Following AGO-mediated cleavage transcript fragments are identified by a characteristic 5′-monophosphate. This end is recognized by an adapter with an attached hydroxyl group. The 5′-adapter contains a *Mme*I binding site. Upon binding the endonucleases *Mme*I cleaves 20 nt downstream. A 3′-adapter is ligated to the produced RNA fragment and the construct is sequenced. Within a computational pipeline the resulting sequences are clipped, trimmed and mapped back to the host transcripts. The mapping allows the identification of the original transcript and indicates the cleavage site. Based on suspected extensive sequence complementarity between guide RNA and transcript, degradome reads start from positions $i = \{1, 2, 3\}$ and are clipped after ten nucleotides each. The resulting truncated reads are mapped as reverse complement back to the respective inoculated PSTVd genome to determine potential vsRNA-mediated cleavage.

Degradome

Leaf samples of the inocuclated plants were collected, prepared and the degradomes sequenced (German et al., 2008, 2009) at LC Sciences (Houston, TX, USA). We processed raw degradome reads with TRIMMOMATIC (Bolger et al., 2014) and clipped reads to 19–21nt length based on the expected length according to the protocol (see Fig. 3.2). Subsequently, we mapped the degradome reads with 100% accuracy to the tomato transcriptome (ITAG2.40) using SEGEMEHL v. 2.0 (Hoffmann et al., 2014).

Differential Degradation

We counted mapped reads to transcripts with HTSEQ-COUNT (Anders et al., 2015) and used DESEQ2 (Love et al., 2014) for differential degradation analysis (filtered for $\log_2(\text{FoldChange}) \geq 1$ and $P \leq 0.05$). We created each subset of the viroid-infected samples by pooling viroid-samples in different combinations with the mock-inoculated sample to identify variant-specific and set-specific degradation regimes (see Fig. 3.3a). We reconstructed set-specific plant pathways connected to differentially degraded transcripts using the Kyoto Encyclopedia of Genes and Genomes (KEGG; Kanehisa and Goto, 2000) to estimate viroid-induced degradation regimes using BLASTKOALA (Kanehisa et al., 2015).

small RNA target prediction

We followed two approaches to computationally validate the pathogenesis theorem.

First, we used CLEAVELAND ver. 4.0 (Addo-Quaye et al., 2009) for the prediction of potential vsRNA targets. Predicted target sites are categorized; we considered categories zero and one; i. e., a predicted target site exhibits more than one read and a unique maximal read peak at the target site or multiple maximal read peaks at different sites.

Second, we developed a method REDEGRADMAP (see Fig. 3.2) to trace back degradome fragments to the small RNA that guided the cleavage. Based on the characteristics of degradation, the target site implies the nucleotide composition of the guide RNA. Small RNA-cleaved transcripts exhibit a near perfect sequence complementarity with the guiding small RNA at least in the so-called “seed region" (pos. 2–8) and the “decision region” (pos. 9–12) (Pasquinelli, 2012). Hence, degradome sequencing-derived reads should exhibit high sequence complementarity to the guide RNA up to pos. 10 because of the cleavage between pos. 10–11 (relative to the guide RNA). Hence, by remapping the reverse complement of pos. 1–10 of the degradome reads, reconstruction of the origin is possible under the assumption of perfect sequence complementarity.

Results

We analyzed the viroid-induced degradome of infected tomato plants. We were unable to reproduce well-established relations between conserved endogenous miRNAs and cleavage sites on tomato transcripts even in the mock-inoculated sample (see Tab. 3.1). The degradome reads contained many inconclusive reads including 5′-to-3′-adapters. After trimming the reads, only about 11% of the original reads where usable.

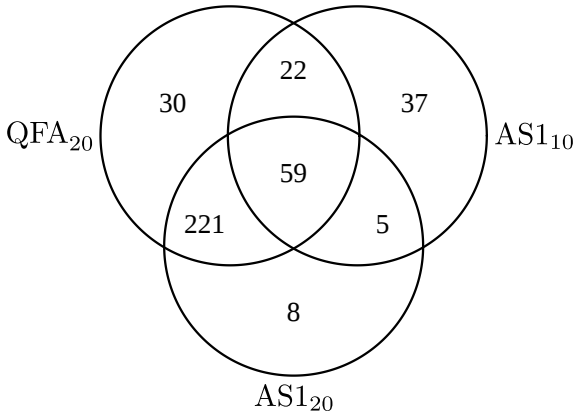

(a) Differentially degradation sets.

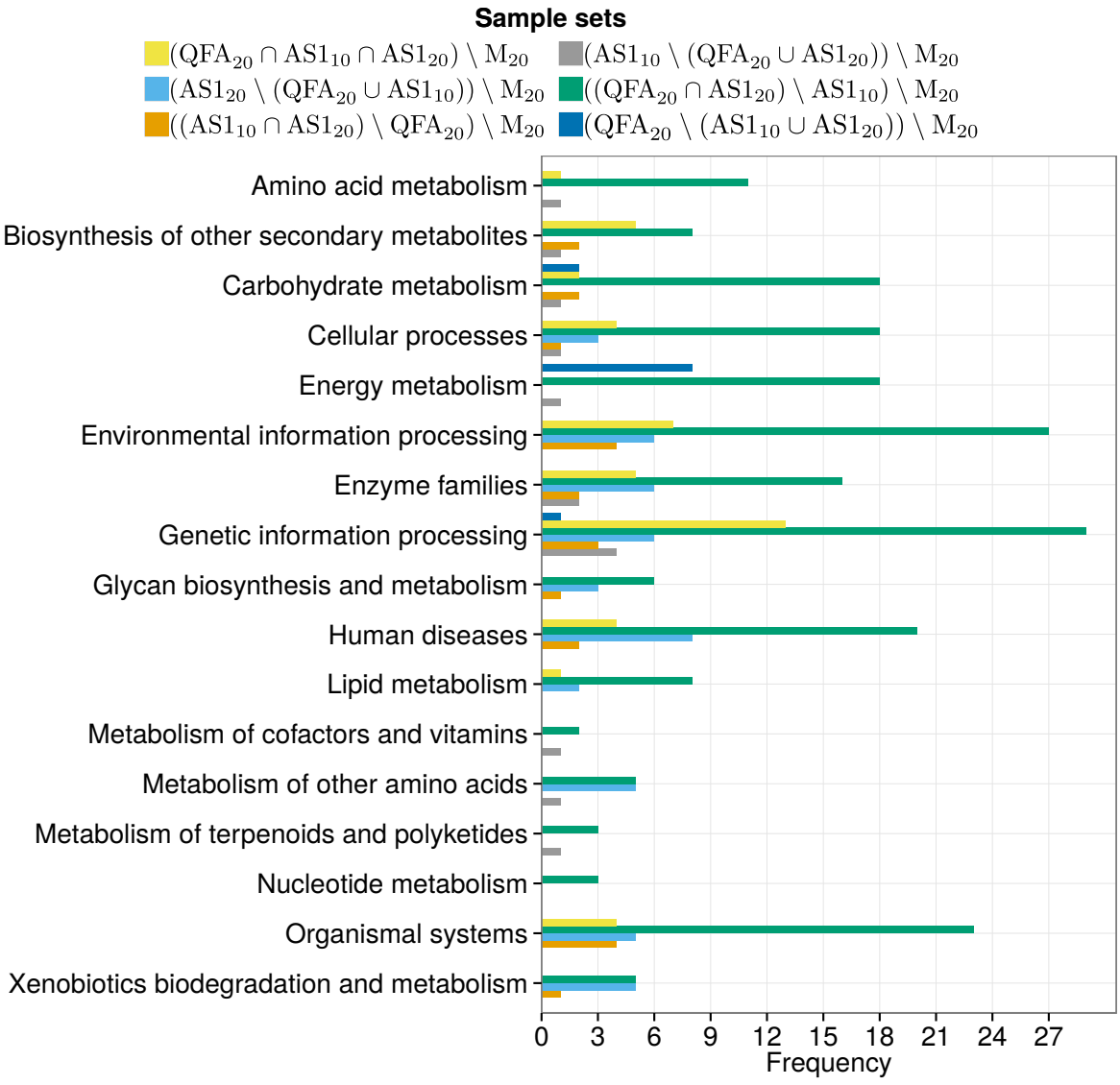

(b) Overview of metabolic pathways affected by differential degradation.

Figure 3.3: Viroid-induced differential degradation of host transcript. (a) Common to all PSTVd-infected samples independent for the point in time are 59 transcripts. Interestingly, both AS1 infected samples share only five exclusive degraded transcripts, whereas QFA_{20} and $AS1_{20}$ share 221. Hence, a time-dependent effect appears in the differential host degradation. (b) BLASTKOALA annotated viroid-induced differential degraded host transcripts based on subsets of samples (see color code at top).

Table 3.1: Endogenous miRNA-guided cleavage of tomato transcripts predicted by CLEAVELAND. Reconstruction of miRNA-transcript relation based on established relations between endogenous miRNAs and cleaved tomato transcripts by Karlova et al. (2013).

			#Reads[a]			
miRNA	Transcript	Slice[b]	M_{20}	QFA_{20}	$AS1_{10}$	$AS1_{20}$
sly-miR160a	Solyc06g075150.2.1	1502	0	0	1	1
sly-miR160a	Solyc11g013470.1.1	554	0	0	0	2
sly-miR160a	Solyc11g069500.1.1	1313	0	1	1	0
sly-miR168a-5p	Solyc06g072300.2.1	2118	0	0	0	1
sly-miR168b-5p	Solyc06g072300.2.1	2118	1	0	0	0
sly-miR171d	Solyc08g078800.1.1	404	0	0	1	0
sly-miR171e	Solyc01g090950.2.1	1578	0	0	0	1
sly-miR172a	Solyc04g049800.2.1	1117	0	0	0	2
sly-miR396a-5p	Solyc04g077510.2.1	895	0	1	0	0
sly-miR396a-5p	Solyc08g005430.2.1	395	0	0	1	0
sly-miR396a-5p	Solyc08g075950.1.1	386	1	1	0	0
sly-miR396b	Solyc02g062740.2.1	1161	0	2	0	1
sly-miR396b	Solyc10g083510.1.1	587	0	1	0	0
sly-miR403-3p	Solyc02g069260.2.1	3260	0	0	0	1
sly-miR5300	Solyc05g005330.2.1	1747	1	0	0	0
sly-miR6027-3p	Solyc04g009660.2.1	1309	0	0	1	0
sly-miR9471a-3p	Solyc01g104400.2.1	147	0	0	1	1

[a] Number of reads starting at the slice position
[b] Transcript cleavage site

Viroid-specific differential degradation

We analyzed the degradome for significantly differentially degraded host transcripts upon PSTVd infection (see Tab. S1). We determined differential degradation regimes for all sample combinations to determine time (in-)dependent effects. Based on the subsets we identified degradation regimes (see Fig. 3.3a). We characterized four selected regimes and analyzed the pathway enrichment using BLASTKOALA (see Fig. 3.3b). We determined 59 commonly transcripts that were differentially degraded in a time-independent manner between the healthy and infected samples. The differentially degraded host transcripts common in all three PSTVd samples are predominantly connected to genetic information processing, environmental information processing and cellular processes. Interestingly, grouping the mild QFA_{20} and "lethal" $AS1_{20}$ yielded the highest overlap with 221 transcripts shared between these samples, indicating a time dependence but not pathogenesis dependence of host transcript degradation. Within this set, we observed an enrichment of degraded transcripts related to genetic information processing, environmental information processing, and organismal systems. Within the PSTVd variant-specific differentially degraded host transcripts, we observed an enrichment of energy metabolism, genetic information processing, and environmental information processing related pathways for QFA_{20}, $AS1_{10}$, and $AS1_{20}$, respectively.

The differential degradation dynamics revealed transcripts with one or more distinct degradome peaks, indicative for a sequence-specific small RNA cleavage. Other transcripts lacked distinct sites but exhibited degradation from many sites. The underlying mode of action acting on the latter transcripts remains an open question. Relation between endogenous or exogenous small RNAs, f. e. vsRNAs, and transcripts with conclusive distinct cleavage sites remain to be established. Common,

Table 3.2: Selected differentially degraded host transcripts.

Transcript	M_{20}	QFA_{20}	$AS1_{10}$	$AS1_{20}$	Description[a]
Solyc02g077040.2.1	0	17	63	234	Phytophthora-inhibited protease 1 (PIP1)
Solyc01g006300.2.1	0	6	42	136	Solanum lycopersicum peroxidase (CEVI-1)
Solyc00g174330.2.1	0	4	32	132	Pathogenesis related protein 1a (PR1a1)
Solyc00g174340.1.1	0	4	149	633	Pathogenesis-related protein 1b (PR1b1)
Solyc09g007010.1.1	0	1	10	90	Pathogenesis-related protein P4 (P4)
Solyc10g086180.1.1	10	99	24	118	Phenylalanine ammonia-lyase (PAL)
Solyc12g015880.1.1	100	403	247	963	Heat shock protein 90 (HSP90)

[a] Annotations where adjusted based on BLAST searches.

time-independent significantly differential degradation were connected to plant defense-related transcripts; selected prominent transcripts are described in the following (see Tab. 3.2 and Fig. 3.4):

- The Phytophthora-inhibited Protein 1 (PIP1, Solyc02g077040.2.1, NM_001247020; Tian et al., 2007) was identified as a pathogenesis-related protein with a role in fungal resistance. PIP1 is SA–induced and closely related to required for *C. fulvum* resistance 3 (*Rcr3*) (Dixon et al., 2000), a papain-like cysteine protease under balancing selection in tomato (Hörger et al., 2012). We determined that it was massively degraded upon viroid infection with two AS1-specific peaks (see Fig. 3.4b).

- We identified the citrus exocortis viroid-induced 1 (CEVI-1) transcript as differentially degraded in viroid-infected plants with extensive cleavage in AS1-infected hosts. CEVI-1 is induced upon viroid infection and is characterized as a lignin-peroxidase that is hypothesized to lead to defects in rooting and cell wall extension. CEVI-1 is the most abundantly expressed protein in leaves after 14 dpi and its induction coincides with PR-1 (Vera et al., 1993).

- The degradomes of QFA-infected and AS1-infected samples exhibit a significant enrichment of different PR-1 transcripts with a PSTVd variant severity-dependent intensity (see Fig. 3.4a). Assumingly, PSTVd-infections down-regulate PR-1 expression blocking the downstream plant defense response (see Fig: 3.5). Silencing of PR-1 genes in tabacco revealed increased susceptibility to infections and PR-1 induction is dependent on SA (Rivière et al., 2008).

- We identified the Phenylalanin ammonia-lyase (PAL, Solyc10g086180.1.1) as a common PSTVd-induced differentially degraded target. PAL is central to the PPP pathway (Vogt, 2010) and its transcript is degraded upon viroid infection (see Fig. 3.4d). In plants, PAL-mediates the production of SA in response to pathogens (Mauch-Mani and Slusarenko, 1996) and is crucial to other secondary metabolic pathways f. e. anthocyanin (for review see MacDonald and D'Cunha, 2007). PAL acts as a positive regulator of SA-dependent defense signaling to combat microbial pathogens via its enzymatic activity in PPP (Kim and Hwang, 2014). In epigenetically PAL-suppressed tobacco plants, a tobacco mosaic virus (TMV) exhibited a different course of pathogenesis including lower SA levels and no induction of pathogenesis-related proteins (Pallas et al., 1996). Because of its central role in the PPP pathway, PAL appears as a plausible target of viroid-directed degradation.

- We identified the heat shock protein 90 (HSP90) to be differential degraded notably in the $AS1_{20}$ infection (see Fig. 3.4e). HSP90 is essential for the resistance to diverse pathogens by facilitat-

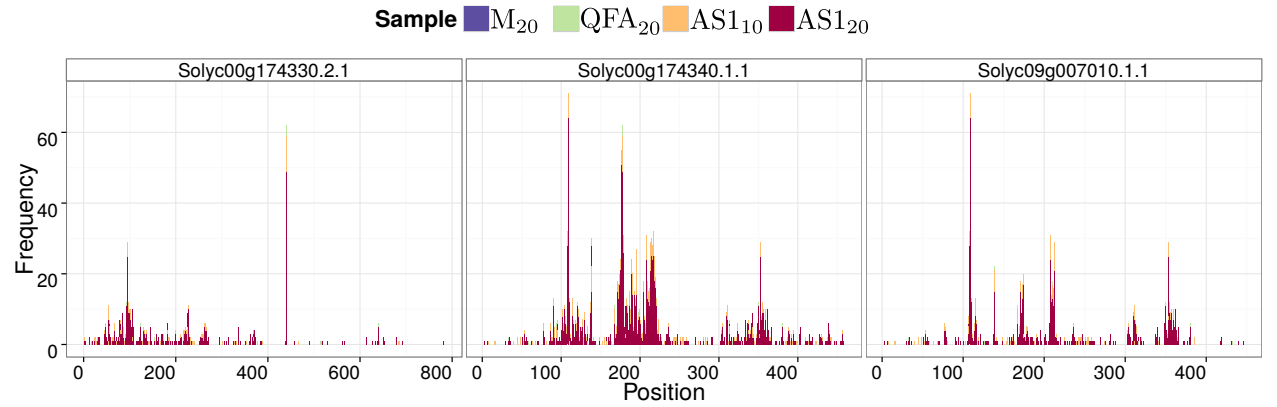

(a) Degradome of three Pathogenesis-related proteins.

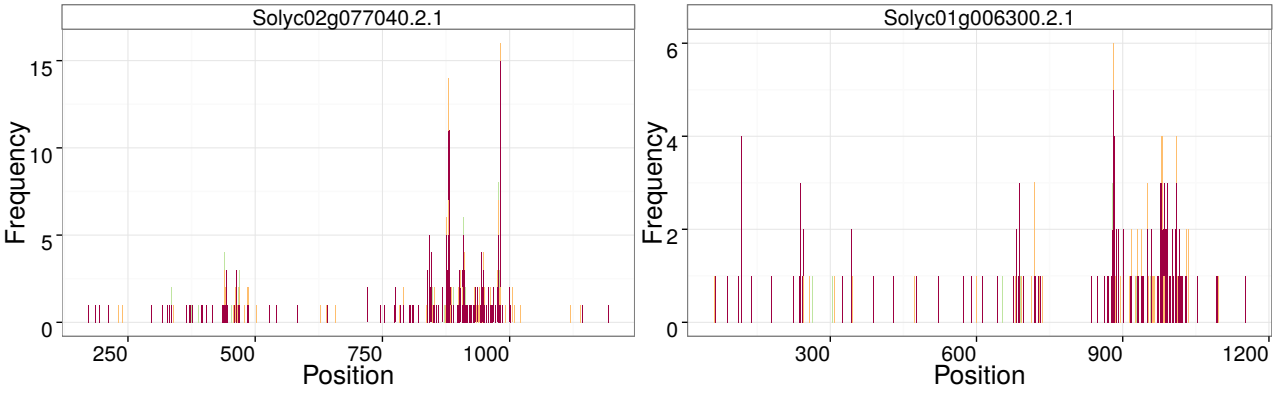

(b) PIP1

(c) CEVI-1

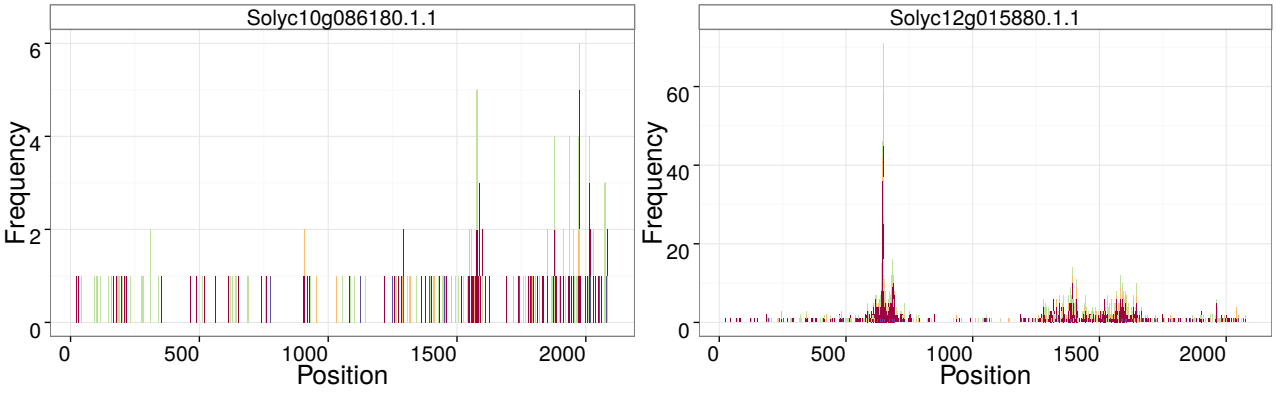

(d) PAL (e) HSP90

Figure 3.4: Selected viroid-induced differentially degraded host transcripts. The amount of reads at cleavage positions are shown. Expression of reads at the most conclusive cleavage site positions are indicated in the following order: (M_{20}/QFA_{20}/$AS1_{10}$/$AS1_{20}$). The color code for the datasets is given at the top. (a) Differentially degradation of host PR-1s transcripts. In PR1a1 (Solyc00g174330.2.1) the main degradation site is located at pos. 440 with (0/3/10/49). PR1b1 (Solyc00g174340.1.1) and P4 (Solyc09g007010.1.1) exhibit a main degradation site at pos. 109 with (0/0/7/64). All PR-1 transcripts exhibit multiple cleavage sites with a suspected formation of phased small RNAs. (b) PIP1 is induced by SA with a critical role in plant pathogen defense. A significant degradation is determined in AS1-infected samples at two positions. The main degradation site at pos. 981 with (0/0/1/15) is exclusive for AS1. (c) CEVI-1 was previously discovered as a viroid-induced host protein connected to PR-1 proteins. The main cleavage products derive from pos. 882 with (0/0/1/5). (d) PAL mediates the production of SA in response to pathogen infection and is central to the PPP pathway. Degradation-derived reads originate from pos. 1975 with (0/1/0/5). (e) HSP90 has key roles in chaperoning PR-1 proteins and facilitates small RNA loading into AGO; a major cleavage site is located at pos. 647 with (2/12/14/43).

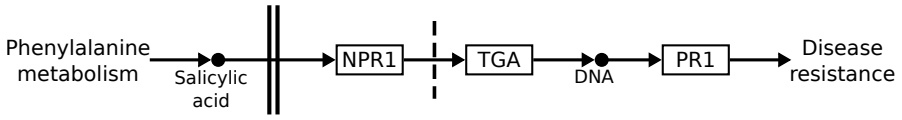

Figure 3.5: The phenylalanine metabolism pathway. The cleavage of PR-1 transcripts block a signal cascade to inhibit downstream disease resistance.

ing correct folding of R proteins (Xu et al., 2012) rendering it a critical target. Furthermore, HSP90 is connected to phenotypic plasticity and plant development (for review see Sangster and Queitsch, 2005). HSP90 is essential to the loading of small RNAs into AGO (for review see Meister, 2013). Thus, HSP90 is crucial for the PTGS pathway that potentially redirects vsRNAs against the viroid genome within the defense system. In the light of its central role, HSP90 transcripts appear as a plausible target for viroid-induced degradation.

vsRNA-mediated Degradome

We determined degradation regimes in infected plants that are either common in PSTVd-infected plants or specific to one of the two variants used. We proceeded to investigate the viroid pathogenesis theorem which suggests that vsRNA instruct host transcript degradations. We used CLEAVELAND to relate predicted small RNAs target sites on transcripts with degradome sequencing-determined cleavage sites for vsRNAs. As queries we generated every possible 21mer from the PSTVd $(+)$-strands and $(-)$-strands. We considered CLEAVELAND-predicted vsRNA target sites as plausible if they belonged to categories zero or one. Additionally, cleavage sites should exhibit at least five reads starting at the predicted position. According to these rules we identified one, seven, and five predicted targets for QFA_{20}, $AS1_{10}$ and, $AS1_{20}$, respectively (see Tab. 3.3). Upon evaluation most targets appear implausible, lacking either convincing expression dynamics or the predicted target site contradicts known complementarity rules (not shown). Among those with plausible sequence complementary and degradation dynamics, Plasminogen activator inhibitor 1 RNA-binding protein-like (PAI-1, Solyc01g090190.2.1, NM_001322024.1; Aoki et al., 2010) was predicted to be a common target of AS1 and QFA (see Fig. 3.6). Plant homologues to the human PAI-1 were previously described in *A. thaliana* and are suspected to be related to cell death processes (Vercammen et al., 2006). The AS1-infected samples revealed that glycine-rich cell wall structural protein 1-like host transcripts (for review see Mangeon et al., 2010) are targeted by vsRNAs. These might explain the observed "lethal" symptoms.

We developed a method named REDEGRADMAP to identify small RNA sources leading to host transcript cleavage from degradation-derived reads. Fig. 3.7 shows that only a very limited amount of degradome reads can be traced back to the infecting viroid genome. Nevertheless, even the control degradome includes reads that can be traced back to the viroid, suggesting some background level.

Discussion

The analysis of PSTVd infected tomato plants with the mild QFA and "lethal" AS1 variants revealed viroid-induced degradation regimes. One might debate that viroids are not recognized as pathogens at all; viroids are lacking most of the signals plants recognize like a capsule, pathogen-induced proteins or cell wall penetration. Additionally, PSTVd is detectable already one to three minutes post

Table 3.3: CLEAVELAND-prediction of degradome-based vsRNA targets.

Set	Transcript	Slice	Cat.	f(Reads)	Hybrid of vsRNA and target site	Annotation†
QFA_{20}	Solyc02g090910.2.1	928	0	5	3′-AGGUGGAGGUGGAGGUGGAGG-5′ 5′-ACCGCUUUUUCUUCUAUCUUA-3′	RNA-binding like protein
	Solyc00g006470.1.1	422	0	15	3′-CCGACAAGCUGUGGGCCCCUUCCGGGGGCU-5′ 5′-GGU--UUC----CCCGGGGA---UCCCUGA-3′	Unknown Protein
	Solyc02g090910.2.1	929	1	5	3′-GAGGUGGAGGUGGAGGUGGAGG-5′ 5′-AACCGCUUUU-UCUCUAUCUUA-3′	RNA-binding like protein
	Solyc04g081880.2.1	577	0	5	3′-UUUCGGAGACCUGGAAGGGGAAGGAG-5′ 5′-CGAGCC-----GCCUUCUUUUUUCUU-3′	Ribonuclease P protein subunit p25
$AS1_{10}$	Solyc05g055460.1.1	487	0	8	3′-GAGGUGGUGG-AGGAGGAGGUG-5′ 5′-CUCC-CCACCGUCCUUUUUUGC-3′	glycine-rich cell wall structural protein 1
	Solyc07g052220.1.1	210	1	5	3′-AGGAGGUGGUCGAGGCGGAGGUU-5′ 5′-UUUUUUGCCAGUUC-GC-UCCAG-3′	glycine-rich cell wall structural protein 1-like
	Solyc08g076900.2.1	423	1	6	3′-GGUGGUGAAGGACAAGGAGGAGG-5′ 5′-CCGCC--UUCUUUUUUCUUUUCU-3′	glycine-rich cell wall structural protein 1.8-like
	Solyc10g081020.1.1	4756	0	9	3′-GGUCGUGGUGGUGGGGUUCUGAGGG-5′ 5′-CCAGU----UCGCUCCAGGUUUCCC-3′	Transcription elongation factor SPT6
$AS1_{20}$	Solyc01g090190.2.1	498	0	11	3′-GGUGGUGGAGAUGGAGGUGGUG-5′ 5′-GAACCGCUUUU-UCUCUAUCUU-3′	Plasminogen activator inhibitor 1 RNA-binding protein-like
	Solyc04g078100.1.1	176	0	5	3′-UGGAGGAGGAGGAGGUGGAGGU-5′ 5′-ACC-GCUUUUUCUCUAUCUUAC-3′	Glycine-rich cell wall structural protein 1
	Solyc06g062540.2.1	649	0	10	3′-ACCAGGUGAGCACCUGGGGACG-5′ 5′-AACUAAACUCGUGG-UUCCUGU-3′	LePS2
	Solyc06g062560.1.1	649	1	10	3′-ACCAGGUGAGCACCUGGGGACG-5′ 5′-AACUAAACUCGUGG-UUCCUGU-3′	LePS2
	Solyc10g051380.1.1	316	0	5	3′-GCGGCGGCGGUGGUUUUGGUGGUG-5′ 5′-CGCUGUCGCUUC---GGCUACUAC-3′	Glycine-rich RNA-binding protein

#The upper sequence represents the hypothetical vsRNA; the lower sequence is the target site of the host transcript.
† Annotations where adjusted based on BLAST searches.

micro-injection in neighboring cells suggesting an active transport (Ding et al., 1997). In contrast, the cleaved host transcripts indicate a viroid-countered PTI response by the host plant.

The question remains whether the degradomes result from overexpression of transcripts enhancing unspecific degradation in response to pathogens or result from a viroid-induced small RNA-mediated pathogenesis network. The translated protein of the viroid-specific differentially degraded PIP1 transcript is targeted and perturbed by EPIC2B, a cystatin-like protease inhibitor of *Phytophthora infestans* (for review see Misas-Villamil and van der Hoorn, 2008; Hein et al., 2009). PIP1 is targeted by different and only distantly related oomycete pathogens, identifying it as an important virulence target (Song et al., 2009). The PSTVd AS1-induced degradation regime includes the PIP1 transcript. The

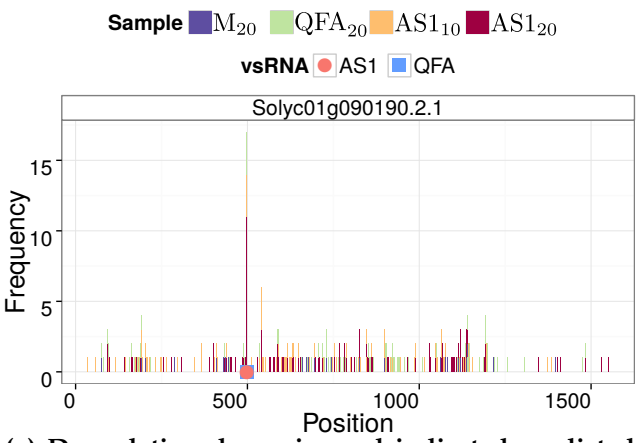

(a) Degradation dynamics and indicated predicted cleavage sites.

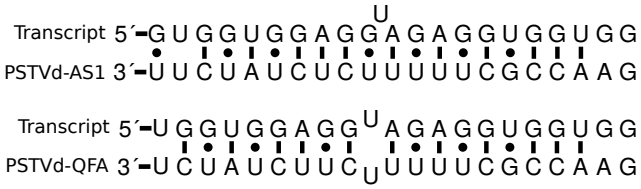

(b) Sequence complementarity of the vsRNAs and predicted target site.

Figure 3.6: CLEAVELAND-predicted vsRNA target site on plasminogen activator inhibitor 1 RNA-binding protein-like (PAI-1) (a) The host transcript exhibits a distinct degradation site that coincides with a vsRNA. (b) The vsRNA derives from the (+)-strand pos. 289 in mild QFA and "lethal" AS1. Hence, the targeted PAI-1 transcript represents a common determinant.

degradation of this key transcript might effectively suppress the PIP1-associated plant pathogen response. PIP1 is under strong diversifying selection (Shabab et al., 2008) potentially indicating a host genotype tolerance determinant. In this framework, selection favors transcript variants with mutated target sites of pathogen-derived small RNAs. The degradation dynamics of CEVI-1 exhibited a rather unspecific degradome (see Fig. 3.4c). CEVI-1 was found to be the most abundant protein in infected leaves 14 dpi (Vera et al., 1993). Thus, we hypothesize that the CEVI-1 degradation dynamic shows a random degradation as a result of viroid-induced overexpression. Most of the differentially degraded transcripts exhibited degradation dynamics not centered around distinct peaks that indicate small RNA cleavage sites. In contrast, transcripts with distinct degradation dynamics like PR-1 may indeed show viroid-induced degradation with distinct target sites. The differentially degraded PR-1 transcripts confirm previous findings, which suggested that host plants modulate a response upon viroid infection (Tornero et al., 1994; Domingo et al., 1994). PR-1 family proteins are part of PTI that mediate HR upon pathogen detection. In order to counter PTI, PR-1 transcripts appear as plausible targets of viroid-induced pathogenesis networks or vsRNAs. We observed that QFA and AS1-induced cleavage of the PR-1 transcripts in a symptom severity-dependent intensity indicating PSTVd variant-dependent efficiency in suppression of the plant response. The small RNAs guiding cleavage to target sites, which were revealed by distinct peaks in the degradomes, remain to be established.

From Table 3.2 follows that *S. lycopersicum* identifies PSTVd as a biotrophic pathogen and induces a SA-mediated plant defense response. This response would lead to PCD but seems to be countered by a PSTVd-induced pathogenesis network. These findings suggest that viroids and tomato plants engage in an evolved host-pathogen interaction. Despite the small genome size of PSTVd, host transcripts with key roles within these defensive pathways are cleaved in a PSTVd variant-specific fashion. The non-coding viroid genomes and reliance on host proteins potentially challenge the host recognition systems.

We identified vsRNA-targeted host transcripts with CLEAVELAND. The identified host transcripts glycine-rich cell wall structural protein 1-like are potential viroid targets that may explain symptoms

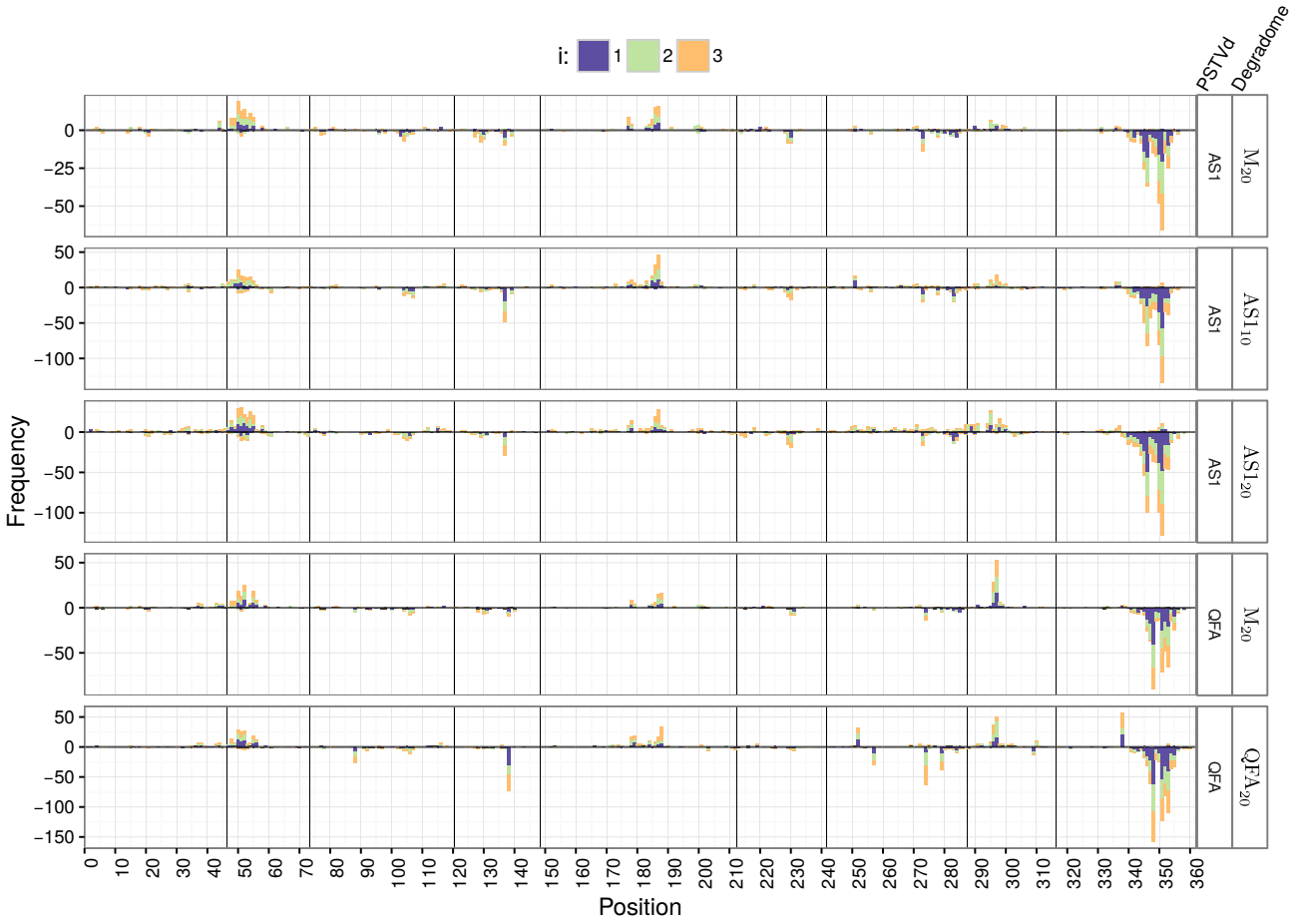

Figure 3.7: Degradome read fragments mapped to PSTVd variants by ReDegradMap. Degradome reads clipped at $j = 10$ from starting position $i = \{1, 2, 3\}$ mapped as reverse complement back to the respective PSTVd genome. The frequency of reconstructions is shown on the y-axis. Reconstructions of vsRNA fragments from the $(+)$-strand have positive algebraic sign and from the $(-)$-strand have negative algebraic sign. Comparisons between viroid-inoculated and mock-inoculated samples reveal no significant considered differential vsRNA expression sites. In contrast, the mapping dynamics show conserved patterns indicating that most degradation is not related to vsRNAs.

like dwarfism, epinasty, and necrosis. Hence, we recommend to validate these targets that potentially constitute pathogenic determinants. Additionally, we identified PAI-1 as a promising target with the highest count of degradome reads starting at the predicted cleavage site.

Based on the limited attributable reads to PSTVd (see Fig. 3.7) we assume that vsRNA-mediated degradation in our samples is at a very minor steady state and that most drastic degradations are orchestrated in a very early stage of the infection. Hence, we recommend to simultaneously determine the degradome and small RNA population via deep sequencing of infected and mock-inoculated cells at different points in time with a focus on early stages of infection.

To sum up, the analyzed PSTVd-induced degradation regimes suggest two implications: First, the *S. lycopersicum* recognizes PSTVd infections and accordingly induces a PTI-response deduced from the induction of PR-1, PIP1, and PAL transcripts to induce PCD. Second, PSTVd is enabled to counter a complex host defense response by inducing degradation of critical PTI-associated transcripts.

References

Addo-Quaye, C., Miller, W., and Axtell, M. J. (2009). CleaveLand: a pipeline for using degradome data to find cleaved small RNA targets. *Bioinformatics*, 25:130–1.

Adkar-Purushothama, C. R., Brosseau, C., Giguère, T., Sano, T., Moffett, P., and Perreault, J.-P. (2015). Small rna derived from the virulence modulating region of the potato spindle tuber viroid silences callose synthase genes of tomato plants. *Plant Cell*, 27:2178–94.

Ameres, S. L. and Zamore, P. D. (2013). Diversifying microRNA sequence and function. *Nat. Rev. Mol. Cell Biol.*, 14:475–88.

Anders, S., Pyl, P. T., and Huber, W. (2015). HTSeq–a Python framework to work with high-throughput sequencing data. *Bioinformatics*, 31:166–9.

Aoki, K., Yano, K., Suzuki, A., Kawamura, S., Sakurai, N., Suda, K., Kurabayashi, A., Suzuki, T., Tsugane, T., Watanabe, M., Ooga, K., Torii, M., Narita, T., Shin-I, T., Kohara, Y., Yamamoto, N., Takahashi, H., Watanabe, Y., Egusa, M., Kodama, M., Ichinose, Y., Kikuchi, M., Fukushima, S., Okabe, A., Arie, T., Sato, Y., Yazawa, K., Satoh, S., Omura, T., Ezura, H., and Shibata, D. (2010). Large-scale analysis of full-length cDNAs from the tomato (*Solanum lycopersicum*) cultivar Micro-Tom, a reference system for the *Solanaceae* genomics. *BMC Genomics*, 11:210.

Avina-Padilla, K., Martinez de la Vega, O., Rivera-Bustamante, R., Martinez-Soriano, J. P., Owens, R. A., Hammond, R. W., and Vielle-Calzada, J.-P. (2015). In silico prediction and validation of potential gene targets for pospiviroid-derived small RNAs during tomato infection. *Gene*, 564:197–205.

Bolger, A. M., Lohse, M., and Usadel, B. (2014). Trimmomatic: a flexible trimmer for Illumina sequence data. *Bioinformatics*, 30:2114–20.

Boller, T. and He, S. Y. (2009). Innate immunity in plants: an arms race between pattern recognition receptors in plants and effectors in microbial pathogens. *Science*, 324:742–4.

Ding, B., Kwon, M.-O., Hammond, R., and Owens, R. (1997). Cell-to-cell movement of potato spindle tuber viroid. *Plant J.*, 12:931–936.

Dixon, M. S., Golstein, C., Thomas, C. M., van Der Biezen, E. A., and Jones, J. D. (2000). Genetic complexity of pathogen perception by plants: the example of Rcr3, a tomato gene required specifically by Cf-2. *Proc. Natl. Acad. Sci. U.S.A.*, 97:8807–14.

Domingo, C., Conejero, V., and Vera, P. (1994). Genes encoding acidic and basic class III beta-1,3-glucanases are expressed in tomato plants upon viroid infection. *Plant Mol. Biol*, 24:725–32.

Etalo, D. W., Stulemeijer, I. J. E., van Esse, H. P., de Vos, R. C. H., Bouwmeester, H. J., and Joosten, M. H. A. J. (2013). System-wide hypersensitive response-associated transcriptome and metabolome reprogramming in tomato. *Plant Physiol.*, 162:1599–617.

Fei, Q., Zhang, Y., Xia, R., and Meyers, B. C. (2016). Small rnas add zing to the zig-zag-zig model of plant defenses. *Mol. Plant Microbe Interact.*, 29:165–9.

Ferrer, J.-L., Austin, M. B., Stewart, C., and Noel, J. P. (2008). Structure and function of enzymes involved in the biosynthesis of phenylpropanoids. *Plant Physiol. Biochem.*, 46:356–70.

German, M. A., Luo, S., Schroth, G., Meyers, B. C., and Green, P. J. (2009). Construction of Parallel Analysis of RNA Ends (PARE) libraries for the study of cleaved miRNA targets and the RNA degradome. *Nat. Protoc.*, 4:356–62.

German, M. A., Pillay, M., Jeong, D.-H., Hetawal, A., Luo, S., Janardhanan, P., Kannan, V., Rymarquis, L. A., Nobuta, K., German, R., De Paoli, E., Lu, C., Schroth, G., Meyers, B. C., and Green, P. J.

(2008). Global identification of microRNA-target RNA pairs by parallel analysis of RNA ends. *Nat. Biotechnol.*, 26:941–6.

Glazebrook, J. (2005). Contrasting mechanisms of defense against biotrophic and necrotrophic pathogens. *Annu. Rev. Phytopathol.*, 43:205–27.

Glazebrook, J., Rogers, E. E., and Ausubel, F. M. (1996). Isolation of Arabidopsis mutants with enhanced disease susceptibility by direct screening. *Genetics*, 143:973–82.

Hadidi, A., Flores, R., Randles, J., and Semancik, J. (2003). *Viroids: properties, detection, diseases and their control*. Csiro Publishing.

Hammann, C. and Steger, G. (2012). Viroid-specific small RNA in plant disease. *RNA Biol.*, 9:809–19.

Hanley-Bowdoin, L., Bejarano, E. R., Robertson, D., and Mansoor, S. (2013). Geminiviruses: masters at redirecting and reprogramming plant processes. *Nat. Rev. Microbiol.*, 11:777–88.

Heath, M. C. (2000). Hypersensitive response-related death. *Plant Mol. Biol*, 44:321–34.

Hein, I., Gilroy, E. M., Armstrong, M. R., and Birch, P. R. J. (2009). The zig-zag-zig in oomycete-plant interactions. *Mol. Plant Pathol.*, 10:547–62.

Hoffmann, S., Otto, C., Doose, G., Tanzer, A., Langenberger, D., Christ, S., Kunz, M., Holdt, L. M., Teupser, D., Hackermüller, J., and Stadler, P. F. (2014). A multi-split mapping algorithm for circular RNA, splicing, trans-splicing and fusion detection. *Genome Biol.*, 15:R34.

Hörger, A. C., Ilyas, M., Stephan, W., Tellier, A., van der Hoorn, R. A. L., and Rose, L. E. (2012). Balancing selection at the tomato RCR3 Guardee gene family maintains variation in strength of pathogen defense. *PLoS Genet.*, 8:e1002813.

Itaya, A., Zhong, X., Bundschuh, R., Qi, Y., Wang, Y., Takeda, R., Harris, A. R., Molina, C., Nelson, R. S., and Ding, B. (2007). A structured viroid RNA serves as a substrate for dicer-like cleavage to produce biologically active small RNAs but is resistant to RNA-induced silencing complex-mediated degradation. *J. Gen. Virol.*, 81:2980–94.

Jones, J. D. G. and Dangl, J. L. (2006). The plant immune system. *Nature*, 444:323–9.

Kanehisa, M. and Goto, S. (2000). KEGG: Kyoto encyclopedia of genes and genomes. *Nucleic Acids Res.*, 28:27–30.

Kanehisa, M., Sato, Y., and Morishima, K. (2015). BlastKOALA and GhostKOALA: KEGG tools for functional characterization of genome and metagenome sequences. *J. Mol. Biol.*, 428:726–731.

Karlova, R., van Haarst, J. C., Maliepaard, C., van de Geest, H., Bovy, A. G., Lammers, M., Angenent, G. C., and de Maagd, R. A. (2013). Identification of microRNA targets in tomato fruit development using high-throughput sequencing and degradome analysis. *J. Exp. Bot.*, 64:1863–78.

Kasschau, K. D. and Carrington, J. C. (1998). A counterdefensive strategy of plant viruses: suppression of posttranscriptional gene silencing. *Cell*, 95:461–70.

Kim, D. S. and Hwang, B. K. (2014). An important role of the pepper phenylalanine ammonia-lyase gene (PAL1) in salicylic acid-dependent signalling of the defence response to microbial pathogens. *J. Exp. Bot.*, 65:2295–306.

Loake, G. and Grant, M. (2007). Salicylic acid in plant defence–the players and protagonists. *Curr. Opin. Plant Biol.*, 10:466–72.

Love, M. I., Huber, W., and Anders, S. (2014). Moderated estimation of fold change and dispersion for RNA-seq data with DESeq2. *Genome Biol.*, 15:550.

MacDonald, M. J. and D'Cunha, G. B. (2007). A modern view of phenylalanine ammonia lyase. *Biochem. Cell Biol.*, 85:273–82.

Macho, A. P. and Zipfel, C. (2014). Plant PRRs and the activation of innate immune signaling. *Mol. Cell*, 54:263–72.

Mangeon, A., Junqueira, R. M., and Sachetto-Martins, G. (2010). Functional diversity of the plant glycine-rich proteins superfamily. *Plant Signal Behav.*, 5:99–104.

Matousek, J., Orctová, L., Steger, G., and Riesner, D. (2004). Biolistic inoculation of plants with viroid nucleic acids. *Journal of virological methods*, 122:153–64.

Mauch-Mani, B. and Slusarenko, A. J. (1996). Production of salicylic acid precursors Is a major function of phenylalanine ammonia-lyase in the resistance of Arabidopsis to *Peronospora parasitica*. *Plant Cell*, 8:203–212.

Meister, G. (2013). Argonaute proteins: functional insights and emerging roles. *Nat. Rev. Genet.*, 14:447–59.

Mendgen, K. and Hahn, M. (2002). Plant infection and the establishment of fungal biotrophy. *Trends Plant Sci.*, 7:352–6.

Misas-Villamil, J. C. and van der Hoorn, R. A. L. (2008). Enzyme-inhibitor interactions at the plant-pathogen interface. *Curr. Opin. Plant Biol.*, 11:380–8.

Navarro, B., Gisel, A., Rodio, M. E., Delgado, S., Flores, R., and Di Serio, F. (2012). Small RNAs containing the pathogenic determinant of a chloroplast-replicating viroid guide the degradation of a host mRNA as predicted by RNA silencing. *Plant J.*, 70:991–1003.

Navarro, L., Jay, F., Nomura, K., He, S. Y., and Voinnet, O. (2008). Suppression of the microRNA pathway by bacterial effector proteins. *Science*, 321:964–7.

Oliva, J., Rommel, S., Fossdal, C. G., Hietala, A. M., Nemesio-Gorriz, M., Solheim, H., and Elfstrand, M. (2015). Transcriptional responses of Norway spruce (*Picea abies*) inner sapwood against *Heterobasidion parviporum*. *Tree Physiol.*, 35:1007–15.

Pallas, J. A., Paiva, N. L., Lamb, C., and Dixon, R. A. (1996). Tobacco plants epigenetically suppressed in phenylalanine ammonia-lyase expression do not develop systemic acquired resistance in response to infection by tobacco mosaic virus. *Plant J.*, 10:281–293.

Papaefthimiou, I., Hamilton, A., Denti, M., Baulcombe, D., Tsagris, M., and Tabler, M. (2001). Replicating potato spindle tuber viroid RNA is accompanied by short RNA fragments that are characteristic of post-transcriptional gene silencing. *Nucleic Acids Res.*, 29:2395–400.

Pasquinelli, A. E. (2012). MicroRNAs and their targets: recognition, regulation and an emerging reciprocal relationship. *Nat. Rev. Genet.*, 13:271–82.

Pieterse, C. M. J., Leon-Reyes, A., Van der Ent, S., and Van Wees, S. C. M. (2009). Networking by small-molecule hormones in plant immunity. *Nat. Chem. Biol.*, 5:308–16.

Pumplin, N. and Voinnet, O. (2013). RNA silencing suppression by plant pathogens: defence, counter-defence and counter-counter-defence. *Nat. Rev. Microbiol.*, 11:745–60.

Qiao, Y., Shi, J., Zhai, Y., Hou, Y., and Ma, W. (2015). Phytophthora effector targets a novel component of small RNA pathway in plants to promote infection. *Proc. Natl. Acad. Sci. U.S.A.*, 112:5850–5.

Rivière, M.-P., Marais, A., Ponchet, M., Willats, W., and Galiana, E. (2008). Silencing of acidic pathogenesis-related PR-1 genes increases extracellular beta-(1→3)-glucanase activity at the onset of tobacco defence reactions. *J. Exp. Bot.*, 59:1225–39.

Sangster, T. A. and Queitsch, C. (2005). The HSP90 chaperone complex, an emerging force in plant development and phenotypic plasticity. *Curr. Opin. Plant Biol.*, 8:86–92.

Seyfferth, C. and Tsuda, K. (2014). Salicylic acid signal transduction: the initiation of biosynthesis, perception and transcriptional reprogramming. *Front. Plant Sci.*, 5:697.

Shabab, M., Shindo, T., Gu, C., Kaschani, F., Pansuriya, T., Chintha, R., Harzen, A., Colby, T., Kamoun, S., and van der Hoorn, R. A. L. (2008). Fungal effector protein AVR2 targets diversifying defense-related cys proteases of tomato. *Plant Cell*, 20:1169–83.

Song, J., Win, J., Tian, M., Schornack, S., Kaschani, F., Ilyas, M., van der Hoorn, R. a. L., and Kamoun, S. (2009). Apoplastic effectors secreted by two unrelated eukaryotic plant pathogens target the tomato defense protease Rcr3. *Proc. Natl. Acad. Sci. U.S.A.*, 106:1654–9.

Tafer, H., Ameres, S. L., Obernosterer, G., Gebeshuber, C. a., Schroeder, R., Martinez, J., and Hofacker, I. L. (2008). The impact of target site accessibility on the design of effective siRNAs. *Nat. Biotechnol.*, 26:578–83.

Thomma, B. P. H. J., Nürnberger, T., and Joosten, M. H. (2011). Of PAMPs and effectors: the blurred PTI-ETI dichotomy. *Plant Cell*, 23:4–15.

Tian, M., Win, J., Song, J., van der Hoorn, R., van der Knaap, E., and Kamoun, S. (2007). A Phytophthora infestans cystatin-like protein targets a novel tomato papain-like apoplastic protease. *Plant Physiol.*, 143:364–77.

Tomato Genome Consortium (2012). The tomato genome sequence provides insights into fleshy fruit evolution. *Nature*, 485:635–641.

Tornero, P., Conejero, V., and Vera, P. (1994). A gene encoding a novel isoform of the PR-1 protein family from tomato is induced upon viroid infection. *Mol. Gen. Genet.*, 243:47–53.

Torres, M. A., Jones, J. D. G., and Dangl, J. L. (2006). Reactive oxygen species signaling in response to pathogens. *Plant Physiol.*, 141:373–8.

Tsuda, K. and Katagiri, F. (2010). Comparing signaling mechanisms engaged in pattern-triggered and effector-triggered immunity. *Curr. Opin. Plant Biol.*, 13:459–65.

Vaucheret, H. (2008). Plant ARGONAUTES. *Trends Plant Sci.*, 13:350–8.

Vera, P., Tornero, P., and Conejero, V. (1993). Cloning and expression analysis of a viroid-induced peroxidase from tomato plants. *Mol. Plant Microbe Interact.*, 6:790–4.

Vercammen, D., Belenghi, B., van de Cotte, B., Beunens, T., Gavigan, J.-A., De Rycke, R., Brackenier, A., Inzé, D., Harris, J. L., and Van Breusegem, F. (2006). Serpin1 of *Arabidopsis thaliana* is a suicide inhibitor for metacaspase 9. *J. Mol. Biol.*, 364:625–36.

Vogt, T. (2010). Phenylpropanoid biosynthesis. *Mol. Plant*, 3:2–20.

Voinnet, O. (2009). Origin, biogenesis, and activity of plant microRNAs. *Cell*, 136:669–87.

Xu, Z.-S., Li, Z.-Y., Chen, Y., Chen, M., Li, L.-C., and Ma, Y.-Z. (2012). Heat shock protein 90 in plants: molecular mechanisms and roles in stress responses. *Int. J. Mol. Sci.*, 13:15706–23.

Zipfel, C. (2014). Plant pattern-recognition receptors. *Trends Immunol.*, 35:345–51.

Supplement

Table S1: Differentially degraded host transcripts. Entries are sorted according to DESEQ2 $\log_2$(FoldChange) and P-value (not shown).

Transcript	M_{20}	QFA_{20}	$AS1_{10}$	$AS1_{20}$	Annotation
					$(QFA_{20} \cap AS1_{10} \cap AS1_{20}) \setminus M_{20}$
Solyc02g077040.2.1	0	17	63	234	Cathepsin B-like cysteine proteinase 5
Solyc10g081570.1.1	9	91	129	328	KED
Solyc01g006300.2.1	0	6	42	136	Peroxidase
Solyc01g097270.2.1	1	7	96	81	Chitinase (Fragment)
Solyc05g054090.2.1	0	19	28	24	Unknown Protein
Solyc05g009490.2.1	2	11	53	160	Unknown Protein
Solyc04g040160.2.1	1	46	12	52	Pheophorbide a oxygenase
Solyc04g054740.2.1	13	224	40	260	Inositol-3-phosphate synthase
Solyc10g085030.1.1	1	22	11	73	Soul heme-binding family protein
Solyc09g018280.1.1	1	11	26	47	Calcium/calmodulin-dependent protein kinase type 1
Solyc07g006890.1.1	1	9	21	64	Cytochrome P450
Solyc01g106620.2.1	0	3	24	39	Pathogenesis-related protein 1a
Solyc08g068870.2.1	0	5	12	50	Aspartic proteinase nepenthesin-1
Solyc12g049220.1.1	1	16	22	37	Mitochondrial import inner membrane translocase subunit tim23
Solyc07g063930.2.1	1	13	21	43	Solute carrier family 22 member 2
Solyc02g082920.2.1	0	2	14	66	Endochitinase (Chitinase)
Solyc01g107820.2.1	8	23	58	269	UDP-glucosyltransferase family 1 protein
Solyc04g079920.2.1	4	31	98	29	Pre-mRNA-splicing factor cwc22
Solyc04g005100.2.1	0	16	3	40	Myb transcription factor
Solyc05g009720.2.1	2	34	17	36	Myb family transcription factor-like
Solyc09g082710.2.1	3	31	48	29	Histone H2A
Solyc12g007120.1.1	3	31	43	31	Signal peptidase I
Solyc09g091800.2.1	0	9	26	9	Unknown Protein
Solyc11g066060.1.1	58	404	218	798	heat shock protein
Solyc08g076900.2.1	20	123	219	133	Unknown Protein
Solyc06g053540.2.1	2	17	27	41	Unknown Protein
Solyc03g033500.2.1	7	40	66	87	Cold shock protein-1
Solyc09g015770.2.1	2	8	24	76	WRKY transcription factor 6
Solyc04g007140.1.1	0	5	5	50	Unknown Protein
Solyc02g079740.1.1	0	9	13	17	U-box domain-containing protein (Fragment)
Solyc06g076020.2.1	2	24	7	76	heat shock protein
Solyc06g066800.1.1	1	13	13	37	Glycosyl transferase family 8
Solyc01g103510.2.1	2	22	19	39	Ribosomal protein L3-like
Solyc03g093140.2.1	15	130	47	201	MFS family major facilitator transporter glycerol-3-phosphate cation symporter
Solyc01g109570.2.1	0	10	13	13	Glucan endo-1 3-beta-glucosidase 7
Solyc09g091390.2.1	13	75	89	134	Unknown Protein
Solyc02g087190.1.1	1	19	12	25	Peroxidase 65
Solyc01g079680.2.1	1	13	19	24	Ran GTPase activating protein (Fragment)
Solyc09g098510.2.1	7	19	57	142	Unknown Protein
Solyc03g080190.2.1	0	5	4	43	Flavanone 3-hydroxylase-like protein
Solyc12g098590.1.1	0	9	4	30	UDP-glucosyltransferase family 1 protein
Solyc11g010380.1.1	8	48	18	197	Mate efflux family protein
Solyc08g082590.2.1	23	146	44	420	Glutaredoxin family protein
Solyc01g099370.2.1	6	35	36	83	SRC2 homolog (Fragment)
Solyc10g086180.1.1	10	99	24	118	Phenylalanine ammonia-lyase
Solyc11g069070.1.1	11	53	62	134	Metal ion binding protein
Solyc03g120780.2.1	4	34	36	34	Ribosomal protein L37
Solyc09g065280.2.1	5	21	56	54	Pre-mRNA-splicing factor 18
Solyc06g009770.1.1	5	34	37	51	Binding protein
Solyc09g062970.1.1	186	634	1587	1343	Unknown Protein
Solyc04g071890.2.1	25	31	261	353	Peroxidase 4
Solyc00g047700.2.1	5	29	41	51	Unknown Protein
Solyc01g110960.2.1	17	82	120	121	Glutamic acid-rich protein
Solyc12g098230.1.1	185	591	1753	1104	Unknown Protein
Solyc03g025270.2.1	21	84	225	106	rRNA 2&apos-O-methyltransferase fibrillarin
Solyc02g094490.2.1	19	94	101	128	Unknown Protein
Solyc09g075010.2.1	62	172	499	398	Prostaglandin E synthase 3
					$(AS1_{10} \cap AS1_{20}) \setminus (QFA_{20} \cup M_{20})$
Solyc00g174340.1.1	0	4	149	633	Pathogenesis-related protein 1b
Solyc01g097270.2.1	1	7	96	81	Chitinase (Fragment)
Solyc00g174330.2.1	0	4	32	132	Pathogenesis related protein PR-1
Solyc01g006300.2.1	0	6	42	136	Peroxidase
Solyc09g082810.2.1	6	3	126	69	Unknown Protein
Solyc04g071890.2.1	25	31	261	353	Peroxidase 4
Solyc05g009490.2.1	2	11	53	160	Unknown Protein
Solyc09g007010.1.1	0	1	10	90	Pathogenesis related protein PR-1
Solyc02g082920.2.1	0	2	14	66	Endochitinase (Chitinase)
Solyc10g055800.1.1	0	0	22	26	Chitinase
Solyc01g107820.2.1	8	23	58	269	UDP-glucosyltransferase family 1 protein
Solyc01g106620.2.1	0	3	24	39	Pathogenesis-related protein 1a

continued on next page

Table S1: (continued)

Transcript	M_{20}	QFA_{20}	$AS1_{10}$	$AS1_{20}$	Annotation
Solyc04g007980.2.1	9	3	60	81	1-aminocyclopropane-1-carboxylate oxidase
Solyc04g048900.2.1	0	0	16	24	Calreticulin 2 calcium-binding protein
Solyc09g098510.2.1	7	19	57	142	Unknown Protein
Solyc07g049530.2.1	0	0	7	33	1-aminocyclopropane-1-carboxylate oxidase
Solyc12g045030.1.1	2	3	21	44	Short-chain dehydrogenase/reductase family protein
Solyc09g015770.2.1	2	8	24	76	WRKY transcription factor 6
Solyc03g078490.2.1	0	1	5	41	UDP-glucuronosyltransferase
Solyc01g006400.2.1	21	19	174	97	Cysteine-rich extensin-like protein-4
Solyc04g071070.2.1	4	1	37	28	Unknown Protein
Solyc09g011630.2.1	1	3	5	67	Glutathione S-transferase-like protein
Solyc06g036330.1.1	4	2	25	40	Ornithine cyclodeaminase protein
Solyc08g068870.2.1	0	5	12	50	Aspartic proteinase nepenthesin-1
Solyc07g006890.1.1	1	9	21	64	Cytochrome P450
Solyc09g075820.2.1	2	2	21	27	Solute carrier family 2, facilitated glucose transporter member 3
Solyc05g005460.2.1	3	8	23	60	Nucleoredoxin 2
Solyc03g121710.2.1	8	12	56	67	RNA-binding motif, single-stranded-interacting protein 1
Solyc11g021060.1.1	16	15	154	45	Proteinase inhibitor
Solyc10g085880.1.1	2	4	4	69	UDP-glucosyltransferase family 1 protein
Solyc10g007280.2.1	0	0	12	13	AAA-ATPase
Solyc02g077050.2.1	7	12	47	66	Cathepsin B-like cysteine proteinase
Solyc05g009310.2.1	6	5	81	13	Zinc finger protein CONSTANS-LIKE 16
Solyc01g103650.2.1	1	1	15	18	Hydrolase alpha/beta fold family
Solyc07g047800.2.1	9	16	46	95	Short-chain dehydrogenase/reductase family protein
					$(QFA_{20} \cap AS1_{20}) \setminus (AS1_{10} \cup M_{20})$
Solyc02g067050.2.1	3	217	24	461	Uncharacterized ACR COG1678 family protein
Solyc09g011080.2.1	9	162	4	266	Ribulose-1 5-bisphosphate carboxylase/oxygenase activase 1
Solyc09g092490.2.1	5	76	3	234	UDP-glucosyltransferase family 1 protein
Solyc08g078700.2.1	1	34	1	89	Heat shock protein 22
Solyc06g036260.2.1	5	105	7	179	Beta-carotene hydroxylase 1
Solyc12g006050.1.1	0	33	1	50	Nitrate transporter
Solyc07g042400.2.1	4	84	16	289	Unknown Protein
Solyc06g036290.2.1	3	41	4	120	Heat shock protein 90 (Fragment)
Solyc01g058720.2.1	14	173	46	648	NaCl-inducible Ca2+-binding protein
Solyc08g007130.2.1	7	73	4	127	Beta-amylase 8
Solyc06g062550.2.1	1	20	0	44	Phosphatase
Solyc10g079620.1.1	3	36	1	54	HAD superfamily (Subfamily IA) hydrolase TIGR02254
Solyc04g054740.2.1	13	224	40	260	Inositol-3-phosphate synthase
Solyc10g084370.1.1	0	15	0	26	MYB transcription factor (Fragment)
Solyc01g067660.2.1	4	50	3	57	Beta-amylase
Solyc05g051850.2.1	7	75	11	112	Inositol-3-phosphate synthase
Solyc05g055460.1.1	1	29	2	31	Unknown Protein
Solyc08g062340.2.1	0	10	0	30	Class II small heat shock protein Le-HSP17.6
Solyc10g005080.2.1	1	21	2	41	Late elongated hypocotyl and circadian clock associated-1-like
Solyc07g063120.2.1	1	25	0	19	WD-40 repeat protein
Solyc04g005100.2.1	0	16	3	40	Myb transcription factor
Solyc08g082590.2.1	23	146	44	420	Glutaredoxin family protein
Solyc02g089610.1.1	3	34	4	49	S-adenosylmethionine decarboxylase proenzyme
Solyc11g010380.1.1	8	48	18	197	Mate efflux family protein
Solyc11g012360.1.1	10	81	10	100	Sodium-dependent dicarboxylate transporter
Solyc06g076020.2.1	2	24	7	76	heat shock protein
Solyc03g031860.2.1	2	32	5	46	Phytoene synthase 1
Solyc02g063000.2.1	6	36	2	70	Glucosyltransferase
Solyc03g098010.2.1	6	62	13	94	Acid phosphatase
Solyc07g064410.1.1	0	13	1	23	Ubiquitin-conjugating enzyme-like protein
Solyc01g091260.2.1	1	23	1	19	AT2G45380 protein (Fragment)
Solyc02g094400.2.1	21	125	34	282	Glycerophosphodiester phosphodiesterase gde1
Solyc06g068300.2.1	1	17	0	18	Unknown Protein
Solyc04g040160.2.1	1	46	12	52	Pheophorbide a oxygenase
Solyc07g055060.2.1	19	140	34	207	Phosphoenolpyruvate carboxylase 1
Solyc01g110360.2.1	124	746	97	948	Fructose-bisphosphate aldolase
Solyc10g086180.1.1	10	99	24	118	Phenylalanine ammonia-lyase
Solyc06g062540.2.1	1	15	2	30	Phosphatase
Solyc05g009420.1.1	1	14	1	25	Unknown Protein
Solyc10g085030.1.1	1	22	11	73	Soul heme-binding family protein
Solyc09g082690.2.1	2	22	5	41	Early light-induced protein 7
Solyc01g110370.2.1	0	9	0	15	Zinc finger protein CONSTANS-LIKE 3
Solyc11g066100.1.1	1	11	2	32	heat shock protein
Solyc07g065340.1.1	5	33	9	70	Serine acetyltransferase
Solyc04g050440.2.1	5	19	2	60	Ammonium transporter
Solyc03g093140.2.1	15	130	47	201	MFS family major facilitator transporter glycerol-3-phosphate cation symporter
Solyc05g007880.2.1	0	9	0	14	Dof zinc finger protein
Solyc02g089120.2.1	0	5	0	21	Ch-cobra
Solyc11g006300.1.1	0	10	0	12	3-oxo-5-alpha-steroid 4-dehydrogenase family protein
Solyc06g073320.2.1	65	314	62	467	GDP-L-galactose phosphorylase 1
Solyc02g078400.2.1	0	14	3	21	Allantoinase
Solyc10g085880.1.1	2	4	4	69	UDP-glucosyltransferase family 1 protein
Solyc12g013840.1.1	1	18	3	21	WD-40 repeat protein
Solyc10g074930.1.1	6	59	18	69	Protein kinase 2

continued on next page

Table S1: (continued)

Transcript	M_{20}	QFA_{20}	$AS1_{10}$	$AS1_{20}$	Annotation
Solyc09g092500.1.1	26	122	71	804	UDP-glucosyltransferase family 1 protein
Solyc09g011630.2.1	1	3	5	67	Glutathione S-transferase-like protein
Solyc04g007140.1.1	0	5	5	50	Unknown Protein
Solyc01g104740.2.1	0	2	1	32	Multiprotein bridging factor 1
Solyc03g080190.2.1	0	5	4	43	Flavanone 3-hydroxylase-like protein
Solyc00g011160.1.1	2	47	4	5	Unknown Protein
Solyc02g089540.2.1	1	12	0	14	Tomato CONSTANS-like 1
Solyc05g011890.1.1	5	36	8	45	Sulfotransferase family protein
Solyc11g066060.1.1	58	404	218	798	heat shock protein
Solyc03g098320.2.1	2	19	2	19	MYB transcription factor (Fragment)
Solyc07g008210.2.1	0	6	0	14	TPR domain protein
Solyc12g098590.1.1	0	9	4	30	UDP-glucosyltransferase family 1 protein
Solyc03g115230.2.1	1	13	4	28	ClpB chaperone
Solyc04g009900.2.1	10	46	17	97	Calcium-dependent protein kinase 2
Solyc06g074800.1.1	1	23	4	14	Cys2/His2 zinc-finger transcription factor
Solyc03g118130.2.1	17	77	17	103	Rubredoxin-like protein
Solyc11g007500.1.1	0	1	1	31	UDP-glucosyltransferase
Solyc12g009480.1.1	9	41	14	78	Xenotropic and polytropic retrovirus receptor
Solyc11g013810.1.1	33	165	42	182	Nitrate reductase
Solyc03g033840.2.1	0	4	2	26	26S protease regulatory subunit 6B homolog
Solyc01g110150.2.1	8	27	19	118	CM0216.450.nc protein
Solyc01g005590.2.1	18	83	8	74	Unknown Protein
Solyc10g085870.1.1	7	17	2	59	UDP-glucosyltransferase family 1 protein
Solyc10g084400.1.1	2	4	5	57	Glutathione S-transferase
Solyc02g073580.1.1	3	22	5	27	BZIP transcription factor
Solyc01g017330.1.1	0	13	0	3	Photosystem I P700 chlorophyll a apoprotein A1
Solyc05g005170.2.1	5	27	7	40	Polygalacturonase 2
Solyc01g107780.2.1	0	3	2	27	UDP-glucosyltransferase family 1 protein
Solyc06g036110.1.1	1	3	1	29	C2 domain-containing protein
Solyc02g072540.2.1	11	43	4	53	CBL-interacting protein kinase 16
Solyc01g080460.2.1	4	17	6	44	Pyruvate phosphate dikinase
Solyc11g065830.1.1	111	442	190	817	2-oxoglutarate/malate translocator-like protein
Solyc04g078460.2.1	2	15	3	21	N(4)-(Beta-N-acetylglucosaminyl)-L-asparaginase
Solyc12g015880.1.1	100	403	247	963	Heat shock protein 90
Solyc09g007760.2.1	1	12	2	15	Aquaporin 2
Solyc03g116730.2.1	48	165	33	243	Stearoyl-CoA 9-desaturase
Solyc09g092130.2.1	0	13	1	5	Sucrose phosphate synthase
Solyc12g096770.1.1	24	93	52	223	Hydroxycinnamoyl CoA quinate transferase
Solyc03g116740.2.1	21	64	16	127	Genomic DNA chromosome 3 P1 clone MSJ11
Solyc01g009430.2.1	2	18	6	27	Os02g0448600 protein (Fragment)
Solyc02g062340.2.1	138	601	226	838	Fructose-bisphosphate aldolase
Solyc02g078480.2.1	3	22	8	34	CBS domain containing protein
Solyc04g077920.2.1	3	33	13	37	Interferon-related developmental regulator family protein
Solyc07g005510.2.1	21	70	21	129	Omega-6 fatty acid desaturase
Solyc01g097340.2.1	9	59	25	77	NAD-dependent epimerase/dehydratase family protein-like protein
Solyc09g075470.2.1	1	6	0	16	Chaperone protein dnaJ
Solyc06g068970.2.1	1	18	7	24	Conserved transmembrane protein
Solyc01g095070.2.1	3	27	8	26	Heavy metal-associated domain containing protein expressed
Solyc09g082630.2.1	18	69	30	133	Acireductone dioxygenase
Solyc05g013380.2.1	34	132	25	146	Alanine aminotransferase 2
Solyc01g087260.2.1	11	49	19	79	Carotenoid cleavage dioxygenase 1B
Solyc01g095530.2.1	43	156	46	228	Unknown Protein
Solyc01g100610.2.1	1	10	5	28	Solute carrier family 40 member 1
Solyc04g080040.2.1	3	18	0	13	UBA/TS-N domain protein
Solyc02g036370.2.1	0	10	1	7	MYB transcription factor (Fragment)
Solyc01g100020.2.1	0	4	1	16	Phospholipase D
Solyc02g069860.2.1	2	21	6	20	Nuclear transcription factor Y subunit A-7
Solyc07g053180.2.1	9	32	3	40	Lrr,resistance protein fragment
Solyc09g008780.2.1	15	49	19	100	Os01g0786800 protein (Fragment)
Solyc02g078150.2.1	1	8	4	26	Plant-specific domain TIGR01615 family protein
Solyc12g088170.1.1	0	5	1	13	Hydroxycinnamoyl CoA quinate transferase
Solyc12g005230.1.1	0	5	2	17	Breast carcinoma amplified sequence 3 (Fragment)
Solyc01g086660.2.1	0	1	1	22	Unknown Protein
Solyc04g007730.2.1	2	15	6	26	Unknown Protein
Solyc01g095140.2.1	0	8	2	12	Late embryogenesis abundant protein (Fragment)
Solyc02g089620.2.1	8	40	18	62	Proline dehydrogenase
Solyc01g100490.2.1	0	6	2	15	Nicotianamine synthase
Solyc05g052270.1.1	2	19	9	30	CBL-interacting protein kinase 13
Solyc05g009720.2.1	2	34	17	36	Myb family transcription factor-like
Solyc01g095980.2.1	5	24	13	52	Acid phosphatase/vanadium-dependent haloperoxidase related
Solyc05g053210.2.1	7	28	8	41	CBL-interacting protein kinase 1
Solyc05g014280.2.1	1	6	0	13	Heat shock protein
Solyc01g009080.2.1	14	73	32	90	FHA domain containing protein
Solyc01g099910.2.1	1	12	5	21	Epoxide hydrolase
Solyc11g069960.1.1	7	39	19	59	Receptor like kinase, RLK
Solyc09g083210.2.1	3	7	9	58	Receptor-like protein kinase
Solyc04g008230.2.1	0	6	0	7	Polygalacturonase
Solyc10g079200.1.1	12	63	28	79	Mitochondrial carrier protein
Solyc08g061130.2.1	0	14	3	7	Transcription factor HY5

continued on next page

Table S1: (continued)

Transcript	M_{20}	QFA_{20}	$AS1_{10}$	$AS1_{20}$	Annotation
Solyc08g060920.2.1	8	32	30	112	Xenotropic and polytropic retrovirus receptor
Solyc02g080510.1.1	1	15	5	16	Arabidopsis thaliana genomic DNA chromosome 5 P1 clone MOK16
Solyc02g082760.2.1	88	266	109	489	Catalase
Solyc08g079180.2.1	52	201	80	263	Elongation factor G
Solyc01g100760.2.1	2	21	9	25	Susceptibility homeodomain transcription factor (Fragment)
Solyc07g051820.2.1	6	19	4	34	Cellulose synthase
Solyc09g007770.2.1	12	44	12	56	Aquaporin 2
Solyc03g025720.2.1	1	11	1	8	Long-chain-fatty-acid–CoA ligase
Solyc11g073020.1.1	1	8	0	9	Metal ion binding protein
Solyc10g017580.2.1	3	10	8	44	Digalactosyldiacylglycerol synthase 2, chloroplastic
Solyc11g011140.1.1	0	12	5	15	50S ribosomal protein L23
Solyc07g026680.2.1	1	8	4	22	Myb transcription factor
Solyc03g095510.2.1	0	5	1	11	Protein kinase 2
Solyc09g010530.2.1	0	4	0	9	Cation/H+ antiporter
Solyc09g011490.2.1	0	4	0	9	Glutathione S-transferase-like protein
Solyc10g005200.2.1	3	18	5	20	Novel protein
Solyc04g054190.2.1	43	160	86	267	ABC-1 domain protein
Solyc07g006710.1.1	11	39	9	46	Pathogenesis-related protein PR-1
Solyc11g071740.1.1	0	6	4	20	Calmodulin-like protein
Solyc04g072160.2.1	4	14	2	22	Prostaglandin E synthase 3
Solyc10g085830.1.1	14	51	22	80	O-methyltransferase 1
Solyc04g077500.2.1	13	55	27	83	Os03g0729100 protein (Fragment)
Solyc04g007530.2.1	0	11	3	9	Multidrug resistance protein mdtK
Solyc10g084430.1.1	1	2	0	19	RING finger protein 44
Solyc11g044620.1.1	4	36	5	6	Imp biosynthesis protein
Solyc01g006720.2.1	11	46	27	84	ABC transporter G family member 22
Solyc10g085850.1.1	16	48	16	78	TPSI1
Solyc06g009020.2.1	25	59	38	179	Glutathione S-transferase
Solyc09g075210.2.1	42	135	28	147	Late embryogenesis abundant protein 5
Solyc12g006810.1.1	1	7	2	15	Soul heme-binding family protein
Solyc05g053060.1.1	13	47	20	71	Unknown Protein
Solyc01g096620.2.1	0	7	0	4	Unknown Protein
Solyc02g084990.2.1	10	47	24	66	Mannan endo-1 4-beta-mannosidase
Solyc09g008470.2.1	0	12	4	10	Splicing factor 3a subunit 2
Solyc05g056470.1.1	2	7	0	15	ABC transporter G family member 5
Solyc05g052950.2.1	0	4	0	8	Regulator of chromosome condensation RCC1 domain-containing protein
Solyc03g007270.2.1	3	19	9	28	Protein phosphatase 2C
Solyc12g007100.1.1	1	11	3	12	Ankyrin repeat domain-containing protein 1
Solyc01g007520.2.1	1	16	1	2	Photosystem II reaction center protein H
Solyc02g088200.2.1	0	1	0	14	Activating signal cointegrator 1 complex subunit 1
Solyc10g054440.1.1	35	142	96	255	Arginine decarboxylase
Solyc12g096860.1.1	0	6	0	5	Acyl-CoA thioesterase 9
Solyc03g096290.2.1	17	78	36	89	Aquaporin-like protein
Solyc04g040190.1.1	6	30	11	32	Lycopene beta-cyclase 1
Solyc10g086580.1.1	738	2314	820	3067	Ribulose-1 5-bisphosphate carboxylase/oxygenase activase 1
Solyc02g084440.2.1	111	388	159	480	Fructose-bisphosphate aldolase
Solyc10g079790.1.1	12	107	40	41	Pathogen-induced calmodulin-binding protein (Fragment)
Solyc02g067230.2.1	0	5	0	6	Dof zinc finger protein
Solyc06g009040.2.1	0	2	0	11	Glutathione S-transferase
Solyc06g076790.1.1	27	88	36	123	Unknown Protein
Solyc09g008200.2.1	7	28	29	90	Heavy metal-associated domain containing protein expressed
Solyc06g060340.2.1	98	309	141	452	Chloroplast photosystem II-associated protein
Solyc01g103990.2.1	6	28	15	43	T-complex protein 11
Solyc01g108630.2.1	27	104	53	138	Nitrite reductase
Solyc10g086730.1.1	16	86	47	93	Fructose-1 6-bisphosphatase class 1
Solyc09g072990.2.1	26	78	40	136	Unknown Protein
Solyc08g008480.2.1	0	7	0	3	Myb transcription factor
Solyc02g087190.1.1	1	19	12	25	Peroxidase 65
Solyc12g042600.1.1	3	8	15	63	UDP-glucosyltransferase family 1 protein
Solyc02g020910.2.1	10	34	26	83	Myosin-like protein
Solyc06g066800.1.1	1	13	13	37	Glycosyl transferase family 8
Solyc05g049990.2.1	3	15	10	33	Heavy metal-associated domain containing protein expressed
Solyc06g009120.2.1	3	15	8	27	Unknown Protein
Solyc09g090570.2.1	91	273	97	347	Proton gradient regulation 5
Solyc02g091500.1.1	5	24	9	26	Calmodulin
Solyc10g083440.1.1	4	17	9	31	UDP flavonoid 3-O-glucosyltransferase (Fragment)
Solyc05g056170.2.1	5	26	13	33	Phenylalanine ammonia-lyase
Solyc09g009830.2.1	9	36	14	40	Carbonic anhydrase (Carbonate dehydratase)
Solyc11g013110.1.1	6	26	13	37	Anthocyanidin synthase
Solyc10g009230.1.1	11	37	17	55	Unknown Protein
Solyc08g016080.2.1	11	37	15	50	NAD-dependent epimerase/dehydratase
Solyc01g110520.2.1	21	79	40	100	Glucosamine–fructose-6-phosphate aminotransferase
Solyc10g054910.1.1	7	20	6	32	Peptidyl-prolyl cis-trans isomerase
Solyc10g083720.1.1	7	32	19	48	Pyruvate kinase
Solyc05g005490.2.1	33	99	35	120	Carbonic anhydrase
Solyc03g114950.2.1	6	14	8	41	Lipid a export ATP-binding/permease protein msba
Solyc03g007370.2.1	6	19	7	30	RNA polymerase sigma factor
Solyc01g099370.2.1	6	35	36	83	SRC2 homolog (Fragment)
Solyc01g007500.2.1	37	216	73	74	Photosystem II CP47 chlorophyll apoprotein

continued on next page

Table S1: (continued)

Transcript	M_{20}	QFA_{20}	$AS1_{10}$	$AS1_{20}$	Annotation
Solyc01g103510.2.1	2	22	19	39	Ribosomal protein L3-like
Solyc02g081190.2.1	29	76	69	209	1-aminocyclopropane-1-carboxylate oxidase
Solyc10g055680.1.1	21	69	34	92	Ubiquinone/menaquinone biosynthesis methyltransferase ubiE
Solyc02g086650.2.1	9	28	10	37	Glucose-6-phosphate/phosphate translocator 2
Solyc07g049440.2.1	18	66	24	58	GDSL esterase/lipase At2g04570
Solyc10g085040.1.1	8	32	28	70	Soul heme-binding family protein
Solyc03g111690.2.1	17	71	37	75	Pectate lyase
Solyc08g005930.1.1	9	23	23	76	F-box family protein
Solyc12g010980.1.1	8	36	32	73	Acyltransferase-like protein
Solyc11g069070.1.1	11	53	62	134	Metal ion binding protein
Solyc10g011820.2.1	6	25	16	39	Delta-6 desaturase
Solyc11g012320.1.1	7	32	21	45	Unknown Protein
Solyc02g092790.2.1	25	73	43	116	Arabinogalactan
Solyc11g065740.1.1	8	30	17	42	RbcX protein
Solyc05g005480.2.1	74	207	113	307	Oxidoreductase zinc-binding dehydrogenase
Solyc07g063430.2.1	36	101	69	184	Mpv17 protein
Solyc07g005370.2.1	45	109	36	149	Norcoclaurine synthase
Solyc12g094640.1.1	106	304	122	348	Glyceraldehyde-3-phosphate dehydrogenase B
Solyc10g078930.1.1	24	78	90	214	Activator of heat shock protein ATPase homolog 1
Solyc08g083320.2.1	21	49	34	110	Granule-bound starch synthase
Solyc07g005390.2.1	36	98	43	126	Aldehyde dehydrogenase
Solyc06g050980.2.1	58	221	155	288	Ferritin
Solyc10g086410.2.1	10	33	39	96	Heat shock protein 70-3
Solyc06g073260.2.1	129	361	172	449	NAD-dependent epimerase/dehydratase
Solyc03g114450.2.1	76	205	108	289	Extracellular calcium sensing receptor
Solyc05g007830.2.1	9	50	43	73	Expansin 2
Solyc09g011140.2.1	16	58	24	48	Tropinone reductase I
Solyc07g006030.2.1	24	75	37	85	Protein TIF31 homolog
Solyc12g044330.1.1	138	295	140	519	Aquaporin
Solyc02g020940.2.1	128	346	204	506	Glyceraldehyde-3-phosphate dehydrogenase
					$(QFA_{20} \cap AS1_{10}) \setminus (AS1_{20} \cup M_{20})$
Solyc01g007690.2.1	93	1485	363	219	Unknown Protein
Solyc08g036520.2.1	6	198	40	33	Unknown Protein
Solyc00g006470.1.1	32	316	83	54	Unknown Protein
Solyc07g052220.1.1	1	10	42	3	Unknown Protein
Solyc11g027690.1.1	9	140	35	32	Unknown Protein
					$QFA_{20} \setminus (AS1_{10} \cup AS1_{20} \cup M_{20})$
Solyc08g036520.2.1	6	198	40	33	Unknown Protein
Solyc00g011160.1.1	2	47	4	5	Unknown Protein
Solyc01g007690.2.1	93	1485	363	219	Unknown Protein
Solyc00g006470.1.1	32	316	83	54	Unknown Protein
Solyc11g027690.1.1	9	140	35	32	Unknown Protein
Solyc05g016120.1.1	7	57	5	8	Photosystem Q(B) protein
Solyc01g048590.1.1	2	23	2	1	Photosystem Q(B) protein
Solyc11g044620.1.1	4	36	5	6	Imp biosynthesis protein
Solyc01g007330.2.1	123	865	258	346	Ribulose bisphosphate carboxylase large chain
Solyc01g007520.2.1	1	16	1	2	Photosystem II reaction center protein H
Solyc01g007500.2.1	37	216	73	74	Photosystem II CP47 chlorophyll apoprotein
Solyc10g079790.1.1	12	107	40	41	Pathogen-induced calmodulin-binding protein (Fragment)
Solyc01g007530.2.1	23	93	27	24	Cytochrome b6
Solyc01g017330.1.1	0	13	0	3	Photosystem I P700 chlorophyll a apoprotein A1
Solyc12g039030.1.1	1	16	5	1	Photosystem Q(B) protein
Solyc09g091110.2.1	1	12	2	1	Unknown Protein
Solyc01g007610.2.1	2	17	6	3	30S ribosomal protein S3 chloroplastic
Solyc09g092130.2.1	0	13	1	5	Sucrose phosphate synthase
Solyc06g074800.1.1	1	23	4	14	Cys2/His2 zinc-finger transcription factor
Solyc00g008570.2.1	0	9	2	1	Unknown Protein
					$AS1_{10} \setminus (QFA_{20} \cup AS1_{20} \cup M_{20})$
Solyc12g010020.1.1	0	0	21	0	Leucyl aminopeptidase
Solyc05g009310.2.1	6	5	81	13	Zinc finger protein CONSTANS-LIKE 16
Solyc10g051390.1.1	92	120	907	208	RNA-binding glycine-rich protein-1b
Solyc07g052210.2.1	85	150	837	206	Unknown Protein
Solyc07g064600.2.1	5	4	44	4	Endoribonuclease L-PSP family protein
Solyc01g109660.2.1	829	285	4394	574	Glycine-rich RNA-binding protein
Solyc11g021060.1.1	16	15	154	45	Proteinase inhibitor
Solyc12g006440.1.1	15	7	92	12	Unknown Protein
Solyc02g063450.2.1	51	52	374	89	Hypothetical YFW family protein 5
Solyc06g071820.2.1	2	1	24	1	Speckle-type poz protein
Solyc08g074630.1.1	12	17	124	38	Polyphenol oxidase
Solyc01g100710.2.1	8	1	45	2	Unknown Protein
Solyc03g093800.1.1	31	9	145	7	Unknown Protein
Solyc04g007000.1.1	1	2	21	1	Ethylene-responsive transcription factor 4
Solyc01g100720.2.1	31	20	176	39	Importin alpha-1b subunit
Solyc10g078920.1.1	19	5	92	10	Thioredoxin-like 5
Solyc07g052220.1.1	1	10	42	3	Unknown Protein

continued on next page

Table S1: (continued)

Transcript	M_{20}	QFA_{20}	$AS1_{10}$	$AS1_{20}$	Annotation
Solyc02g077420.2.1	9	5	52	5	Lipase-like
Solyc02g067690.2.1	19	11	101	16	Glucosyltransferase-like protein
Solyc07g024000.2.1	5	7	42	4	Dehydrogenase/ reductase 3
Solyc12g042950.1.1	22	13	108	12	ADP/ATP carrier protein
Solyc01g111350.2.1	6	4	39	4	Nodulin family protein
Solyc12g088310.1.1	3	3	31	6	Unknown Protein
Solyc10g008720.2.1	3	3	28	4	GDSL esterase/lipase At1g28580
Solyc07g041900.2.1	26	2	109	9	Cathepsin L-like cysteine proteinase
Solyc03g083770.1.1	20	6	86	4	Pectinesterase
Solyc01g067680.2.1	7	4	40	6	Tubby-like F-box protein 6
Solyc11g008460.1.1	10	14	69	14	U4/U6.U5 tri-snRNP-associated protein 1
Solyc09g082810.2.1	6	3	126	69	Unknown Protein
Solyc11g071460.1.1	3	1	21	0	Dehydrogenase/reductase SDR family member 13
Solyc01g080910.2.1	6	5	45	13	Unknown Protein
Solyc00g071180.2.1	4	3	29	5	Cysteine proteinase inhibitor
Solyc11g068710.1.1	8	5	47	12	F-box family protein
Solyc05g009470.2.1	109	127	642	237	Alpha-glucosidase
Solyc07g055050.2.1	51	21	190	29	ATP synthase I-like protein
Solyc04g079920.2.1	4	31	98	29	Pre-mRNA-splicing factor cwc22
Solyc10g078540.1.1	8	19	93	43	H/ACA ribonucleoprotein complex subunit 1-like protein 1
Solyc01g006400.2.1	21	19	174	97	Cysteine-rich extensin-like protein-4
Solyc06g016750.2.1	16	33	132	52	Transcription factor (Fragment)
Solyc09g092710.2.1	32	23	147	49	Glycine rich protein
Solyc01g079470.2.1	157	78	532	87	CP12
Solyc03g123630.2.1	64	43	237	63	Pectinesterase
Solyc01g098760.2.1	48	65	256	114	Heavy metal-associated domain containing protein expressed
					$AS1_{20} \setminus (QFA_{20} \cup AS1_{10} \cup M_{20})$
Solyc09g011630.2.1	1	3	5	67	Glutathione S-transferase-like protein
Solyc10g085880.1.1	2	4	4	69	UDP-glucosyltransferase family 1 protein
Solyc09g092500.1.1	26	122	71	804	UDP-glucosyltransferase family 1 protein
Solyc11g007500.1.1	0	1	1	31	UDP-glucosyltransferase
Solyc01g107820.2.1	8	23	58	269	UDP-glucosyltransferase family 1 protein
Solyc10g084400.1.1	2	4	5	57	Glutathione S-transferase
Solyc03g078490.2.1	0	1	5	41	UDP-glucuronosyltransferase
Solyc01g104740.2.1	0	2	1	32	Multiprotein bridging factor 1
Solyc04g007140.1.1	0	5	5	50	Unknown Protein
Solyc02g082920.2.1	0	2	14	66	Endochitinase (Chitinase)
Solyc11g011340.1.1	0	0	1	22	Alcohol dehydrogenase
Solyc03g080190.2.1	0	5	4	43	Flavanone 3-hydroxylase-like protein
Solyc09g083210.2.1	3	7	9	58	Receptor-like protein kinase
Solyc05g009490.2.1	2	11	53	160	Unknown Protein
Solyc01g086660.2.1	0	1	1	22	Unknown Protein
Solyc01g097240.2.1	1	0	1	22	Pathogenesis-related protein 4B (Fragment)
Solyc06g036110.1.1	1	3	1	29	C2 domain-containing protein
Solyc11g010380.1.1	8	48	18	197	Mate efflux family protein
Solyc08g068870.2.1	0	5	12	50	Aspartic proteinase nepenthesin-1
Solyc01g107780.2.1	0	3	2	27	UDP-glucosyltransferase family 1 protein
Solyc12g042600.1.1	3	8	15	63	UDP-glucosyltransferase family 1 protein
Solyc09g015770.2.1	2	8	24	76	WRKY transcription factor 6
Solyc02g093710.1.1	3	3	10	44	Genomic DNA chromosome 3 TAC clone K1G2
Solyc01g110150.2.1	8	27	19	118	CM0216.450.nc protein
Solyc07g056480.2.1	7	2	15	62	Glutathione S-transferase-like protein
Solyc01g008620.2.1	0	0	2	19	Beta-1 3-glucanase
Solyc01g006290.2.1	1	0	0	18	Peroxidase
Solyc03g033840.2.1	0	4	2	26	26S protease regulatory subunit 6B homolog
Solyc09g098510.2.1	7	19	57	142	Unknown Protein
Solyc07g006890.1.1	1	9	21	64	Cytochrome P450
Solyc08g079870.1.1	0	1	4	22	Subtilisin-like protease
Solyc11g007950.1.1	5	12	20	71	Unknown Protein
Solyc03g078500.2.1	0	0	0	13	UDP-glucuronosyltransferase
Solyc05g050750.1.1	0	0	0	13	Calmodulin-like protein
Solyc08g006470.2.1	0	1	3	19	Zinc finger family protein
Solyc08g082590.2.1	23	146	44	420	Glutaredoxin family protein
Solyc10g084430.1.1	1	2	0	19	RING finger protein 44
Solyc06g076020.2.1	2	24	7	76	heat shock protein
Solyc01g067120.2.1	1	2	1	19	Cullin 1-like protein C
Solyc04g040180.2.1	0	1	4	20	S-adenosylmethionine-dependent methyltransferase (Fragment)
Solyc10g085030.1.1	1	22	11	73	Soul heme-binding family protein
Solyc05g005460.2.1	3	8	23	60	Nucleoredoxin 2
Solyc10g017580.2.1	3	10	8	44	Digalactosyldiacylglycerol synthase 2, chloroplastic
Solyc02g088200.2.1	0	1	0	14	Activating signal cointegrator 1 complex subunit 1
Solyc10g051020.1.1	4	4	8	35	Cytochrome P450
Solyc08g060920.2.1	8	32	30	112	Xenotropic and polytropic retrovirus receptor
Solyc10g045180.1.1	1	1	3	18	Cytokinesis negative regulator RCP1
Solyc12g013690.1.1	0	0	3	16	Monooxygenase FAD-binding protein
Solyc12g006380.1.1	2	2	3	21	1-aminocyclopropane-1-carboxylate oxidase-like protein
Solyc03g095770.2.1	0	2	8	25	WRKY transcription factor 6
Solyc07g008140.2.1	0	0	0	11	Blue copper protein (Fragment)

continued on next page

Table S1: (continued)

Transcript	M_{20}	QFA_{20}	$AS1_{10}$	$AS1_{20}$	Annotation
Solyc10g081570.1.1	9	91	129	328	KED
Solyc11g011440.1.1	6	8	10	44	Aspartic proteinase nepenthesin-1
Solyc04g050440.2.1	5	19	2	60	Ammonium transporter
Solyc10g079930.1.1	8	12	33	77	UDP-glucosyltransferase HvUGT5876
Solyc05g014550.1.1	8	8	13	50	DNA-binding protein (Fragment)
Solyc10g084170.1.1	0	1	1	13	Bcl-2-associated athanogene-like protein
Solyc12g006980.1.1	19	51	91	207	Leucine-rich repeat receptor-like protein kinase PEPR2
Solyc09g007010.1.1	0	1	10	90	Pathogenesis related protein PR-1
Solyc09g011540.2.1	0	1	0	12	Glutathione S-transferase-like protein
Solyc10g049580.1.1	6	13	35	75	Unknown Protein
Solyc07g047800.2.1	9	16	46	95	Short-chain dehydrogenase/reductase family protein
Solyc06g009020.2.1	25	59	38	179	Glutathione S-transferase
Solyc09g008200.2.1	7	28	29	90	Heavy metal-associated domain containing protein expressed
Solyc04g051690.2.1	0	0	1	11	WRKY transcription factor 16
Solyc08g062450.1.1	1	1	0	13	class II heat shock protein
Solyc08g078020.1.1	104	184	337	720	Methionine rich arabinogalactan
Solyc12g015880.1.1	100	403	247	963	Heat shock protein 90
Solyc03g117630.1.1	0	1	0	10	heat shock protein
					$M_{20} \setminus (QFA_{20} \cup AS1_{10} \cup AS1_{20})$
Solyc03g117590.2.1	77	24	48	27	Chaperone protein dnaJ
Solyc06g035940.2.1	8	0	3	3	Homeobox-leucine zipper protein PROTODERMAL FACTOR 2
Solyc10g005100.2.1	140	72	119	93	Salt stress root protein RS1
Solyc06g060640.1.1	166	93	182	115	Cortical cell-delineating protein